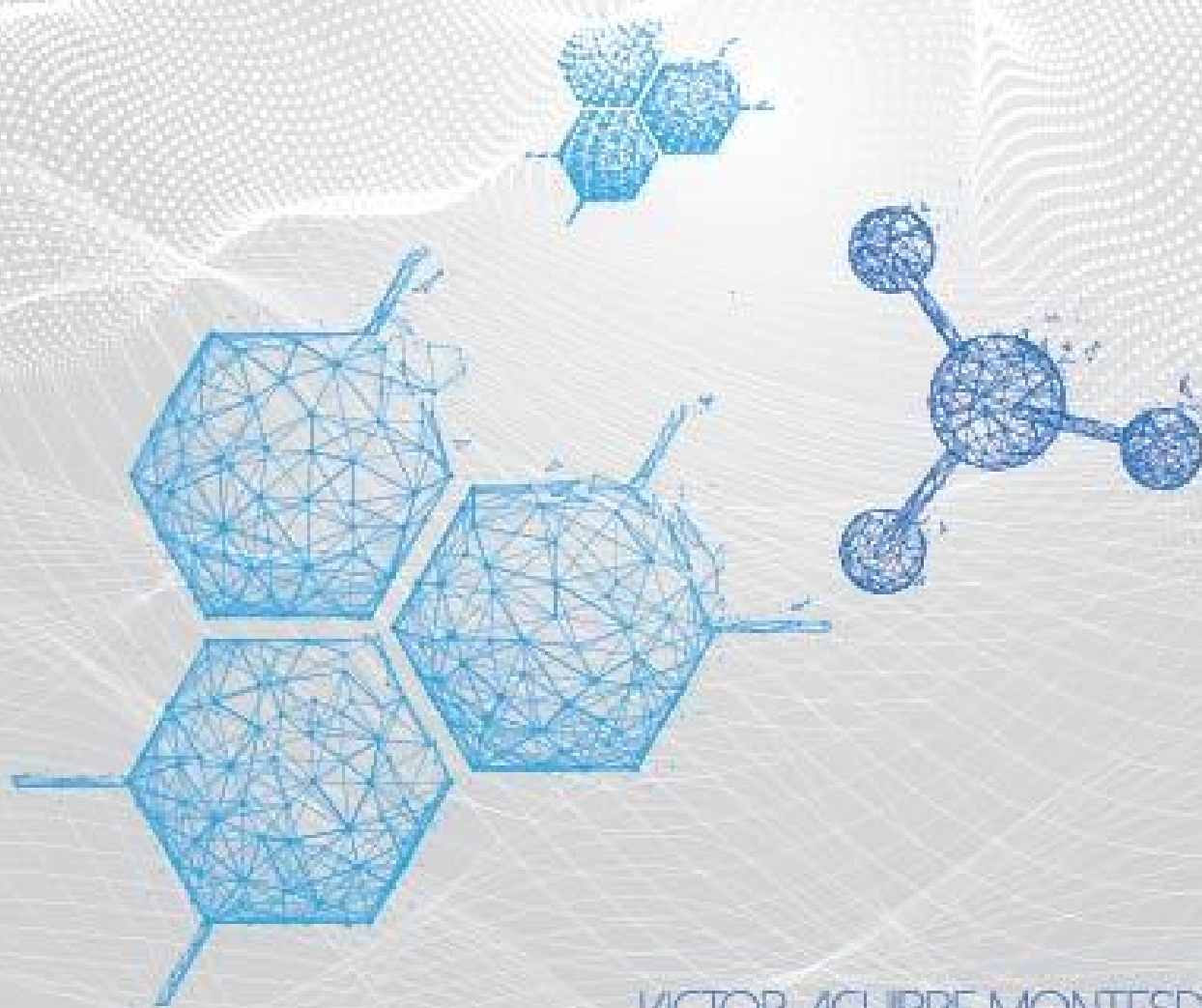


MEMBRANE FILTRATION OF FOOD STREAMS: MECHANISMS AND MODELLING



VICTOR AGUIRRE MONTESDEOCA

Membrane filtration of food streams: Mechanisms and modelling.

Víctor Aguirre Montesdeoca

Thesis committee

Promotors

Prof. Dr Albert van der Padt

Special Professor of Sustainable Production of Food.

Wageningen University & Research

Prof. Dr Remko M. Boom

Professor of Food Process Engineering

Wageningen University & Research

Co-promotors

Dr Anja E. M. Janssen

Associate professor at the laboratory of Food Process Engineering

Wageningen University & Research

Other members

Prof. Dr van der Linden, Wageningen University & Research

Prof. Dr FAM Leermakers, Wageningen University & Research

Prof. Dr HDW Roesink, University of Twente

Dr R. Noordman, Pentair, Netherlands.

This research was conducted under the auspices of the Graduate School VLAG (Advanced studies in Food Technology, Agrobiotechnology, Nutrition and Health Sciences).

Membrane filtration of food streams: Mechanisms and modelling.

Víctor Aguirre Montesdeoca

Thesis

submitted in fulfilment of the requirements for the degree of doctor
at Wageningen University
by the authority of the Rector Magnificus
Prof. Dr A.P.J Mol,
in the presence of the
Thesis Committee appointed by the Academic Board
to be defended in public
on Monday 12 November 2018
at 4 p.m. in the Aula.

Victor Aguirre Montesdeoca

Membrane filtration of food streams: Mechanisms and modelling.

194 pages

PhD thesis, Wageningen University, Wageningen, NL (2018)

With references, with summary in English

ISBN: 978-94-6343-509-3

DOI: <https://doi.org/10.18174/459186>

To my grandmas:

Mariana and Clementina

Contents

	Page
Chapter 1. Introduction	1
Chapter 2. Modelling of membrane cascades for the purification of oligosaccharides	17
Chapter 3. Nanofiltration of non-spherical molecules.	49
Chapter 4. Nanofiltration of concentrated oligosaccharide solutions – hydration and pore size distribution effects.	85
Chapter 5. Modelling UF performance by integrating local (critical) fluxes along the membrane length.	129
Chapter 6. General discussion	169
Summary	185

Chapter 1

General Introduction

1.1 THE EVOLUTION OF MEMBRANE TECHNOLOGY

The principle of separation via synthetic membranes is not new. Ultrafiltration (UF) was a novelty at the research level in early 1960's, and its industrial applications started appearing already in the 1970's [1]. Over the years, the developments in the understanding of the separation mechanisms and in material science, allowed the expansion of membrane filtration applications to many different fields. Originally, size exclusion was the main mechanism to be exploited for the purification or concentration of solutions, in which pressure or concentration gradients act as driving force for the transport of the components in the mixture. Later on, other driving forces such as electrical potential and temperature gradients were used in the development of processes that allow the separation of molecules with specific properties. In the former case, components with specific type of charge (electrodialysis), and in the latter case, allowing the transport of only molecules in vapour phase (membrane distillation). Likewise, in line with the process intensification trend, combinations of membrane filtration with other technologies have been developed in the last decades. That is the case for membrane reactors, in which the aim is to combine a reaction and a separation process in a single step. Other type of synergetic combinations are membrane absorption/stripping and membrane crystallization [2]. A summary of the main membrane processes, their driving force and typical selectivity range is shown in Table 1-1.

Table 1-1. Primary membrane processes and their characteristics. *Adapted from Koros [3].*

Process	Typical driving force	Selectivity range [$\times 10^{-9}$ m]
Microfiltration (MF)	TMP (0.7 - 2 bar)	100 – 20000
Ultrafiltration (UF)	TMP (0.7 - 7 bar)	2 – 10
Dialysis (D)	Concentration difference (10 - 200 mg/L)	1 – 4
Nanofiltration (NF)	TMP (7 – 30 bar)	0.5 – 2
Reverse Osmosis (RO)	TMP (7 – 100 bar)	0.3 – 0.5
Pervaporation (PV)	Fugacity difference (0.3 – 1.4 bar)	0.3 – 0.5
Gas or vapour separation (GS)	TMP (7 – 100 bar)	0.3 – 0.5
Electrodialysis (ED)	Voltage difference (1-2 V per membrane par)	0.3 – 0.5

TMP: Trans-membrane Pressure.

Nowadays, after more than five decades of its initial discovery, membrane technology is still a growing area. Its applications in industry are still expanding due to mainly its relatively low energy consumption, compared with processes such as evaporation or distillation, which require a phase change in the mixture that is to be separated. For example, in the case of distillation, despite the great efforts in increasing its efficiency over the years, this process alone accounts for approximately 50% of the energy consumption in the chemical and oil industries [4]. Therefore, membrane separations are likely to play an increasingly important role in reducing the environmental impact and operational costs of industrial processes. Other advantages of membrane separations over other processes are: simplicity, manufacturing scalability, and small footprint [5].

1.2 APPLICATIONS OF MEMBRANE TECHNOLOGY IN THE FOOD INDUSTRY

Although most of the industrial applications of membrane technology are related with water treatment, in the food and biotechnology industry many membrane separation processes can also be found. A general summary of these applications is presented in Table 1-2.

Table 1-2. Main applications of membrane processes in the Food and Biotechnology industry [6-9].

Process	Food industry		Biotechnology industry
	Dairy applications	Other	
Microfiltration (MF)	Bacterial reduction. Fat removal. Whey and casein standardisation. Removal of casein from whey.	Clarification of juices/wine Clarification of beer Sterilization of soy sauce.	Enzyme polishing. Pyrogen removal. Sterile water for injections.
Ultrafiltration (UF)	Whey concentration. Fractionation of hydrolysates. Separation of β -lactoglobulin and α -lactalbumin.	Clarification and chillproofing of juices. Clarification of soy sauce.	Recovery of antibiotics from fermentation broth. Concentration of enzymes. Clarification of organic compounds and amino acids.
Nanofiltration (NF)	Partial demineralisation of whey. Removal of lactose from milk.	Decoloration and partial desalination of soy sauce.	Enzyme and antibiotic concentration. Diafiltration water recovery.
Reverse Osmosis (RO)	Concentration of milk and whey. Solid recovery. Water reclamation.	Concentration of juices.	Water polishing for recycling. Recovery of low molecular weight xanthan gum. Pre-concentration of amino acids. Diafiltration water preparation.
Electrodialysis (ED)	Demineralization of whey		

The incorporation of a new process technology comes together with a need of understanding about the involved physicochemical mechanisms at every length scale. From the basic molecular level to the upscaling and staging of the process (membrane cascading). This need goes beyond the gathering of experimental data that may or may not be useful to predict the behaviour of the process. Current theory, however, is not yet sufficient to be applied in systems with complex feeds. It is only applicable to the more standard membrane technology applications, which are often related with water purification. In the next section, these theories and models are briefly introduced.

1.3 TRANSPORT MECHANISMS IN MEMBRANE SYSTEMS

1.3.1 Transport through membranes

Many models and theories have been developed over the years for the description of the mass transfer of a component through a membrane. The so-called ‘black-box’ model was one of the first models to be created, based on irreversible thermodynamics and developed by Kedem and Katchalsky in 1958. It was actually first obtained to represent the transport of non-electrolytes through biological membranes [10]. It was later on used for synthetic membranes with great success [11-13]. Another well-known model, which follows a complete different approach, is the so called pore-model. This is a more physics-based model which assumes the pore to be cylindrical and uses Poiseuille flow to relate the size of the pore, the pressure gradient and the resulting water flux [14-16]. Both of these models require initial characterization experiments to estimate important parameters of the system.

1.3.2 Concentration Polarization

Apart from the description of the actual transport of the solute through the membrane pores, it was also found necessary to describe the rise in the solute concentration just before the membrane. This phenomenon, called concentration polarization, occurs due to the size exclusion effect of the membrane. It was found that the size of this concentration polarization layer was dependent on the diffusivity of the solutes and in the cross flow velocity of the process. Commonly, the effect on the permeate flux (J) of a concentration at the membrane (C_m) higher than that at the bulk of the retentate (C_b) can be expressed as follows:

$$J = k \ln \left(\frac{C_m - C_p}{C_b - C_p} \right), \quad (1.1)$$

in which k is the mass transfer coefficient and C_p is the solute concentration in the permeate. Eq. 1.1 is the result of a mass balance of the solute in the concentration polarization layer, in which two transport mechanisms are involved: convection (towards the membrane) and diffusion (towards the bulk of the retentate) [17].

In filtration processes that include macromolecules such as proteins, the formation of a gel layer in the membrane is likely to occur. As consequence, the concentration at the membrane surface can reach the gel concentration (C_g). For a membrane that rejects completely the proteins, Eq.1.1 can be simplified in the following way, resulting in what is called: the gel layer model[18].

$$J_{lim} = k \ln \left(\frac{C_g}{C_b} \right) \quad (1.2)$$

1.4 MULTICOMPONENT, CONCENTRATED FEED MIXTURES

The aforementioned models and descriptions are developed for thermodynamically ideal mixtures [19]. They do not consider the interactions between components that determine ‘cross effects’ in the system. Hence, they are not suitable for concentrated multicomponent mixtures, which are precisely the type of mixtures that are commonly used in the food and biotechnology industry. If these models would be used for the filtration of such feed mixtures, the obtained solutes fluxes would be independent of each other. This means that the components of the mixture would not affect each other separation with respect to single solute systems. In reality, it has been found experimentally that the final outcome of a separation is quite different when extra solutes are added to the feed [20-23].

Van Oers et al., already in 1992, found out that the rejection of PEG was greatly reduced as dextran was added to the feed [20]. Likewise, Bargeman measured the effect of adding salts during the nanofiltration of glucose. They found that the almost complete rejection of glucose was notoriously decreased as NaCl and other salts were added [21]. The common observation in these studies was that these ‘cross effects’ were greater as the solutes concentration in the feed increased.

Based on the models available in literature, and on the type of real systems currently used in industry, 6 aspects (Figure 1-1) can be recognized as ‘points for improvement’ in order to develop mathematical descriptions that can actually represent such complex systems:

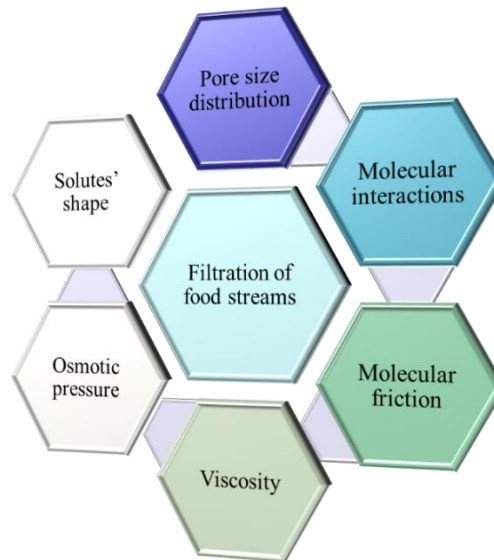


Figure 1-1. Aspects to consider when modelling the filtration of food streams.

Molecular shape: Molecular dimensions and shape are important because they define the probability of a solute entering a membrane pore [24]. In practice, neither the solute nor the pores have a regular shape; nevertheless, much more information is available about the molecular structure of the solute [25, 26]. Hence, it makes more sense to improve the representation of the shape and dimensions of the solute, and assume a regular shape for the pores (cylinders) [27, 28]. Current models usually consider molecules to be spherical and use their Stokes radii to represent their physical dimensions (see Figure 1-2). Assuming a solute molecule to be spherical, however, can be far away from reality; chained molecules like oligomers or polymers are very elongated and are normally found in food streams (e.g. oligosaccharides, fibers, peptides, etc) [29].

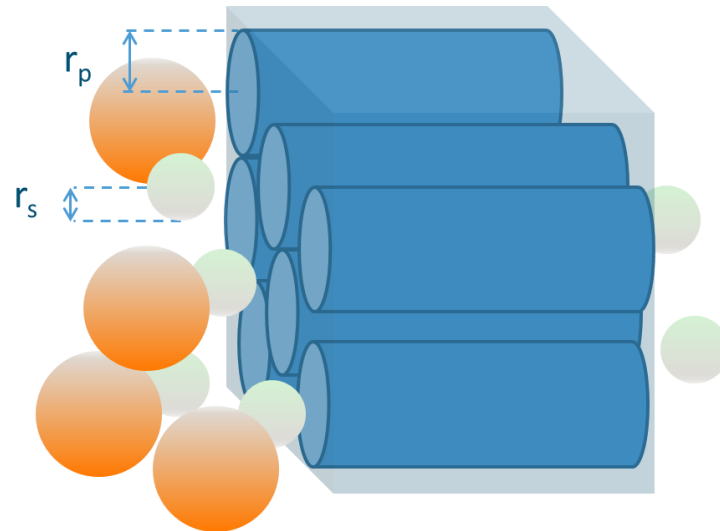


Figure 1-2. Graphical representation of the Pore model. Solutes with a Stokes radius (r_s) larger than the pore radius (r_p) are rejected by the membrane. The opposite occurs with smaller molecules. (Figure taken from Jaap Bakker's MSc. thesis).

Pore size distribution: Membranes normally do not have a uniform pore size (except track-etched membranes). Especially in nanofiltration systems, the distribution of pore size is a very important variable that it is often overlooked. Although it might seem intuitively convenient to use only the average pore size during modelling, it has already been proved that this simplification leads to erroneous results [30, 31]. Including the pore size distribution in a model represents a large burden in the computation resources needed for the calculations. Therefore, efficient model coding and making use of fast modern computers are critical to tackle this issue.

Interaction between components: Solutes in a mixture always interact; they interact between them and with the solvent. In diluted systems, these interactions are often negligible, but as the system gets concentrated such interactions determine non-idealities that should not be ignored [32]. Phenomena like hydration, adsorption, electrical effects and volume exclusion can be found in concentrated systems [33]. Available knowledge about these phenomena allow us to mathematically represent it and incorporate it in a model.

Friction between components: The components of a mixture moving at different speeds produce molecular friction between them. This friction is proportional to the difference in the components' velocities [34]. It is expected that if one component is totally rejected by the membrane, the difference in velocity (and hence friction) with components that do pass through the membrane would be large (See Figure 1-3). The friction proportionality constant between two components is caught by the diffusion coefficient between them. Diffusivities are normally

considered only for solutes with water, while diffusivities between solutes are much more difficult to determine and their relevance in the final outcome is not yet well established [35].

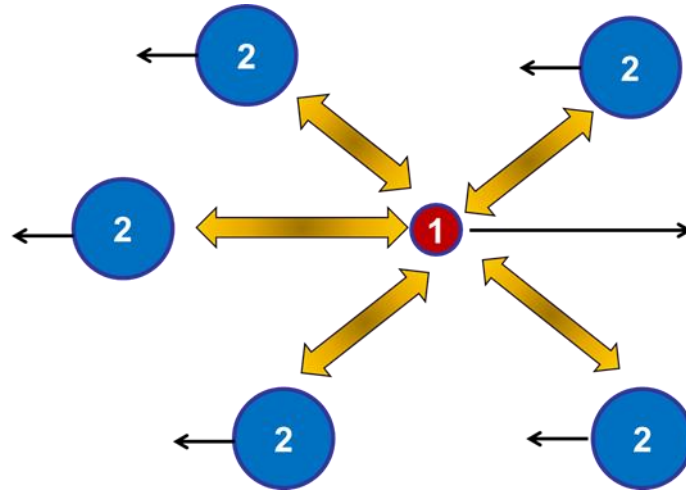


Figure 1-3. Sketch of the friction forces working over two components moving in different directions.

Viscosity: Concentrated systems are expected to have an increased viscosity with respect to that of water. Viscosity is normally important in the mass transfer of solutes outside the membrane, where the concentration is the highest. It becomes then critical to take into account this increase, since it can definitely have an impact in the overall process efficiency. Empirical equations to estimate the mass transfer coefficient, like the Sherwood relations, rely on variables such as Reynolds and Schmidt numbers, which are functions of viscosity [36].

Osmotic pressure: Due to the difference in concentration at both sides of the membrane, the resulting difference in osmotic pressure counteracts the effect of the transmembrane pressure. Van't Hoff equation is useful to estimate the osmotic pressure at each sides of the membrane based on the local compositions [32]. Unfortunately, this relation is only valid for ideal systems. The complexity of food streams demands the use of thermodynamics to estimate the water activity of the solutions, and subsequently, calculate the osmotic pressure.

1.5 MAXWELL STEFAN EQUATIONS

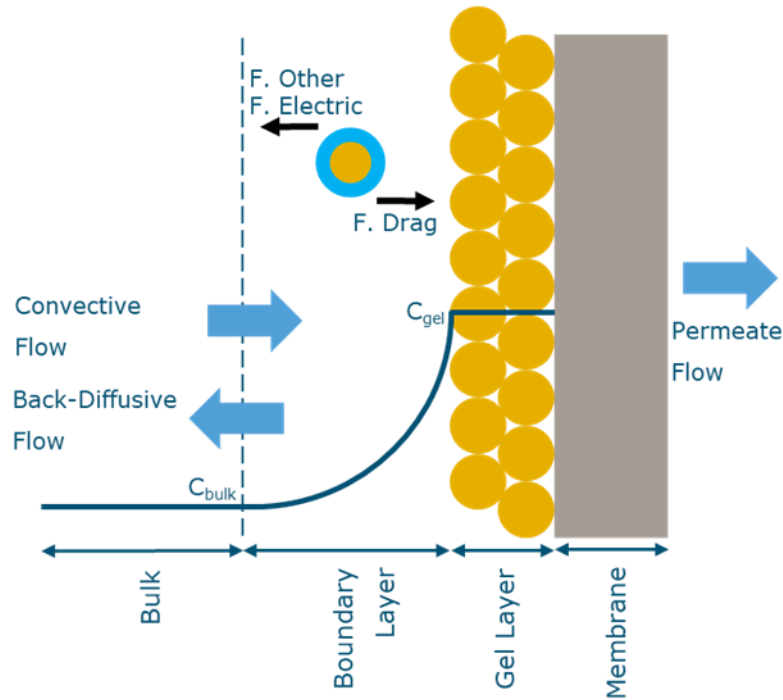


Figure 1-4. Schematic view of the forces acting over an approaching protein molecule for a membrane covered by a gel layer. (Taken from the MSc. thesis of Bobby Oka Mahendra).

The Maxwell-Stefan equations are the conjunction of the work made by James Clerk Maxwell (1866) and Josef Stefan (1871). They both studied molecular transport at the end of the 19th century. This approach is a rigorous way to represent the molecular transport in multicomponent systems like the ones shown in Figure 1-4. The Maxwell-Stefan equations can be envisaged as a force balance between the molecules in a system, in which the driving forces are equal to the friction forces as represented in Eq. 1.3 [34]. The left hand side term represents the driving forces for component i , and the right hand side account for the friction forces acting over i . x represents the solutes mole fraction and u are their linear velocities. \mathfrak{D}_{ij} is the Maxwell-Stefan cross diffusion coefficient between species i and j .

$$\frac{x_i}{RT} \nabla_{T,P} \mu_i = - \sum_{\substack{j=1 \\ j \neq i}}^m \frac{x_i x_j (u_i - u_j)}{\mathfrak{D}_{ij}} \quad (1.3)$$

The Maxwell-Stefan cross diffusion coefficient (\mathfrak{D}_{ij}), differs from the diffusion coefficient defined in Fick's law ($D_{i,j}$). The main difference is that in Fick's law, the non-idealities of the system are accounted in the $D_{i,j}$, while in the Maxwell-Stefan Equations, the non-idealities are

accounted in the driving forces term [37, 38]. As consequence, \mathfrak{D}_{ij} are much less dependent on concentration and obey the Onsager reciprocal relation: $\mathfrak{D}_{ij} = \mathfrak{D}_{ji}$ [35, 39].

Interestingly, the driving forces are expressed as a function of the gradient in chemical potential at constant temperature (T) and pressure (P). This description is very suitable considering that in the concentration polarization layer, pressure and temperature are indeed constant. Additionally, the fact that chemical potential is used in the equation, is a generalization that implies that the driving forces are not necessarily the negative of the concentration gradient. It gives room for ‘corrections’ if needed, to account for the non-idealities of the system [34].

As consequence, the term for the driving forces can be worked out in the following way:

$$driving\ force = \frac{x_i}{RT} \sum_{j=1}^{m-1} \left(\frac{\partial \mu_i}{\partial x_j} \right)_{T,P} \frac{dx_j}{dz} \quad (1.4)$$

$$driving\ force = x_i \sum_{j=1}^{m-1} \left(\frac{\partial \ln x_i}{\partial x_j} + \frac{\partial \ln \gamma_i}{\partial x_j} \right)_{T,P} \frac{dx_j}{dz} \quad (1.5)$$

$$driving\ force = \sum_{j=1}^{m-1} \Gamma_{ij} \frac{dx_j}{dz} \quad (1.6)$$

Γ_{ij} is the so-called thermodynamic factor, which corrects for the non-idealities existing in the system. It can be calculated based on thermodynamic data about the interactions that the mixture components might have with each other [34]. Therefore, the Maxwell-Stefan Equations not only allow us to relate driving forces with friction forces between the components, but also allow us to incorporate non-idealities in the driving forces. This make the Maxwell-Stefan equations the best approach to deal with complex solutions, such as food streams [40].

Table 1-3. Summary of the advantages and disadvantages of the Maxwell Stefan and Fick approaches to represent mass transfer of multicomponent mixtures (after Wesselingh and Krishna, 2000) [35].

	Maxwell- Stefan	Fick
Simple behaviour of coefficients	Yes	No
Independence of reference frame	Yes	No
Easily extended to other driving forces	Yes	No
Number of ternary coefficients	3	4
Coefficients are independent of driving forces	Yes	No
Coefficients independent of sequence	Yes	No
Explicit fluxes	No*	Yes
Integration with thermodynamics	Yes	No
Looks like ‘chemical engineering’	No	Yes

*Fluxes in the Maxwell-Stefan equations are relative to a reference frame. To calculate their absolute values, an extra equation is needed; this equation is called ‘Bootstrap’.

1.6 SCOPE OF THIS THESIS

The fundamentals about mass transfer in membrane systems have already been established over the last 50 years. Many theories and models have been developed to represent most of the existing membrane systems. A big gap, however, still exists in the area of the industrial applications of such membrane systems. More specifically, the filtration of the streams used in the food and biotechnological industry cannot yet be modelled, and several observations cannot yet be explained. In this thesis, we try to reduce the gap in the understanding of these complex systems. Using as starting point the available theory in literature, the aim is to improve the models accuracy in the field of pressure driven filtration by adapting new concepts and descriptions. These new concepts come from the understanding of the underlying phenomena taking place under realistic conditions.

In **Chapter 2**, we start our research studying the overall behaviour of a staged nanofiltration system. Based on experimental rejection data obtained using single stage filtration, we model

and optimize a three-stage cascade system for the purification of oligosaccharides. An ideal combination of process parameters dependent on the feed mixture composition is determined.

In **Chapter 3**, to avoid the need of experimental data on solute rejection, the transport of solutes through membrane pores is studied. We revisit the effects of solutes molecular shape in membrane rejection for nanofiltration systems. The possibility of considering elongated solutes to be capsule-shaped instead of spherical is evaluated. Under the capsular approach, not only position but also molecular orientation are relevant in determining whether a solute enters or not a pore. Simultaneously, the consideration of a pore size distribution instead of a uniform pore size is included in the analysis.

In **Chapter 4**, the effect of high concentration is assessed using as a model system the nanofiltration of an oligosaccharides mixture. Although the analysis is mostly based on thermodynamic effects due to hydration, effects emerging from the pore size distribution and high osmotic pressure are also discussed. Likewise, the importance of the different transport mechanisms at high concentration is assessed and compared with that at diluted conditions.

In **Chapter 5**, the analysis of the interactions between components is expanded in a twofold manner: Electrical interactions between components are considered and excluded volume effects are also assessed by using the Carnahan-Starling description. The effect of this interactions on the resulting permeate flux is assessed for a system containing BSA, NaCl and water. The formation of a gel layer is also analysed and a model that considers local fluxes depending on the changing boundary layer thickness is proposed.

In **Chapter 6**, the findings and conclusions of this thesis are discussed. Opportunities for improvement for membrane manufacturers and membrane users are analysed within the scope of the application of membrane technology in food processes. Finally, remaining challenges about scientific aspects that could not been completely covered in this thesis are also presented.

REFERENCES

- [1] R. Baker, *Membrane Technology and Applications* 2nd ed., Wiley, California, USA, 2004.
- [2] A. Stankiewicz, M. J., *Re-engineering the chemical processing plant. Process Intensification*, Marcel Dekker, New York, 2004.
- [3] W.J. Koros, *Evolving beyond the thermal age of separation processes: Membranes can lead the way*, *AIChE J.*, 50 (2004) 2326-2334.
- [4] J.A. Caballero, I.E. Grossmann, A. Górak, E. Sorensen, Chapter 11 - Optimization of Distillation Processes, in: *Distillation*, Academic Press, Boston, 2014, pp. 437-496.
- [5] H.B. Park, J. Kamcev, L.M. Robeson, M. Elimelech, B.D. Freeman, *Maximizing the right stuff: The trade-off between membrane permeability and selectivity*, *Science*, 356 (2017).
- [6] F. Lipnizki, Z.F. Cui, H.S. Muralidhara, Chapter 7 - Membrane Processes for the Production of Bulk Fermentation Products, in: *Membrane Technology*, Butterworth-Heinemann, Oxford, 2010, pp. 121-153.
- [7] Y. Wan, J. Luo, Z. Cui, Z.F. Cui, H.S. Muralidhara, Chapter 4 - Membrane Application in Soy Sauce Processing, in: *Membrane Technology*, Butterworth-Heinemann, Oxford, 2010, pp. 45-62.
- [8] S.A. Ilame, S. V. Singh, *Application of Membrane Separation in Fruit and Vegetable Juice Processing: A Review*, *Crit. Rev. Food Sci. Nutr.*, 55 (2015) 964-987.
- [9] Y. Pouliot, *Membrane processes in dairy technology—From a simple idea to worldwide panacea*, *Int. Dairy J.*, 18 (2008) 735-740.
- [10] O. Kedem, A. Katchalsky, *Thermodynamic analysis of the permeability of biological membranes to non-electrolytes*, *Biochim. Biophys. Acta*, 27 (1958) 229-246.
- [11] K. Spiegler, O. Kedem, *Thermodynamics of hyperfiltration (reverse osmosis): criteria for efficient membranes*, *Desalination*, 1 (1966) 311-326.
- [12] S.-I. Nakao, S. Kimura, *Analysis of solutes rejection in ultrafiltration*, *J. Chem. Eng. Jpn.*, 14 (1981) 32-37.
- [13] W. Li, J. Li, T. Chen, Z. Zhao, C. Chen, *Study on nanofiltration for purifying fructo-oligosaccharides: II. Extended pore model*, *J. Membr. Sci.*, 258 (2005) 8-15.
- [14] W.R. Bowen, A.W. Mohammad, *Characterization and Prediction of Nanofiltration Membrane Performance—A General Assessment*, *Chem. Eng. Res. Des.*, 76 (1998) 885-893.
- [15] W.R. Bowen, J.S. Welfoot, *Modelling the performance of membrane nanofiltration—critical assessment and model development*, *Chem. Eng. Sci.*, 57 (2002) 1121-1137.

- [16] S. Bandini, D. Vezzani, Nanofiltration modeling: the role of dielectric exclusion in membrane characterization, *Chem. Eng. Sci.*, 58 (2003) 3303-3326.
- [17] M. Mulder, Transport in Membranes, in: *Basic Principles of Membrane Technology*, Springer Netherlands, 1996, pp. 210-279.
- [18] J.G. Wijmans, S. Nakao, C.A. Smolders, Flux limitation in ultrafiltration: Osmotic pressure model and gel layer model, *J. Membr. Sci.*, 20 (1984) 115-124.
- [19] C. Rodrigues, A.I. Cavaco Morão, M.N. de Pinho, V. Geraldes, On the prediction of permeate flux for nanofiltration of concentrated aqueous solutions with thin-film composite polyamide membranes, *J. Membr. Sci.*, 346 (2010) 1-7.
- [20] C.W. van Oers, M.A.G. Vorstman, R.v.d. Hout, P.J.A.M. Kerkhof, The influence of thermodynamic activity on the solute rejection in multicomponent systems, *J. Membr. Sci.*, 136 (1997) 71-87.
- [21] G., J.M. Vollenbroek, J. Straatsma, C.G.P.H. Schroën, R.M. Boom, Nanofiltration of multi-component feeds. Interactions between neutral and charged components and their effect on retention, *J. Membr. Sci.*, 247 (2005) 11-20.
- [22] A.E. Yaroshchuk, Negative rejection of ions in pressure-driven membrane processes, *Adv. Colloid Interface Sci.*, 139 (2008) 150-173.
- [23] A.W. Mohammad, R.K. Basha, C.P. Leo, Nanofiltration of glucose solution containing salts: Effects of membrane characteristics, organic component and salts on retention, *J. Food Eng.*, 97 (2010) 510-518.
- [24] J.C. Giddings, E. Kucera, C.P. Russell, M.N. Myers, Statistical theory for the equilibrium distribution of rigid molecules in inert porous networks. Exclusion chromatography, *The Journal of Physical Chemistry*, 72 (1968) 4397-4408.
- [25] Y. Kiso, K. Muroshige, T. Oguchi, M. Hirose, T. Ohara, T. Shintani, Pore radius estimation based on organic solute molecular shape and effects of pressure on pore radius for a reverse osmosis membrane, *J. Membr. Sci.*, 369 (2011) 290-298.
- [26] Y. Kiso, K. Muroshige, T. Oguchi, T. Yamada, M. Hhirose, T. Ohara, T. Shintani, Effect of molecular shape on rejection of uncharged organic compounds by nanofiltration membranes and on calculated pore radii, *J. Membr. Sci.*, 358 (2010) 101-113.
- [27] J.L.C. Santos, P. de Beukelaar, I.F.J. Vankelecom, S. Velizarov, J.G. Crespo, Effect of solute geometry and orientation on the rejection of uncharged compounds by nanofiltration, *Sep. Purif. Technol.*, 50 (2006) 122-131.

- [28] F. Vinther, M. Pinelo, M. Brøns, G. Jonsson, A.S. Meyer, Statistical modelling of the interplay between solute shape and rejection in porous membranes, *Sep. Purif. Technol.*, 89 (2012) 261-269.
- [29] B. Van der Bruggen, J. Schaep, D. Wilms, C. Vandecasteele, Influence of molecular size, polarity and charge on the retention of organic molecules by nanofiltration, *J. Membr. Sci.*, 156 (1999) 29-41.
- [30] W.R. Bowen, J.S. Welfoot, Modelling of membrane nanofiltration—pore size distribution effects, *Chem. Eng. Sci.*, 57 (2002) 1393-1407.
- [31] A.L. Zydney, P. Aimar, M. Meireles, J.M. Pimbley, G. Belfort, Use of the log-normal probability density function to analyze membrane pore size distributions: functional forms and discrepancies, *J. Membr. Sci.*, 91 (1994) 293-298.
- [32] P. Walstra, *Physical Chemistry of Foods*, Marcel Dekker Inc., New York, 2003.
- [33] T.R. Noordman, T.H. Ketelaar, F. Donkers, J.A. Wesselingh, Concentration and desalination of protein solutions by ultrafiltration, *Chem. Eng. Sci.*, 57 (2002) 693-703.
- [34] R. Taylor, R. Krishna, *Multicomponent Mass Transfer*, John Wiley & Sons, Inc, New York, 1993.
- [35] J.A. Wesselingh, R. Krishna, *Mass Transfer in Multicomponent Mixtures*, VSSD, Delft, 2000.
- [36] G.B. van den Berg, I.G. Rácz, C.A. Smolders, Mass transfer coefficients in cross-flow ultrafiltration, *J. Membr. Sci.*, 47 (1989) 25-51.
- [37] X. Liu, T.J.H. Vlught, A. Bardow, Maxwell–Stefan diffusivities in liquid mixtures: Using molecular dynamics for testing model predictions, *Fluid Phase Equilib.*, 301 (2011) 110-117.
- [38] H.A. Kooijman, R. Taylor, Estimation of diffusion coefficients in multicomponent liquid systems, *Industrial & Engineering Chemistry Research*, 30 (1991) 1217-1222.
- [39] J. Newman, Stefan–Maxwell mass transport, *Chem. Eng. Sci.*, 64 (2009) 4796-4803.
- [40] J.A. Wesselingh, How on earth, can I get chemical engineers to do their multi-component mass transfer sums properly?, *J. Membr. Sci.*, 73 (1992) 323-333.

Chapter 2

Modelling of membrane cascades for the purification of oligosaccharides

This chapter has been published as:

Victor Aguirre Montesdeoca, A. Van der Padt, R. M. Boom, and Anja E. M. Janssen (December 2016). “Modelling of membrane cascades for the purification of oligosaccharides”. In: *Journal of Membrane Science* 520 712-722.

ABSTRACT

The aim of this study was to evaluate the potential of NF membrane cascades for continuous oligosaccharide purification. Three different nanofiltration membranes were evaluated, and the best combination in terms of membrane type and process parameters was determined for two commercial oligosaccharide mixtures of fructooligosaccharides (FOS) and galactooligosaccharides (GOS). To represent the cascade mathematically, a dynamic model was built based on film theory and on measurements performed in single-stage conditions. The model predictability was demonstrated with experiments in a membrane cascade set-up.

Considering an initial purity of 84% for FOS and 40.4% for GOS, the model predicted a maximum attainable purity of 94.9% and 46.7% for FOS and GOS respectively. A minimum yield of 90% was used as constraint during the optimisation process, in which the physical limitations of the set up were also taken into account. This paper demonstrates that the trade-off situation between purity and yield can be overcome by using cascade configuration, leading to an efficient separation that cannot be achieved by single-stage membrane systems.

2.1 INTRODUCTION

Oligosaccharides such as fructooligosaccharides (FOS) and galactooligosaccharides (GOS) have recently become quite important as food ingredients, due to their prebiotic effect and apparent anti-cancer functionality [1, 2]. Commercially, they are not found or produced in pure state, but are always combined with small molecular weight sugars that lack this prebiotic function and can add undesirable calories and sweetness to the mixture. As a consequence, separation methods are necessary [3].

Membrane technology has emerged as a convenient alternative for downstream processing because it does not require much energy or many chemicals in operation and is easy to scale up; however, the low level of purity achievable in single-stage filtration is still an important drawback that needs to be overcome [4-6]. In the case of oligosaccharide purification, some work has been done using UF [7] and NF membranes [3, 6, 8-10]. Goulas et al. studied the fractionation of oligosaccharides using NF membranes in a dead end [3] and in a cross flow filtration system [9], in both cases diafiltration processes were necessary to improve purification efficiency. Likewise, Li et al. experimented with many types of diafiltration methods with FOS mixtures as feed [6], and modelled FOS purification using an extended pore model [8]. Kuhn et al. used a two-stage NF system to further increase the efficiency of the process, and to reduce the necessity of diluting the feed stream with water, demonstrating the convenience of recirculating streams and additional filtration stages to achieve a higher purity [10].

Over the last few years, the application of membrane cascades for the purification of complex mixtures has gained interest, because increased purities can be attained and solvent consumption can be lowered. Some work has been completed on the designing of cascades, in which the solvent is recycled after recovery through the use of extra filtration stages [11], or by coupling to an adsorptive solvent recovering unit [12]. It has even been experimentally proven that under some conditions, it is possible to achieve high purity and yield, when using membrane cascades without the addition of extra solvent, through the use of an in situ, solvent-recovery stage [13]. Lightfoot defined an 'ideal cascade' as a configuration of individual membrane units determined by the fact that streams entering mixing points must have the same solvent-free composition; in this way, the benefits from counter-flow are reflected in a higher process efficiency [5]. Figure 2-1 depicts this 'ideal' configuration for a three-stage cascade. Recently, the advantages of NF cascades in continuous oligosaccharide purification were assessed in our group by Patil et al., who purified a FOS mixture using a three-stage cascade,

and compared it with a diafiltration process in terms of yield and purity [14]. Similarly, using the same set up with GOS mixture as feed, we used membranes with different MWCO at each cascade stage to improve the separation process, in what was called an ‘inhomogeneous cascade’[15]. Nevertheless, quantification of the effect of each process parameter on the separation process is still required to estimate the maximum performance of the membrane cascade. This can be achieved by modelling the system considering its physical boundaries and the mass transfer through the membrane.

The aim of this study was to evaluate the potential of NF membrane cascades for oligosaccharide purification. In order to simulate experiments and optimise the process parameters, the cascade system was mathematically represented by a dynamic model. A three-stage cascade configuration, as shown in Figure 2-1, was used to perform experiments and validate the model using commercial mixtures of FOS and GOS as feed.

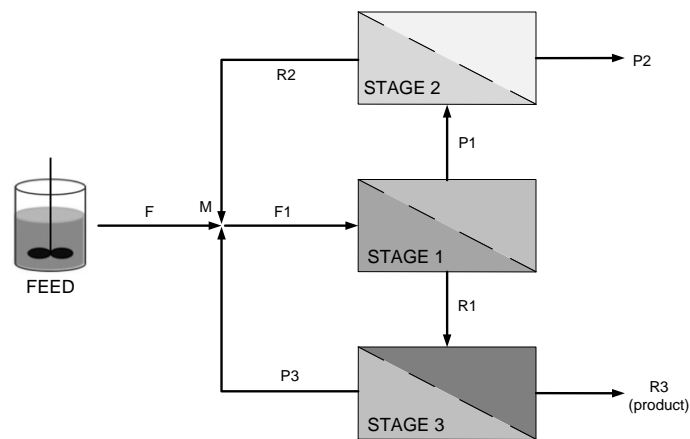


Figure 2-1. Three-stage cascade configuration. (F) is the feed, (P) the permeate and (R) the retentate of each stage of the cascade. (M) stands for the mixing point, at which the recirculating streams and feed join.

2.2 THEORY

2.2.1 Modelling permeate flux

The osmotic pressure model, which is derived from Darcy’s law, can be used to describe the permeate flux, J , in a filtration process (Eq. 2.1). Here, J is expressed in terms of the transmembrane pressure, TMP , osmotic pressure difference $\Delta\pi$, viscosity of the permeate μ_p and membrane resistance, R_m , which should be previously determined using demineralised

water as feed. Darcy's law can be derived from the Navier-Stokes equation [16], and can be used also for non-steady state conditions [17].

$$J = \frac{TMP - \Delta\pi}{\mu_p R_m} \quad (2.1)$$

Eq. 2.1 differs from the expression based on irreversible thermodynamics, in which a reflection coefficient, σ , is included, $J = L_p(TMP - \sigma\Delta\pi)$. Both equations are analogous only when there is total rejection ($R = 1, \sigma = 1$), thus, only water is passing through the membrane. However, it has been shown experimentally that, under not too concentrated conditions, the simplification of considering $\sigma = 1$ is valid, even at low rejections [10]. Kuhn et al. used this assumption in his study on FOS purification[10], and Bowen and Welfoot did the same for nanofiltration of charged solutes[18]; therefore, in this paper $\sigma = 1$ is considered.

The driving force exerted by the applied pressure is diminished by the difference in π at both sides of the membrane. In ideal systems, π is calculated using the Van't Hoff equation, as shown in Eq. 2.2, in which R is the ideal gas constant, T is the temperature and M is the molarity of each species [19]. As shown in Eq. 2.3, $\Delta\pi$ can be expressed considering the concentration of each molecule i present in the solution at the membrane wall $C_{w,i}$ and at the permeate side $C_{p,i}$.

$$\pi_i = M_i RT \quad (2.2)$$

$$\Delta\pi = \sum_{i=1}^n \Delta\pi_i = \sum_{i=1}^n \frac{RT}{MW_i} (C_{w,i} - C_{p,i}) \quad (2.3)$$

Due to concentration polarisation, the concentration of the sugars at the membrane surface is higher than that at the bulk of the retentate. The film model can be used to calculate $C_{w,i}$:

$$C_{w,i} - C_{p,i} = (C_{r,i} - C_{p,i}) \exp\left(\frac{J}{k}\right) \quad (2.4)$$

within which, the mass transfer coefficient k , can be calculated using the Sherwood, Reynolds and Schmidt numbers, as follows:

$$k_i = \frac{Sh_i D_i}{d_h} \quad (2.5)$$

$$Sh_i = A Re^{0.875} Sc_i^{0.25} \text{ with } A = 0.065 \quad (2.6)$$

$$Re = \frac{\rho_r v d_h}{\mu_r} \quad (2.7)$$

$$Sc_i = \frac{\mu_r}{\rho_r D_i} \quad (2.8)$$

To calculate the hydraulic diameter d_h and the cross-flow velocity v in the spiral wound membrane, the procedure presented by Schock and Miquel can be used [20], in which the effect of the retentate spacer is considered, and the parameter A in the Sherwood relation is equal to 0.065 for spiral wound membranes. ρ_r and μ_r stand for the density and the viscosity of the solution at the bulk of the retentate, and D_i is the diffusion coefficient of each molecule.

The viscosity of the permeate and retentate can be calculated according to the model presented by Chirife and Buera. As shown in Eq. 2.9, it expresses the viscosity of the solution as a function of the solution concentration and composition. μ_0 is the viscosity of pure water at a given temperature, E is the average, non-dimensional, free-energy parameter, which depends on the average molecular weight of the mixture, and x_i is the molar fraction of the component i in the solution [21].

$$\mu = \mu_0 \exp(E \sum x_i) \quad (2.9)$$

2.2.2 Modelling membrane retention

The membrane and process conditions determine the retention at each stage of the cascade. The observed retention, R_o , and the real retention, R_r , are defined in Eqs. 2.10 and 2.11, respectively. In principle the membrane retention is a dimensionless parameter. However, it slightly varies depending on the units used to express the concentration of the solutes. From this point forward, all the concentrations are expressed in g/Kg.

$$R_{o,i} = 1 - \frac{C_{p,i}}{C_{r,i}} \quad (2.10)$$

$$R_{r,i} = 1 - \frac{C_{p,i}}{C_{w,i}} \quad (2.11)$$

Whilst it has been observed that R_o decreases as the feed gets more concentrated [9], mainly due to the viscosity increase in the concentration polarisation layer, and a subsequently higher accumulation of solutes at the membrane wall, R_r can be considered an intrinsic property that remains constant under diluted conditions. Likewise, a change in the cross-flow velocity will affect R_o exclusively, and not R_r [22]. Therefore, once the R_r values at different TMP are experimentally determined, the flux of solutes through the membrane can be predicted using Eq. 2.12, in which \dot{m}_i is the mass flux of component i , from the retentate towards the permeate stream.

$$\dot{m}_i = C_{w,i}(1 - R_{r,i})J\rho_r \quad (2.12)$$

To illustrate the separation potential of each membrane, weighted averaged observed retentions (\bar{R}_o) were calculated for two groups of molecules: oligosaccharides (DP3, DP4 and \geq DP5) and mono- & di- saccharides. The mass fractions of each species in the total mixture (Table 2-1) were used as weight for the calculation of \bar{R}_o . Finally, the separation factor (Ψ) was defined as the ratio between these two \bar{R}_o values (Eq. 2.13).

$$\Psi = \frac{\bar{R}_{o,oligo}}{\bar{R}_{o,mono-di}} \quad (2.13)$$

2.2.3 Diffusivities

In order to model the concentration polarisation effect and calculate C_w for each molecule, D values of each molecule must be estimated. They play an important role in the mass transfer in the concentration polarisation layer as can be seen in Eq. 2.5. Considering that sucrose and lactose solutions with concentrations lower than 25% (w/w) behave almost ideally [23, 24], and that FOS and GOS mixtures contain exclusively neutral sugars that resemble sucrose's structure, it can be assumed that the feed solutions used (4% FOS, 10% GOS) are thermodynamically ideal. This assumption is also in accordance with the data on water activity as a function of sugar concentration presented by other researchers, in which, they used sucrose, fructose and apple juice [25, 26]. Therefore, D values can be considered constant and can be estimated using Stokes-Einstein equation (Eq.) for the mono- and disaccharides, since their Stokes radius r_s are widely available in literature. k_B is the Boltzmann constant ($1.38 \cdot 10^{-23} \text{ JK}^{-1}$).

$$D_i = \frac{k_B T}{6\pi\mu_0 r_{s,i}} \quad (2.14)$$

Since for bigger molecules (DP3, DP4 and >DP5) the Stokes radii are uncertain, it is more convenient to use the empirical equation proposed by Sano and Yamamoto, as shown in Eq. 2.15, which is based on the M_w of the solute [24].

$$\frac{T}{D_i \mu_0} = 9.5 \cdot 10^{13} M_w^{1/3} \quad (2.15)$$

2.2.4 Mass balances

Some mass balances are required to represent how the different streams recirculate inside the cascade. Thus, the mass flow in every stream can be determined using the following equations derived from Figure 2-1:

$$F = P_2 + R_3 \quad (2.16)$$

$$F_1 = P_1 + R_1 \quad (2.17)$$

$$R_1 = P_3 + R_3 \quad (2.18)$$

$$P_1 = P_2 + R_2 \quad (2.19)$$

In the case of the component balances, since six different molecule types are quantified, six mass balances are solved for the retentate and six for the permeate stream at each stage. Additionally, six extra mass balances are calculated at point M, at which F, R2 and P3 meet together to form F1. In total, 42 mass balances are required in a three-stage cascade configuration. Taking stage 1 as an example, a retentate mass balance for solute i is presented in Eq. 2.20, in which the re-circulation loop inside the same stage is considered to be part of the retentate (see Figure 2-2), V_r is its total volume, and A_1 is the membrane area in that stage.

$$\frac{d(\rho_r V_r C_{R1,i})}{dt} = F_1 C_{F1,i} - R_1 C_{R1,i} - \dot{m}_i A_1 \quad (2.20)$$

V_r is constant and ρ_r is considered to be constant and equal to water density, so both terms come out of the derivative. Combining this with Eq. 2.12:

$$\frac{dC_{R1,i}}{dt} = \frac{1}{\rho_r V_r} (F_1 C_{F1,i} - R_1 C_{R1,i} - C_{W,i} (1 - R_{r,i}) J \rho_r A_1) \quad (2.21)$$

In the same way, the mass balance of the permeate side is represented as a differential equation in Eq. 2.22, in which V_p is the volume of the permeate channel in the membrane module.

$$\frac{dC_{P1,i}}{dt} = \frac{1}{\rho_p V_p} (C_{w,i}(1 - R_{r,i})J\rho_r A_1 - P_1 C_{P1,i}) \quad (2.22)$$

The mass balance of the mixing point (M in Figure 2-1) is shown in Eq. 2.23, in which V_M is the volume of the mixing point.

$$\frac{d(C_i)}{dt} = \frac{1}{\rho_M V_M} (F C_{F,i} + R_2 C_{R2,i} + P_3 C_{P3,i} - F_1 C_{F1,i}) \quad (2.23)$$

In this study, the effect of concentration on the density of the solutions is not considered, so ρ_r , ρ_p and ρ_{mix} are constants and equal to the water density under experimental conditions.

2.3 MATERIALS AND METHODS

2.3.1 Materials

Experiments were performed using aqueous solutions of commercial mixtures of dietary fibre from chicory oligosaccharide (Fibrelite, Sensus B.V., Roosendaal, The Netherlands) and GOS syrup (Vivinal GOS, FrieslandCampina, Amersfoort, The Netherlands); their composition in terms of dry matter is shown in Table 2-1, in which only molecules with a degree of polymerisation (DP) of three or higher were accounted as oligosaccharides. Pure glucose and sucrose, both with a purity of $\geq 99.5\%$ (Sigma-Aldrich, St. Louis - MO, USA), were used during the viscosity measurements.

Table 2-1. Composition, as weight percentage, %(w/w), and average molecular weight of commercial FOS and GOS mixtures.

Molecules	Fibrelite (FOS)	Vivinal (GOS)
≥DP5	70.5%	6.7%
DP4	7.0%	11.0%
DP3	6.5%	22.7%
DP2	9.2%	35.5%*
Glucose	1.0%	22.1%
Fructose	5.7%	-
Galactose	-	2.0%
\overline{M}_w [g mol ⁻¹]	848	326

*Includes lactose and other DP2 molecules, which were not classified as GOS in this study.

Thin film, NF, spiral wound membranes GE, GH and GK (GE Osmonics, Sterlitech, Kent – WA, United States) (Model 1812C-34D) were used for all experiments. Table 2-2 shows that the MWCOs of the membranes were higher than the actual compounds to be separated. The reason for this is that bigger pores allow more transfer of solutes through the membrane, increasing the purity of the retentate stream. Oligosaccharides that might permeate through the membrane can be recovered in the next stage of the separation (see Figure 2-1).

Table 2-2 Properties of the spiral wound membranes used in this study.

Membrane type	MWCO [Da]	R_m [10 ¹³ m ⁻¹]*	Spacer height [10 ⁻⁴ m]	Total Area [m ²]**
GE	1,000	9.46	8.6	0.32
GH	2,500	11.7	8.6	0.32
GK	3,500	17.7	8.6	0.32

* Estimated with experiments using demineralised water.

**Values for one membrane element.

2.3.2 Experimental set-up

The NF cascade system is composed of three stages that can be used independently or connected to each other. They can be freely linked by connecting the tubing of the permeate and retentate streams, as used for single-stage and three-stage experiments. Each stage of the cascade works with spiral wound membranes. Stage 1 can be adapted to work with two membrane modules connected in series to duplicate the membrane area with respect to Stages 2 and 3. Each stage has its own pressure sensors and valves, flow meters, and heat exchanger to maintain a uniform temperature during the experiments. Additionally, each stage has a recirculation pump that controls the cross flow velocity of the solution with respect to the membrane. The volume of each stage is 2.5 L and the feed tank has a maximum capacity of 10L. The operating pressure range of the system extends from 0 to 30 bar.

Figure 2-2 depicts the single-stage set-up and Figure 2-3 shows the three-stage cascade configuration.

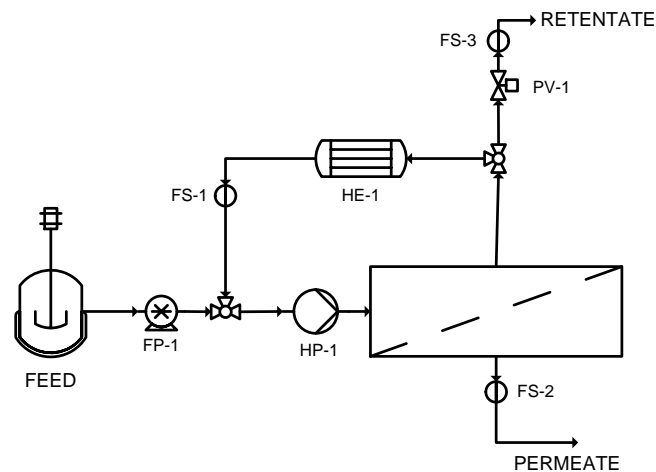


Figure 2-2. Single stage configuration. FP: Feed pump, HP: recirculation pump, PV: Pressure valve, HE: Heat exchanger, FS: Flow meter & Brix meter.

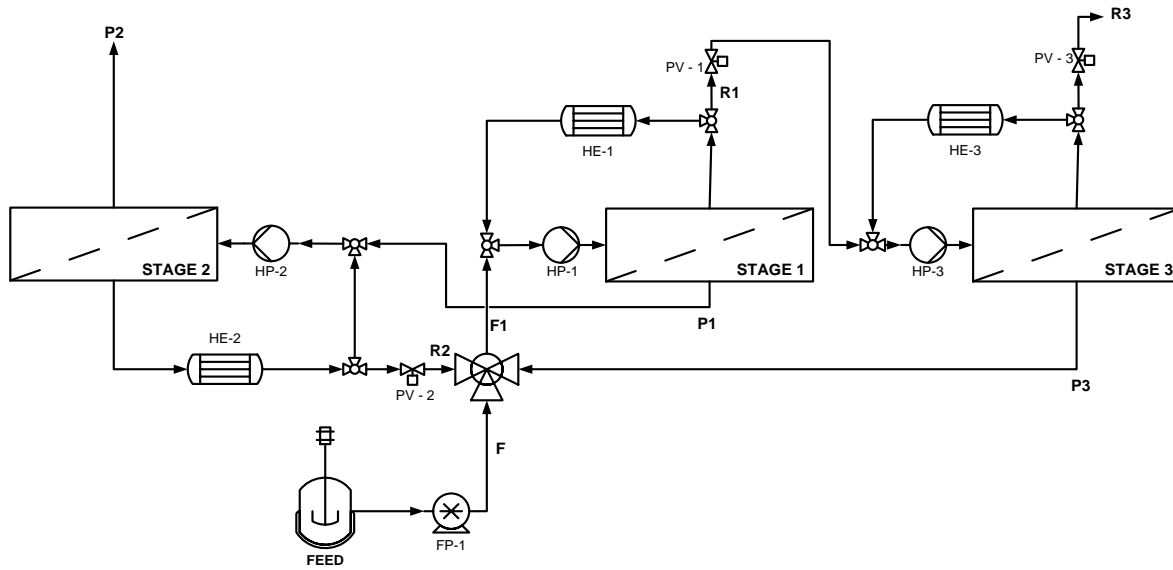


Figure 2-3. Three-stage NF cascade configuration. FP: Feed pump, HP: recirculation pumps, PV: Pressure valves, HE: Heat exchanger

2.3.3 Viscosity measurements

Viscosity measurements at different concentrations of glucose, sucrose, GOS and FOS were performed at 50°C using different shearing rates (0 - 400 s⁻¹). With the data obtained, E values were estimated using Eq. 2.9. To calculate the average molecular weight (\overline{M}_W) of the solutes of the mixture, Eq. 2.24 was used, where W_i is the solvent-free mass fraction of a molecule i . The concentrations used here were 4 – 10%(w/v) for glucose, sucrose and FOS, and in the case of GOS they ranged from 6 – 20%(w/v).

$$\overline{M}_W = \sum_i \frac{M_{W,i}}{W_i} \quad (2.24)$$

2.3.4 Single stage experiments

The resistances of all three types of membranes (GE, GH and GK) were estimated through experiments with demineralised water and using Eq. 2.1 to fit the experimental data. The values obtained are presented in Table 2-2.

Purification experiments were performed using a single-stage configuration (Figure 2-2) and an aqueous solution of 4%(w/v) FOS as feed. This concentration was chosen to avoid the

formation of sugar crystals based on previous tests made in our group [14]. Since Fibrelite is prone to crystallisation at low temperatures, the feed solution was not concentrated during filtration and it was prepared following the procedure specified by Patil et al. [14]. Under steady state conditions, we measured $C_{p,i}$ and $C_{r,i}$ at different TMPs, to calculate $R_{r,i}$ by using Eqs. 2.1 to 2.9 and 2.11. Likewise, for GOS, $R_{r,i}$ values were calculated from data presented by Patil et al. from experiments performed in our group with the same type of membranes, under the same process conditions, and using 10%(w/v) GOS mixtures as feed [15]. In both cases, an iteration procedure was used to solve the system of equations. Furthermore, some additional measurements were taken with different FOS concentrations to evaluate the accuracy of the model. To avoid microbial growth and crystallisation problems, the system was maintained at $50\pm 1^\circ\text{C}$. A cross flow velocity of 0.08 m s^{-1} was used for all the experiments.

2.3.5 Dynamic model and three-stage experiments

When representing the separation process in a three-stage NF cascade, some assumptions were necessary to simplify calculations, namely that:

- Both streams in each stage of the system (retentate and permeate) are well mixed.
- Since we are working at diluted conditions, $R_{r,i}$ values do not change with concentration and reflection coefficients (σ) can be assumed to be 1 during the calculation of J in Eq. 2.1.
- Thermodynamically, the system is expected to behave ideally.
- No fouling takes place in the membranes.

At different TMP, the values of $R_{r,i}$ were slightly different. Thus, for the dynamic model, they were estimated via interpolation depending upon the TMP used in each stage of the cascade.

Considering an initial concentration of zero (pure water) in the cascade, the previously presented calculation procedure (Eqs. 2.1 to 2.9 and 2.12) is repeated for each time interval whilst coupling the mass balances (Eqs. 2.16 to 2.23) to the model. The viscosities of the retentate and permeate streams are also calculated for each time interval, so their effect in the mass transfer is dynamically represented.

To evaluate the accuracy of the dynamic model, three-stage experiments were performed to obtain data of the variables of the system as a function of time and under steady state conditions using the three-stage configuration presented in Figure 2-3. FOS and GOS solutions were used

as feed and many process parameter values were randomly modified between experiments. The temperature of $50\pm 1^\circ\text{C}$ and the cross-flow velocity of 0.08m s^{-1} were the same for all experiments.

2.3.6 Analytical methods

The collected samples were analysed using High Performance Liquid Chromatography (HPLC). For FOS measurements, the column Shodex KS-802 8.0 x 300 (mm) ID x Length + Guard column Shodex KS-G was used at 50°C . For the GOS analysis, the column Rezex RSO-Oligosaccharide 10 x 200 (mm) ID x Length + Guard column Rezex RSO-Guard was used at 80°C . In both cases, the solvent was MilliQ water (flow rate= $0.3\text{mL}/\text{min}$) and detection was achieved by measuring the refractive index with an RI detector (Shodex R9-101).

Viscosity measurements were performed at 50°C in a rheometer MCR 301 (Anton Paar, Graz, Austria). The measuring system was DG26.7 with the following dimensions: diameter 26.667 mm, diameter int. 24.641 mm, length 40,000 mm.

2.3.7 Computational analysis

The Runge-Kutta method was used for the resolution of the system of differential equations summarized in Eqs. 2.21, 2.22 and 2.23. In the optimisation section, Matlab function 'Fmincon' was used to find the optimum set of parameters values that determines the highest purity in R3 stream by using the 'sqp' algorithm. This function finds a minimum or a maximum of a nonlinear function of several variables considering system bounds and constraints.

2.4 RESULTS AND DISCUSSION

2.4.1 Viscosity measurements

After the viscosity measurements, an expected linear relation between the estimated E parameters and the \overline{Mw} of the solutes of the mixture was obtained as described by Chirife and Buera (Figure 2-4) [21]. This linear relation allows us to calculate E and, consequently, the viscosity at 50°C of any sugar solutions with a known concentration and composition by using Eq. 2.9. In this way, precise viscosity values of retentate and permeate streams can be estimated at each time interval. Additionally, it has been verified that oligosaccharides solutions present Newtonian behaviour, as described in [27], thus Eq. 2.1 is useful, as its validity is restricted to incompressible Newtonian flow [28].

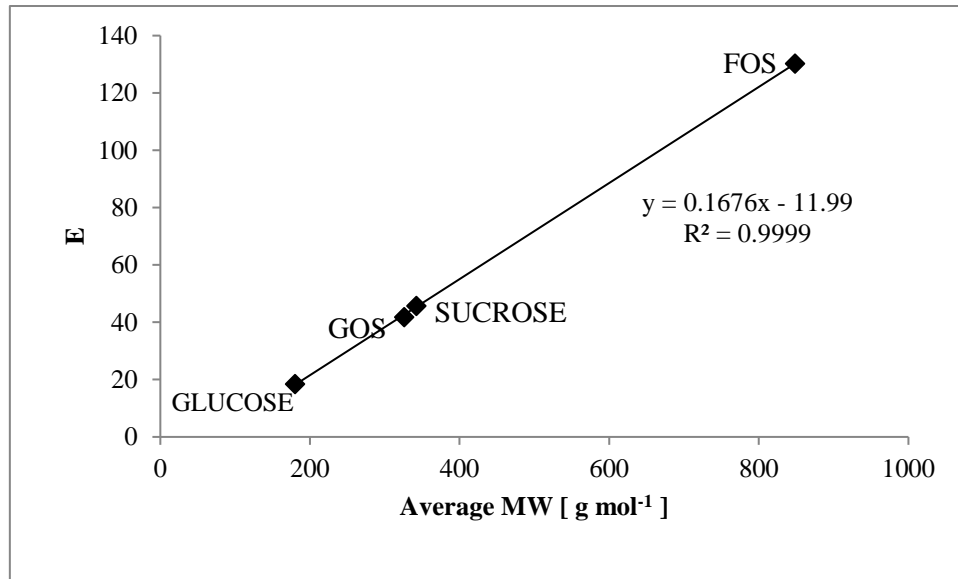


Figure 2-4. Linear dependency of E values with respect to \overline{M}_w . The measurements considered in this calculation were at a shearing rate of 100 s^{-1} and 50°C .

2.4.2 Single stage experiments

By measuring the steady state concentration of each molecule at different pressures, at both sides of the membrane, the permeate flux can be estimated using Eqs. 2.1 to 2.9. Figure 2-5 shows the accuracy of the permeate flux estimations with respect to the experimentally obtained values. The calculated diffusion coefficients, which are included in these calculations, are listed in Table 2-3.

Table 2-3. Data of the diffusivities of the species in the oligosaccharide mixtures

	Fructose	Galactose	Glucose	Sucrose	Lactose	DP3	DP4	\geq DP5 (FOS)	\geq DP5 (GOS)
MW [g mol ⁻¹]	180	180	180	342	342	504	666	2350	896
r_s [10^{-10} m]	3.55	3.60	3.60	4.40	4.50				
D [10^{-10} m ² /s]	11.10	10.90	10.90	8.96	8.76	7.13	6.50	4.27	5.89

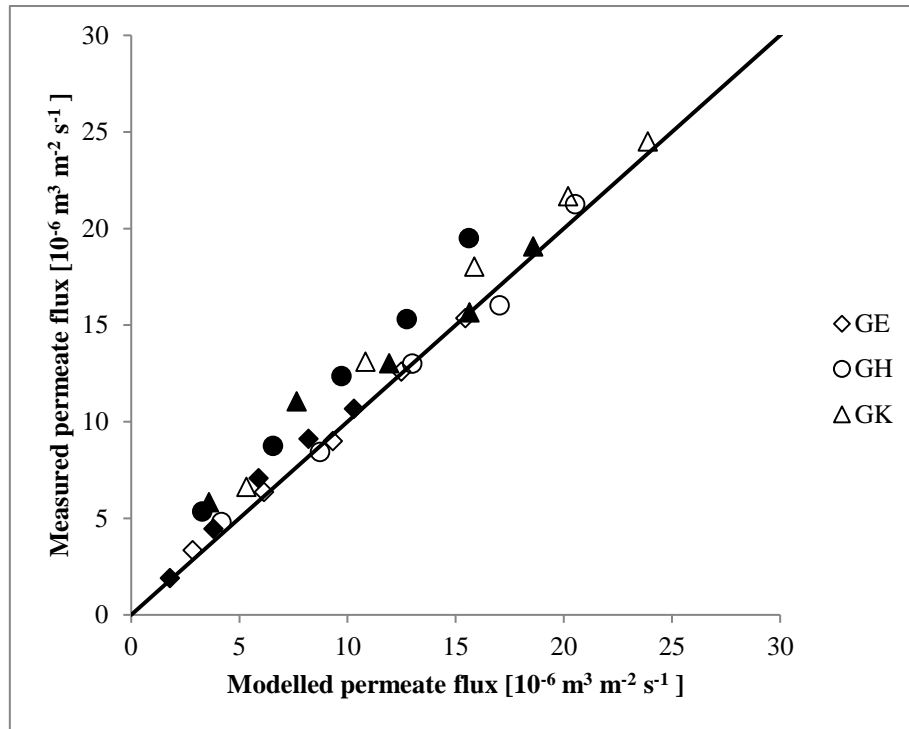


Figure 2-5. Measured permeate flux vs. Modelled permeate flux (Eqs. 2.1 to 2.9) using solutions of 4%(w/v) FOS (open symbols) and 10%(w/v) GOS (closed symbols) for all three membranes. The data for GOS was obtained from Patil et al.[15]. The continuous line represents the point where the prediction and the measurement are similar.

The model very slightly underestimates the permeate flux, probably, because we consider $\sigma = 1$ in Eq. 2.1, obtaining a too high effect of $\Delta\pi$ in the flux, as explained in Section 2.2.1. For this reason, it is also observed that the predictions for the GE membrane, the one with the lowest MWCO, are more accurate than those for the other membranes. Since GE membrane has the highest retentions, the effect of using $\sigma = 1$ is less important. In general, the predictions of the model are satisfactory, considering that the values of all the parameters, other than R_m , are independently calculated or estimated with Eqs. 2.2 to 2.9. If the data presented in Figure 2-5 was fitted, using the A parameter from the Sherwood relation (Eq. 2.6) as a free parameter, the obtained value for A would be 0.081, which is quite close to the original 0.065, indicating that the model has a good level of accuracy. Furthermore, with the data collected from these experiments, R_r values were calculated for all membranes at different pressures. The complete set of R_r values can be found in the Appendices Section (Table 2-A.1).

The model was also evaluated with experiments at different FOS concentrations, at which the flux was modelled using the previously collected R_r values at 4% FOS. In this case, only the

concentration at the retentate was required as an input for the model, and depending on the type of membrane and pressure, the corresponding R_r was selected for the computation. As shown in Figure 2-6, the achieved predictability was reasonably good. The curves flatten as TMP increases especially at higher concentrations since the higher amount of sugars retained in the membrane determine a higher osmotic pressure which affects the flux (see Eq. 2.1). Additionally, the local viscosity increases with higher concentrations of solutes, reducing the mass transfer in the boundary layer and increasing the concentration polarisation effect.

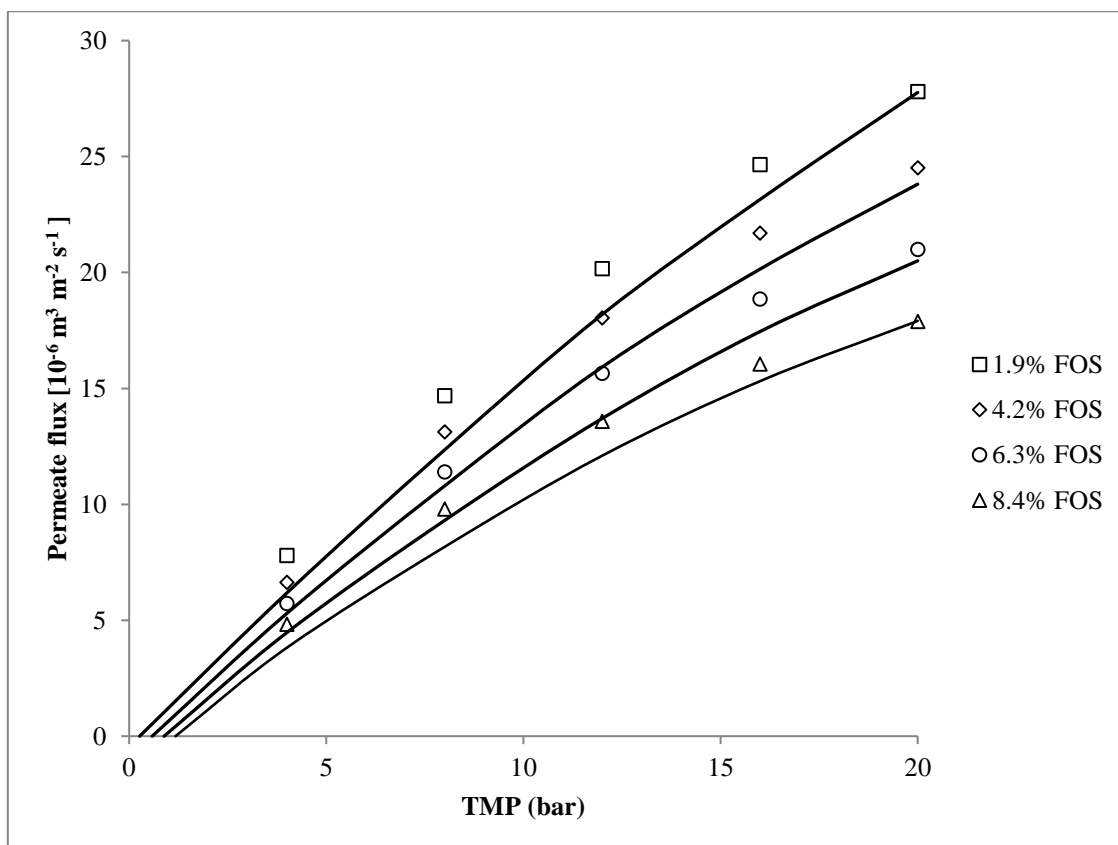


Figure 2-6. Modelled and measured steady state permeate fluxes as a function of TMP for different feed concentrations of FOS mixture using GK membrane. The continuous line represents the modelled flux (Eqs. 2.1 to 2.9 and 2.11) using the previously estimated R_r values. FOS concentrations are given in % (w/v).

In Figure 2-7, the separation factors calculated with data from single-stage experiments (Eq. 2.13) are presented as a function of stage cut for all three membranes. GK membrane is clearly the best option for FOS, because a higher ψ is obtained at any stage cut; whilst for GOS, ψ is almost similar for all the membranes. A higher separation potential for FOS can be observed due to a larger difference in size and molecular weight between the oligosaccharides and small sugars (mono and disaccharides).

It is also evident that at low TMP (stage cut < 0.1), ψ is higher. The reason for this is that concentration polarisation is more pronounced for larger solutes (lower diffusivity); therefore, at higher TMP, the observed retention of larger solutes will decrease faster than the observed retention of smaller solutes, leading to a decrease of ψ .

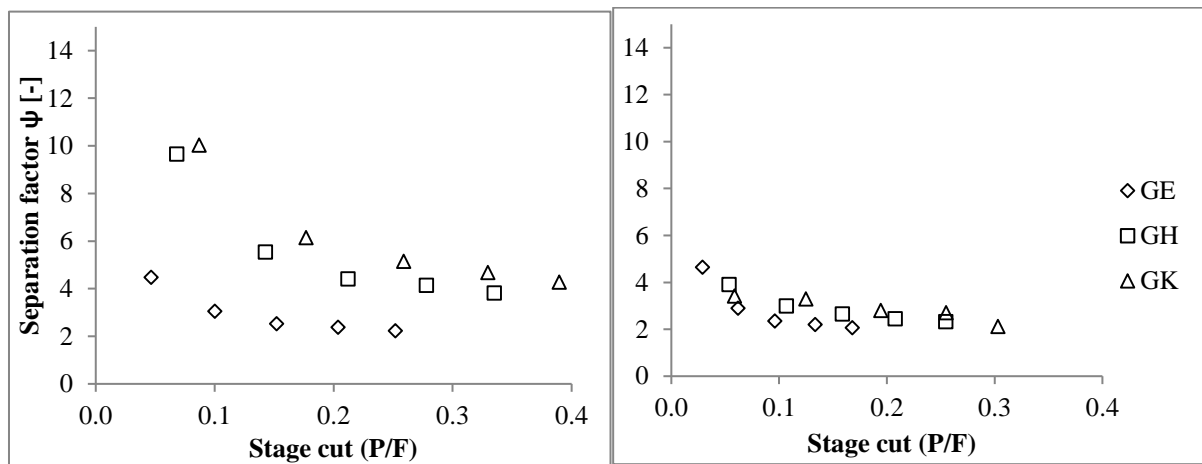


Figure 2-7. Separation factor as a function of stage cut for FOS (left) and GOS (right).

It is important to realise that ψ only considers the equilibrium concentrations in the permeate and retentate, but does not take into account the amount of permeate flow. Thus, in terms of ψ , working at low pressures is convenient, but if the permeate is too low, the composition of the retentate (product stream) will remain unaffected. Additionally, ψ values from Figure 2-7 are a good reference only for considerations in Stages 1 and 3; these results could not be extrapolated to Stage 2, since the mixture composition was quite different.

2.4.3 3-stage experiments

Experiments were performed in a three-stage nanofiltration cascade set-up using the configuration illustrated in Figure 2-3. The process conditions for each experiment are presented in Table 2-4. The sampling and the modelling was performed as a function of time.

Table 2-4. Process conditions during validation experiments

#	Feed	Membranes arrangement*	Feed flow [Kg h ⁻¹]	Feed conc. [%]	TMP in Stages 1, 2 and 3 [bar]
1	FOS	GK ₂ -GH-GE	30	4.5	8, 4, 8
2				4.1	8, 8, 8
3					8, 12, 8
4		GK-GH-GE		4.8	8, 8, 16
5					8, 8, 12
6					12, 8, 8
7					16, 8, 8
8					12, 8, 8
9		GK-GK-GE		30	2.8
10	GOS	GK ₂ -GK-GH	37	11.2	8, 9, 20
11			30		8, 4, 20
12					12, 4, 20
13					12, 6, 20
14					12, 9, 20

* To represent the arrangement of the membranes in the cascade the position of each name of the membrane (1st, 2nd or 3rd) represents the corresponding stage number in the cascade. Subscript 2 in Stage 1 indicates that two membranes elements were used in that stage (membrane area=0.64m²).

A comparison between the measured- and modelled molecule concentrations in the R3 stream is shown in Figure 2-8 and Figure 2-9. An acceptable agreement was obtained at all the time intervals, implying that the assumptions made whilst developing the dynamic model did not significantly affect its predictability.

The time to achieve steady state was longer for Experiment 2 (Figure 2-8) than for Experiment 10 (Figure 2-9), mainly due to the lower feed flow in Experiment 2. Since both outgoing streams P2 and R3 are recirculated to the feed tank, the faster this recirculation, the faster the system will stabilise and reach steady state. Additionally, TMP values used in each stage were higher in Experiment 10, this also determines higher permeate flows that make the system achieve steady state in less time.

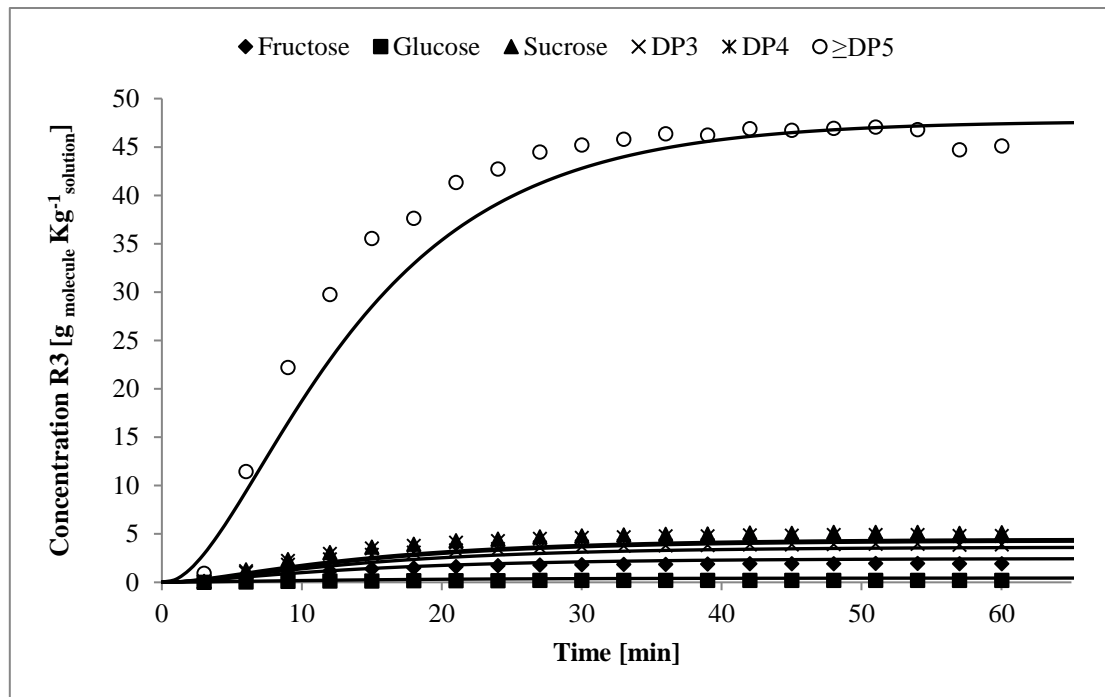


Figure 2-8. Validation experiment 2. Concentration of molecules in R3 stream as a function of time. Lines represent the modelled concentrations.

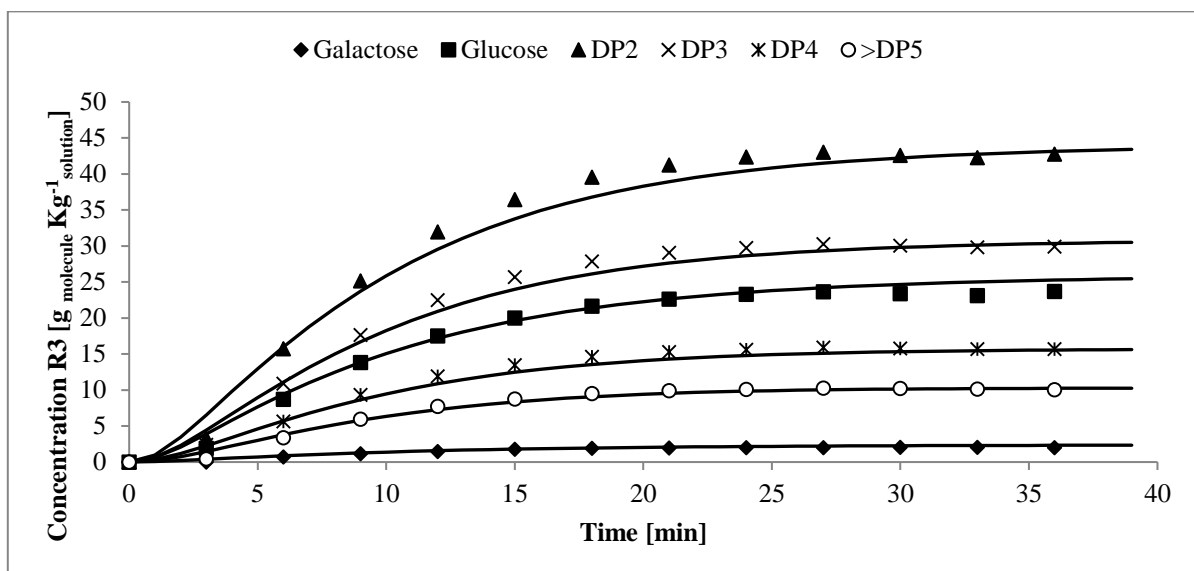


Figure 2-9. Validation experiment 10. Concentration of molecules in R3 stream as a function of time. Lines represent the modelled concentrations.

The steady state flow measurements of the outgoing streams of the cascade P2 and R3 were compared with the values predicted by the model. Figure 2-10 shows good agreement between these set of values, meaning that the model adequately describes the effect of the osmotic pressure and viscosity in the permeate flux calculation. Additionally, it is evident that, regardless of the process conditions inside the cascade, the flow rate in P2 will determine the flow rate in R3 since the feed is constant and there is no internal accumulation (see Eq. 2.16).

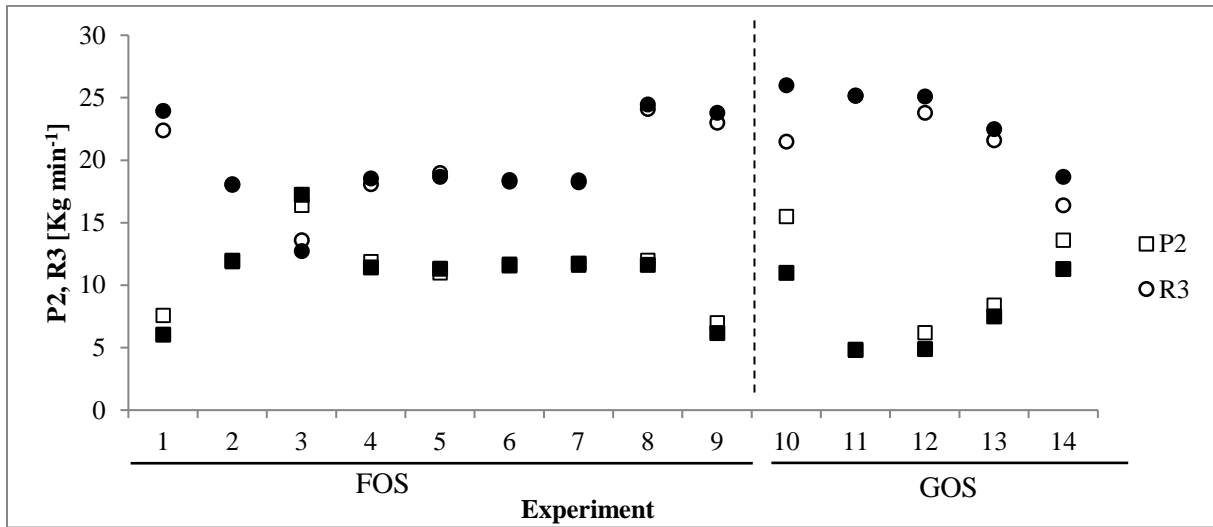


Figure 2-10. Flow rates for P2 and R3 stream during validation experiments. Open symbols represent the experimental values and closed symbols represent the outcome of the model. Values correspond to steady state conditions.

Likewise, the output of the model was compared with measurements at steady state, using yield and purity as variables of interest. The yield is defined as: ‘the percentage of oligosaccharides of the feed solution that are recovered in the product stream R3 at steady state conditions’. Eq. 2.25 was used to calculate the yield considering the concentrations and the flow in streams F and P2, whilst Eq. 2.26 was used to calculate purity at the steady state of each experiment. For the purity calculation, only molecules with a DP 3, or higher, were included as oligosaccharides.

$$Yield = \left[1 - \frac{(C_{DP3} + C_{DP4} + C_{\geq DP5})_{P2} \cdot P2}{(C_{DP3} + C_{DP4} + C_{\geq DP5})_F \cdot F} \right] \cdot 100 \quad (2.25)$$

$$Purity = \frac{(C_{DP3} + C_{DP4} + C_{\geq DP5})_{R3}}{\sum_{DP1}^{\geq DP5} C_{R3}} \cdot 100 \quad (2.26)$$

Figure 2-11 shows some trade-off situations between yield and purity, in which a higher purity can be achieved to the expense of an inherent yield reduction. For instance, Experiments 12, 13 and 14 reflect that increasing the pressure in Stage 2 decreases the yield and slightly increases the oligosaccharide purity in R3. The same observation can be made with Experiments 2 and 3.

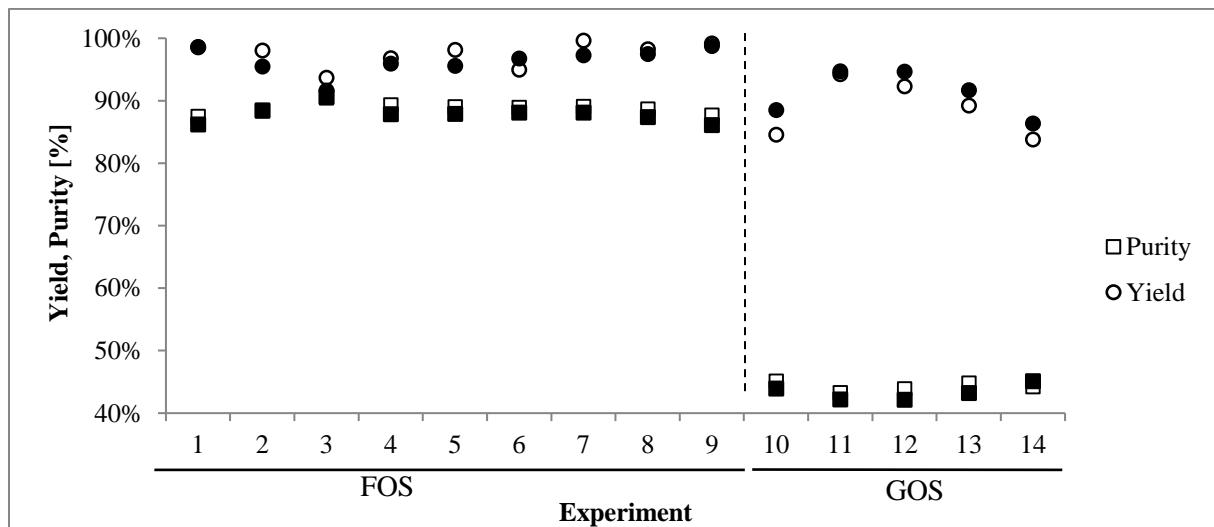


Figure 2-11. Yield and purity during validation experiments in the nanofiltration cascade. Open symbols represent the experimental values and closed symbols represent the outcome of the model. All values correspond to steady state conditions.

2.4.4 Optimisation

Overall, the model is in good accordance with the measurements and predicts the behaviour of the cascade under different conditions. Therefore, it was used for the identification of the set of process parameters that yield the highest purity in R3 stream considering the physical constraints of the set-up.

It was decided to optimise two parameters that were considered more important, based on their effect on the model outcome during simulations: membrane area in Stage 1 and pressure in Stage 2. The other process parameters were previously selected based on the results from Figure 2-7, and after trialling some simulations, in which many combinations of parameters were utilised. As in the real set-up, the membrane areas of Stages 2 and 3 were fixed (0.32m²), and a constant feed flow of 0.5 Kg/min was used in the calculations.

Purity was selected as the variable to maximise, whilst some boundaries and constraints were also established. Table 2-5 shows the optimal process conditions and specifies the set boundaries that represent the physical limits of the system. To deal with the trade-off between yield and purity, a constraint of a minimum yield of 90% was included in the optimisation procedure.

Table 2-5. Optimised process parameters

Feed solution	FOS mixture	GOS mixture	Boundaries
Feed Concentration (% w/w)	4%	10%	
Membrane Area in Stage 1 (m ²)	0.96*	0.96*	(0.32 - 0.96)
Pressure in Stage 1	GK 8 bar	GH 20 bar	
Pressure in Stage 2	GH 17.5 bar*	GH 20 bar*	(4 - 20)
Pressure in Stage 3	GK 20 bar	GH 20 bar	
Feed Purity	84%	40.4%	
R3 Purity	95.0%	46.7%	
R3 Yield **	90%	91.9%	
R3 Total concentration	17.9%	14.9%	

* Optimised Parameters.

** The minimum yield constraint was 90%.

Figure 2-12 depicts the resulting purity and yield in steady state conditions as a function of the pressure in Stage 2. It is shown that the compromise between purity and yield occurs regardless of the composition of the solution and the membrane area. As pressure in Stage 2 increases, the purity in R3 stream goes up and the yield decreases. This remains until the point where the pressure is such that all the feed of Stage 2 ends up going to the permeate stream, in our case, this happens at 10 bars, when the membrane area is 0.32m². As consequence, R2 stream becomes zero, so further pressure increments produce no effects in the system. Although purity values may seem acceptable under these conditions, yields are low; this situation is similar in applying only two stages instead of three. As membrane area is increased in Stage 1, the system

can work at higher pressures in Stage 2 before reaching this 'R2=0' situation, where P1=P2 (see Figure 2-1).

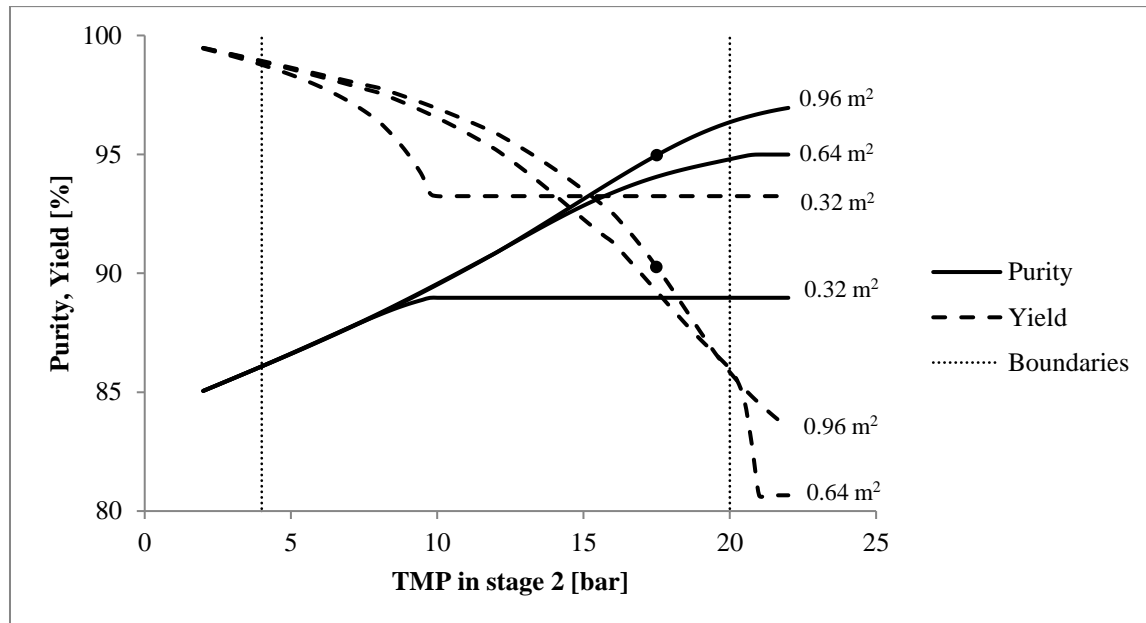


Figure 2-12. Purity and yield as a function of pressure in Stage 2. Results belong to the output of the simulation for different membrane areas in Stage 1, using FOS as feed. The process parameters utilised in the simulation are those found during the optimisation procedure, (●) symbolises the optimal conditions, as presented in Table 2-5.

Figure 2-13 shows the dependency of purity, yield and total concentration in R3 on the membrane area in Stage 1. At optimum conditions, whilst the purity curve flattens at larger membrane areas, the total concentration in R3 rises steadily, and even more importantly, yield also goes up, which means that the trade-off between purity and yield does not take place. A larger membrane area in Stage 1 allows more water and small molecules to be removed in Stage 1, enriching the stream R1 without decreasing the yield of the system, since the excess of FOS molecules in Stage 2 is recycled back to the mixing point of the cascade. As consequence, not only purity and yield increase, but the total concentration in R3 also increases, which makes the process more convenient, since less water will have to be removed from the final product. Overcoming the trade-off between purity and yield is only possible in a cascaded process; it cannot be achieved when using conventional (single stage) filtration systems. Additionally, Figure 2-13 shows that, under the chosen conditions, the membrane area, at which the 'R2=0' situation is overcome, is approximately 0.55m^2 ; therefore, at lower membrane areas, all the feed going to Stage 2 ends up in the P2 stream.

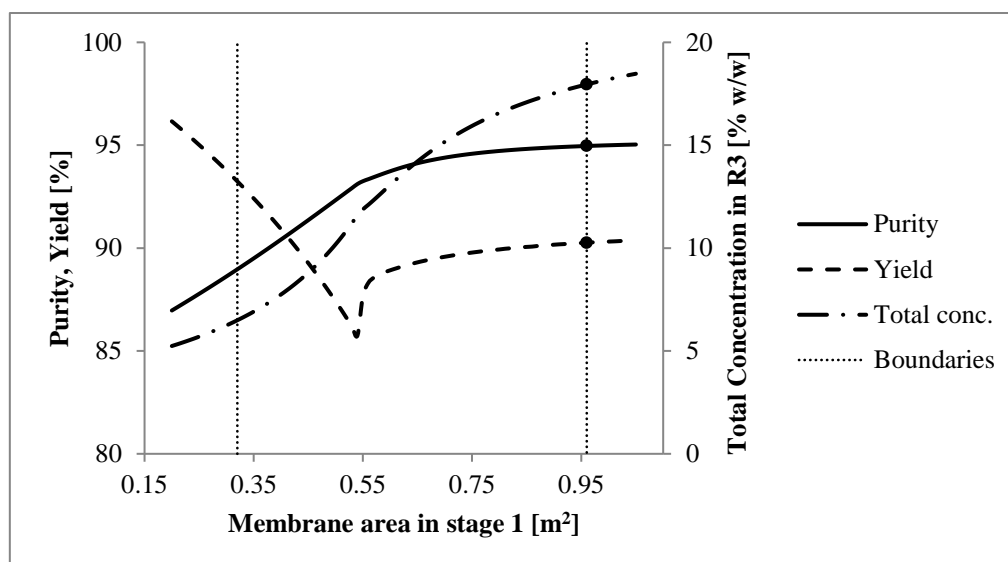


Figure 2-13. Effect of membrane area on purity, yield and total concentration in R3 using the FOS mixture as feed. The boundaries for the membrane area in Stage 1 extend from one membrane element (0.32m^2) to three membrane elements (0.96m^2). The rest of the process parameters are detailed in Table 2-5. (●) indicates the variable values at the optimal membrane area.

In the case of GOS mixtures, the behaviour of the system is similar to FOS. The main difference is that, due to the smaller size of GOS molecules, the separation process is less effective. Figures on the effects on purity using the GOS mixture as feed can be found in the Appendices (Figure A.1 and A.2).

2.5 CONCLUSIONS

We showed that membranes cascades are a viable option for a continuous separation of complex liquid systems such as oligosaccharide mixtures. No addition of water was required, which represents an advantage over diafiltration processes. It was shown that the trade-off between purity and yield can be overcome by increasing the membrane area in the Stage 1 in the cascade. Under these conditions, the total concentration in the product stream also increases, making the process more efficient.

With membrane cascades, the separation potential for FOS is higher than for GOS. The reason for this is the higher molecular weight of the oligosaccharides in the FOS mixture. After our optimisation procedure, the highest achievable oligosaccharide purity was 46.7 %, starting from a 40.4% GOS mixture. For FOS, the maximum purity was 94.9%, starting with a 84% FOS

mixture. In both cases, yields were higher than 90%. Such purification values might not seem too impressive at first glance, but considering that this is a continuous process that does not require the addition of water, such percentages become undoubtedly appealing.

It has been shown that the dynamic model used in this study produces acceptable predictions, in terms of flux and species concentrations. For a good prediction, it is critical to consider the effect of concentration polarisation and the viscosity changes of the solution in every stream, as a function of time. The applicability of this model can be extended to the design of more complex filtration cascades and the development of online control systems.

ACKNOWLEDGEMENTS

This work was carried out as part of a project of the Institute for Sustainable Process Technology, The Netherlands: project number FO-00-02 and CM-20-05.

APPENDIX A

Table 2-A.1. Calculated R_{ri} coefficients for each component i of the commercial mixtures of FOS and GOS.

	TMP	FOS						GOS*					
		Fructose	Glucose	Sucrose	DP3	DP4	DP5	Galactose	Glucose	DP2	DP3	DP4	DP5
GE	4	0.09	0.19	0.31	0.60	0.77	0.97	0.15	0.07	0.15	0.41	0.65	0.84
	8	0.18	0.30	0.50	0.76	0.88	0.99	0.19	0.11	0.36	0.63	0.79	0.91
	12	0.27	0.40	0.61	0.83	0.92	0.99	0.20	0.21	0.49	0.73	0.86	0.94
	16	0.32	0.44	0.67	0.86	0.93	0.99	0.25	0.25	0.57	0.78	0.89	0.95
	20	0.39	0.53	0.73	0.89	0.95	1.00	0.27	0.31	0.63	0.82	0.91	0.96
GH	4	0.02	0.07	0.16	0.38	0.59	0.93	0.08	0.04	0.12	0.24	0.37	0.54
	8	0.07	0.17	0.31	0.57	0.75	0.97	0.11	0.09	0.25	0.44	0.58	0.71
	12	0.14	0.24	0.43	0.69	0.82	0.98	0.17	0.14	0.37	0.58	0.71	0.82
	16	0.18	0.30	0.49	0.73	0.85	0.98	0.17	0.19	0.46	0.67	0.78	0.87
	20	0.24	0.36	0.56	0.78	0.88	0.99	0.20	0.25	0.53	0.73	0.83	0.90
GK	4	0.02	0.07	0.15	0.37	0.57	0.92	0.17	0.08	0.16	0.31	0.49	0.72
	8	0.08	0.15	0.29	0.58	0.72	0.96	0.14	0.13	0.26	0.52	0.65	0.83
	12	0.14	0.26	0.39	0.65	0.80	0.97	0.23	0.15	0.35	0.57	0.72	0.85
	16	0.18	0.30	0.47	0.74	0.85	0.98	0.30	0.20	0.43	0.68	0.78	0.88
	20	0.24	0.36	0.54	0.77	0.87	0.99	0.28	0.26	0.57	0.73	0.81	0.90

* Calculated with data from Patil et al.[15].

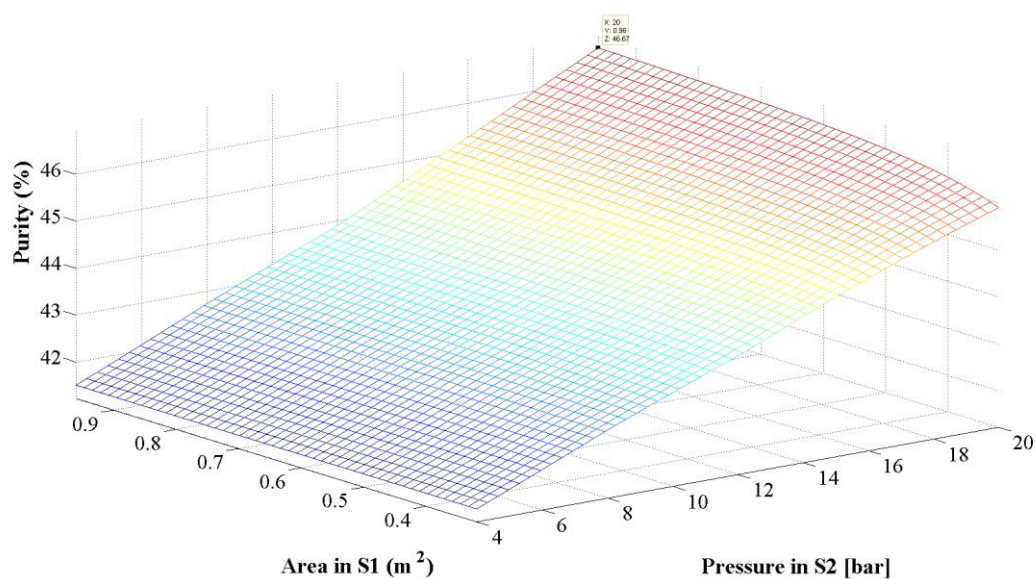


Figure 2-A.1. Purity as a function of area in Stage 1 and pressure in Stage 2 using the GOS mixture as feed. The marker in the top of the surface response represents the optimal point (Table 2-5).

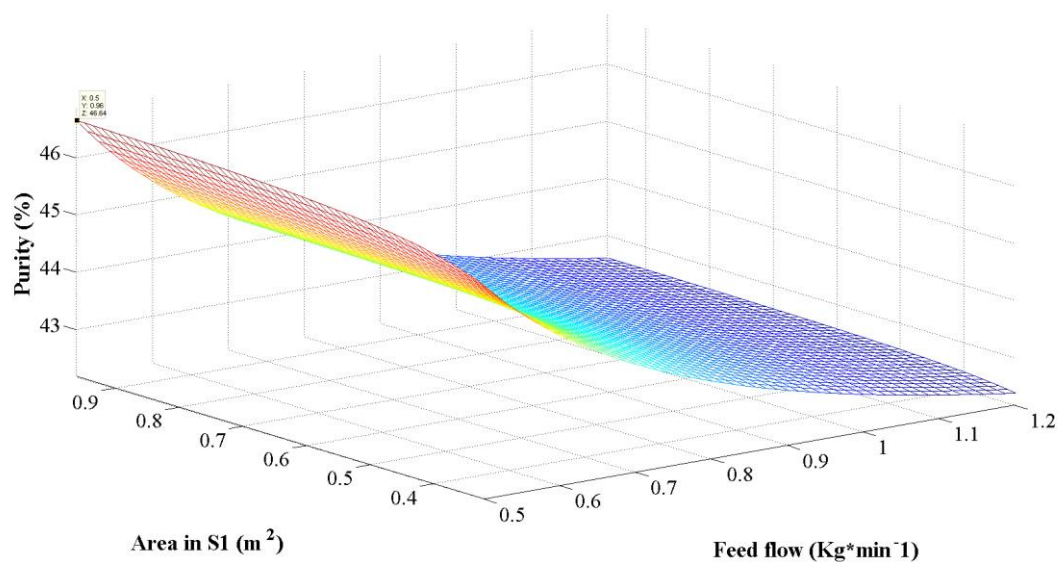


Figure 2-A.2. Purity as a function of area in Stage 1 and feed flow using the GOS mixture as feed. The marker in the top of the surface response represents the optimal point (Table 2-5).

NOMENCLATURE

A	membrane area [m^2]
C	solute concentration [g Kg^{-1}]
D	diffusion coefficient [m s^{-2}]
d_h	hydraulic diameter
E	Parameter related to the free energy of activation for viscous flow in Eq. 2.9[]
$F_{\#}$	feed flow at stage # [Kg min^{-1}]
J	permeate flux [$\text{m}^3 \text{m}^{-2} \text{s}^{-1}$]
k	mass transfer coefficient [m s^{-1}]
k_B	Boltzmann constant [J K^{-1}]
\dot{m}_i	Mass migration rate of component i [$\text{g min}^{-1} \text{m}^{-2}$]
M_w	molecular weight [g mol^{-1}]
$\overline{M_w}$	average molecular weight of the solutes of the mixture [g mol^{-1}]
M_i	concentration of component i [mol L^{-1}]
$P_{\#}$	permeate flow at stage # [Kg min^{-1}]
R	ideal gas constant [$\text{L bar K}^{-1} \text{mol}^{-1}$]
Re	Reynolds number
R_m	membrane resistance [m^{-1}]
R_o	observed rejection
R_r	real rejection
r_s	Stokes radius
$R_{\#}$	retentate flow at stage # [Kg min^{-1}]
Sc	Schmidt number []
Sh	Sherwood number []
T	temperature [K]
TMP	Transmembrane pressure [bar]
v	cross flow velocity [m s^{-1}]
V	Volume of the solution [m^3]
W_i	solvent free mass fraction of component i

X mole fraction []

Greek letters

μ dynamic Viscosity [Pa.s]

μ_{rel} relative viscosity []

π osmotic pressure [bar]

ρ density; assumed to be the same as the water density at 50° C [988 Kg m⁻³]

Ψ separation factor []

Subscripts

1,2,3 number of filtration stage

p permeate

r retentate

w membrane wall

i denote mixture components

M mixing point

mono – di mono and di-saccharides

oligo oligosaccharides

REFERENCES

- [1] G.R. Gibson, M.B. Roberfroid, Dietary modulation of the human colonic microbiota: introducing the concept of prebiotics, *J. Nutr.*, 125 (1995) 1401-1412.
- [2] C.E. Rycroft, M.R. Jones, G.R. Gibson, R.A. Rastall, A comparative in vitro evaluation of the fermentation properties of prebiotic oligosaccharides, *J. Appl. Microbiol.*, 91 (2001) 878-887.
- [3] A.K. Goulas, A.S. Grandison, R.A. Rastall, Fractionation of oligosaccharides by nanofiltration, *J. Sci. Food Agric.*, 83 (2003) 675-680.
- [4] A. Caus, L. Braeken, K. Boussu, B. Van der Bruggen, The use of integrated countercurrent nanofiltration cascades for advanced separations, *J. Chem. Technol. Biotechnol.*, 84 (2009) 391-398.
- [5] E. Lightfoot, Can membrane cascades replace chromatography? Adapting binary ideal cascade theory of systems of two solutes in a single solvent, *Sep. Sci. Technol.*, 40 (2005) 739-756.
- [6] W. Li, J. Li, T. Chen, C. Chen, Study on nanofiltration for purifying fructo-oligosaccharides: I. Operation modes, *J. Membr. Sci.*, 245 (2004) 123-129.
- [7] D. Nabarlantz, C. Torras, R. Garcia-Valls, D. Montané, Purification of xylo-oligosaccharides from almond shells by ultrafiltration, *Sep. Purif. Technol.*, 53 (2007) 235-243.
- [8] W. Li, J. Li, T. Chen, Z. Zhao, C. Chen, Study on nanofiltration for purifying fructo-oligosaccharides: II. Extended pore model, *J. Membr. Sci.*, 258 (2005) 8-15.
- [9] A.K. Goulas, P.G. Kapasakalidis, H.R. Sinclair, R.A. Rastall, A.S. Grandison, Purification of oligosaccharides by nanofiltration, *J. Membr. Sci.*, 209 (2002) 321-335.
- [10] R.C. Kuhn, F. Mauger Filho, V. Silva, L. Palacio, A. Hernández, P. Prádanos, Mass transfer and transport during purification of fructooligosaccharides by nanofiltration, *J. Membr. Sci.*, 365 (2010) 356-365.
- [11] M. Schaeperstoens, C. Didaskalou, J.F. Kim, A.G. Livingston, G. Szekely, Solvent recycle with imperfect membranes: A semi-continuous workaround for diafiltration, *J. Membr. Sci.*, 514 (2016) 646-658.
- [12] J.F. Kim, G. Szekely, I.B. Valtcheva, A.G. Livingston, Increasing the sustainability of membrane processes through cascade approach and solvent recovery-pharmaceutical purification case study, *Green Chemistry*, 16 (2014) 133-145.
- [13] J.F. Kim, G. Szekely, M. Schaeperstoens, I.B. Valtcheva, M.F. Jimenez-Solomon, A.G. Livingston, In Situ Solvent Recovery by Organic Solvent Nanofiltration, *ACS Sustainable Chemistry & Engineering*, 2 (2014) 2371-2379.
- [14] N.V. Patil, X. Feng, J.J.W. Sewalt, R.M. Boom, A.E.M. Janssen, Separation of an inulin mixture using cascaded nanofiltration, *Sep. Purif. Technol.*, 146 (2015) 261-267.

- [15] N.V. Patil, T. Schotel, C.V. Rodríguez Gómez, V. Aguirre Montesdeoca, J.J.W. Sewalt, A.E.M. Janssen, R.M. Boom, Continuous purification of galacto-oligosaccharide mixtures by using cascaded membrane filtration, *Journal of Chemical Technology & Biotechnology*, 91 (2016) 1478-1484.
- [16] S. Whitaker, Flow in porous media I: A theoretical derivation of Darcy's law, *Transport in Porous Media*, 1 (1986) 3-25.
- [17] S.P. Neuman, Theoretical derivation of Darcy's law, *Acta Mechanica*, 25 (1977) 153-170.
- [18] W.R. Bowen, J.S. Welfoot, Modelling the performance of membrane nanofiltration—critical assessment and model development, *Chem. Eng. Sci.*, 57 (2002) 1121-1137.
- [19] M. Mulder, Transport in Membranes, in: *Basic Principles of Membrane Technology*, Springer Netherlands, 1996, pp. 210-279.
- [20] G. Schock, A. Miquel, Mass transfer and pressure loss in spiral wound modules, *Desalination*, 64 (1987) 339-352.
- [21] J. Chirife, M.P. Buera, A simple model for predicting the viscosity of sugar and oligosaccharide solutions, *J. Food Eng.*, 33 (1997) 221-226.
- [22] S.-I. Nakao, S. Kimura, ANALYSIS OF SOLUTES REJECTION IN ULTRAFILTRATION, *J. Chem. Eng. Jpn.*, 14 (1981) 32-37.
- [23] P. Walstra, *Physical Chemistry of Foods*, Marcel Dekker Inc., New York, 2003.
- [24] Y. Sano, S. Yamamoto, Mutual Diffusion Coefficient of Aqueous Sugar Solutions, *J. Chem. Eng. Jpn.*, 26 (1993) 633-636.
- [25] O. Ferreira, E.A. Brignole, E.A. Macedo, Phase equilibria in sugar solutions using the A-UNIFAC model, *Industrial & engineering chemistry research*, 42 (2003) 6212-6222.
- [26] A. Gharsallaoui, B. Rogé, J. Génotelle, M. Mathlouthi, Relationships between hydration number, water activity and density of aqueous sugar solutions, *Food Chem.*, 106 (2008) 1443-1453.
- [27] K.S. Kwon, J.H. Auh, S.K. Choi, G.J. Kang, J.W. Kim, K.H. Park, Characterization of Branched Oligosaccharides Produced by *Bacillus licheniformis* Maltogenic Amylase, *J. Food Sci.*, 64 (1999) 258-261.
- [28] T. Sochi, Non-Newtonian flow in porous media, *Polymer*, 51 (2010) 5007-5023.

Chapter 3

Nanofiltration of non-spherical molecules

This chapter is based on:

Victor Aguirre Montesdeoca, Jaap Bakker, R. M. Boom, Anja E. M. Janssen, and A. Van der Padt. "Ultrafiltration of non-spherical molecules". (*Accepted in J. Memb Sci*).

ABSTRACT

Information about the sizes of the solute molecules and membrane pores is needed to estimate solute rejection in nanofiltration processes. Molecules are normally regarded as spheres, and the Stokes radius is commonly used to represent their molecular size. However, many molecules used in food and pharma processes are oligomers or polymers which are strongly elongated; therefore, considering them spherical affects the accuracy of the model predictions.

We here adapt the so-called Steric Pore Model to a more realistic representation of the transfer of rigid elongated molecules into and through nanofiltration membrane pores. To do so, sugars with different degree of polymerization were used as model molecules. They were considered to be capsule-shaped to facilitate their size estimation. In order to represent the system as accurately as possible, the effect of hydration on the sugars size was included, and the membrane pore size distribution was estimated based on rejection data.

It was demonstrated that considering these molecules to be capsule-shaped instead of spherical generates better predictions over the entire rejection spectrum using a unique pore size distribution. Additionally, this capsular geometry lets us simplify the calculations, making the estimation of the rejection straightforward.

3.1 INTRODUCTION

Nanofiltration (NF) has gained popularity in the food and biotechnology industry in the last decades due to its simplicity, low costs and sustainable features [1]. Together with this increase in popularity, the need of a mathematical representation of NF has emerged. Disciplines such as Process Design, Process Optimization and Process Control require a mathematical representation of the system to proceed. Additionally, the convenience of knowing in advance the outcome of a separation, without actually performing it, is unquestionable. Therefore, many efforts have been done in the last 20 years to understand and model NF.

When modelling NF, two main methods can be distinguished: The ‘Black Box’ method, in which phenomenological equations based on non-equilibrium thermodynamics are used [2, 3], and the so-called Steric Pore Model (SPM), which is a more mechanistic model, that has been improved and modified over the years [4, 5]. Both methods require preliminary experiments for the estimation of parameters that later on are used to predict the behaviour of the system under different process conditions [6]. The SPM model has the advantage that it is more adaptable and the estimated parameters have a clear physical meaning, making them easier to grasp and relate.

NF modelling comprises the representation of the mass transfer outside and inside the membrane. Thus, information about the physical dimensions and properties of the transient solute molecules and the membrane pores is needed to mathematically represent the solute rejection. To simplify this representation, solute molecules are normally regarded as spheres, using the Stokes radius (r_s) as a measure of their molecular dimension. For non-spherical molecules, however, this simplification produce large deviations in the calculation of the solute rejection [7].

Many molecules used in food and pharma processes are oligomers or polymers with a strongly elongated shape. For this type of molecules chain flexibility is a critical factor that determines their hydrodynamic properties [8-10]. Fortunately, small chains (oligomers) can normally be considered rigid, facilitating their representation, since they can be regarded as a continuous capsule-shaped body[9]. This capsular geometry (cylinders bounded along the edges by semispherical surfaces) is also referred as ‘spherocylinders’ by other authors [8].

Some efforts have already been made to consider the actual shape of elongated solute molecules in the modelling of their rejection in membrane pores. Their shape have been approximated to

different geometries such as cylinders [7, 11], rectangular parallelepipeds [12, 13] and spheroids [14, 15]. In order to condense the molecular dimensions of such molecules in one unique parameter, Van der Bruggen et al. calculated an ‘Effective diameter’ based on the dimensions obtained after the minimisation of the molecular energy in the three-dimensional configuration of the molecules [7, 11]. Similarly, Kiso et al, estimated the ‘Molecular width’, which was found to be more appropriate than r_s for the modelling of the rejection [12, 13]. These methods, however, require the use of sophisticated software to model the 3D structure of each solute molecule. Additionally, these studies consider the bare molecule *in vacuo*, without considering any interaction with the solvent (such as hydration). Therefore, more convenient and better methods are needed to model the nanofiltration of elongated molecules while keeping the problem complexity low. Preferably, these methods should use input parameters that are readily available in the literature or can be determined easily.

We here report on the adaptation of the existing nanofiltration theory (SPM model) to a more realistic representation of the mass transfer of rigid elongated molecules through membrane pores. To do so, sugars with different degree of polymerization (DP) were used as model molecules, which were considered to be capsule-shaped to facilitate their size estimation. For accurate predictions, the effect of hydration on the sugars size was included, while the membrane pore sizes were assumed to follow a log-normal distribution.

3.2 THEORY

3.2.1 Solute molecules as capsules

The exclusion of an uncharged non-interacting solute molecule is entirely due to the steric constraints of the pore wall. An excluded volume originates near the pore wall where the centre of solute molecules cannot access because of their finite dimensions [16]. It is generally assumed that the membrane pores are perfect cylinders and that the solute molecule is a perfect sphere. As shown in Eq. 3.1, under these conditions the calculation of a partition coefficient (Φ) at the membrane interface is straightforward, being a function of the radius of the pore (r_p) and the radius of the spherical molecule (r_i) [17].

$$\Phi = \left(1 - \frac{r_i}{r_p}\right)^2 \quad (3.1)$$

For modelling purposes, r_i is commonly represented with r_s , which, by definition, is the radius of a sphere of equal diffusivity as that of the solute molecule. r_s can be calculated from the bulk diffusivity as shown in Eq. 3.2 [18]. Evidently, the simplification $r_i = r_s$ loses accuracy as the molecule shape departs from sphericity.

$$r_s = \frac{k_B T}{6\pi\eta D} \quad (3.2)$$

In a study of exclusion chromatography, Giddings et al. assessed the effects of different molecular shapes on the partition coefficient Φ in pores of different geometries. In the case of elongated molecules, the calculation of Φ in the pore interface turns into a complex problem where molecular orientation and position play an important role [16, 19]. They found that it is more convenient to represent elongated molecules as capsules rather than as spheroids [16]. While the interested reader is advised to read the original paper for a more detailed explanation, we will here give a summary of the reasoning.

In the case of a capsule-shaped molecule and a cylindrical pore, Φ can be considered to be the configuration–space average of the probability q of no intersection with pore walls (Eq. 3.3).

$$\Phi = \frac{\iint q(p, \psi) dp d\psi}{\iint dp d\psi} = \frac{\int \varphi'(p) dp}{\int dp} = \frac{\int \varphi''(\psi) d\psi}{\int d\psi} \quad (3.3)$$

where p and ψ are generalized coordinates that describe the position and the orientation of the molecule respectively. Likewise, the local partition coefficients (φ' and φ'') can be defined as shown in Eq.3.4 and 3.5.

$$\varphi'(p) = \frac{\int q(p, \psi) d\psi}{\int d\psi} \quad (3.4)$$

$$\varphi''(\psi) = \frac{\int q(p, \psi) dp}{\int dp} \quad (3.5)$$

Given a molecule with a specific p and ψ , the probability q that this molecule is not intersected by a pore wall is going to be 1 or 0. Evidently, the restraints imposed by the pore wall will reduce the concentration of solutes near the wall. Additionally, since the surface of the cylindrical pore is assumed to have axial symmetry, ψ can be simply represented by the angle (θ) of the molecular axis with respect to the pore axis.

The size of a capsule-shaped molecule can be represented by its length L_1 and its width (which is equal to its depth) L_0 . Thus, parameters r_1 and r_0 can be defined as the half of L_1 and L_0

respectively. While r_0 represents the radius of the spherical caps at the sides of the capsule, r_1 is not a radius but the half-length. As a limiting case, Giddings et al. derived expressions for Φ and φ'' when the molecule is a rod with an infinitely small thickness ($r_0 = 0$). Since rods have only one dimension (r_1) the resulting equations are straightforward to solve.

$$b = \sqrt{r_p^2 - r_1^2 \sin^2 \theta} \quad (3.6)$$

$$\varphi'' = \frac{4}{r_p^2 \pi} \int_0^b \left(\sqrt{r_p^2 - p^2 - r_1 \sin \theta} \right) dp \quad (r_1 \sin \theta \leq r_p; \text{ otherwise } \varphi'' = 0) \quad (3.7)$$

$$\Phi = \frac{\int_0^{\pi/2} \varphi'' \sin \theta \, d\theta}{\int_0^{\pi/2} \sin \theta \, d\theta} = \int_0^{\pi/2} \varphi'' \sin \theta \, d\theta \quad (3.8)$$

The limiting case represented in Eqs. 3.6, 3.7 and 3.8 is useful because the area available for the centre of a capsule-shaped molecule (with dimensions r_1 and r_0) in a pore with radius r_p is the same as the available area for the centre of an infinitely thin rod ($\hat{r}_0 = 0$) with a new r_1 equal to $r_1 - r_0$ in a pore with radius $r_p - r_0$ (Figure 3-1). As consequence, by defining two new parameters $\hat{r}_1 = r_1 - r_0$ and $\hat{r}_p = r_p - r_0$ and using them in the aforementioned equations, a value for $\Phi(\hat{r}_1, \hat{r}_p)$ can be calculated. This value is still not equal to $\Phi(r_1, r_p)$ since the free volume in the pore is higher with r_p as the radius of the pore. The final correction can be done as shown in Eq. 3.9.

$$\Phi = \frac{(r_p - r_0)^2}{r_p^2} \Phi(\hat{r}_1, \hat{r}_p) \quad (3.9)$$

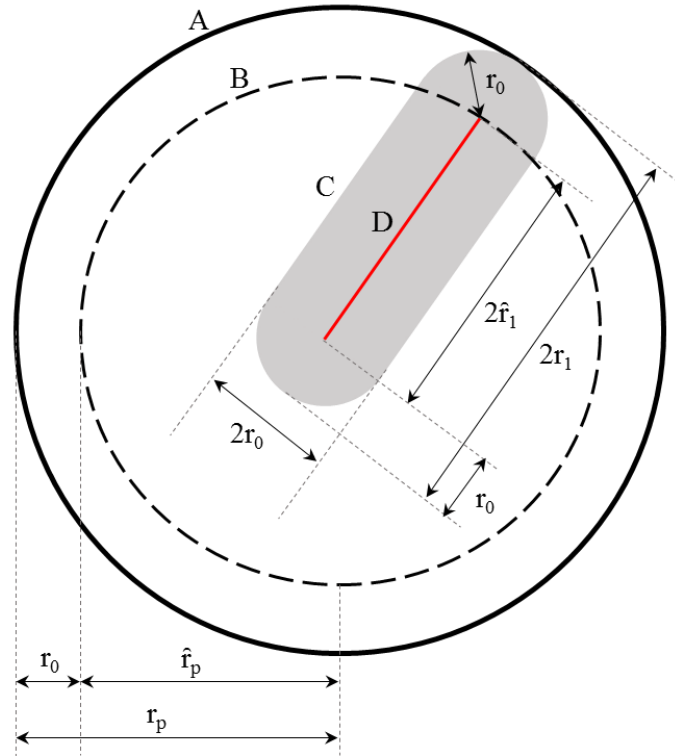


Figure 3-1. Representation of equivalent free available pore area for an infinitely thin rod D in pore B and capsule C in pore A. The dimensions of the rod are $\hat{r}_1 = r_1 - r_0$ and $\hat{r}_0 = 0$ while the dimensions of the capsule are r_1 and r_0 .

As shown in Figure 3-1, this methodology is specially suitable for capsules. Additionally, using these results, Giddings et al. found empirically that one could obtain a good estimation of Φ by calculating an Average radius (r_G), based on the two values that define a capsule r_1 and r_0 (Eq. 3.10). Thus, considering r_G as a dimensional parameter and using Eq.3.1, as if the molecule would be spherical, can also lead to straight forward approximations of Φ for capsule-shaped molecules.

$$r_G = \frac{r_1 + r_0}{2} \quad (3.10)$$

Apart from the convenience in the calculation of Φ , one extra advantage of considering elongated molecules to be capsules is the suitability, in the case of chain-like molecules, of calculating their dimensions from information about their monomers as it is explained in section 3.2.2.

3.2.2 Hydration of molecules

The interaction of solute and solvent molecules influences the physical properties of the solution and the effective dimension of the solute molecules. For sugars, the proximity of many hydroxyl moieties suggests that the molecular properties of water are critical for an understanding of the structure and dynamics of the sugars [20]. Hence, each sugar molecule and the water in its hydration layer will be regarded as a whole.

The hydration of a sugar can be estimated by the method of Gharsallaoui et al. (2008), which uses density data of single sugar solutions and hydration numbers from literature to estimate the hydrated molar volume (V_m) of the sugar [21]. Once this is done for the monosaccharides of interest, their radii can be calculated by considering them to be spherical. Subsequently, the length and width of the whole capsular oligosaccharide can be estimated by aligning the spherical monosaccharides next to each other as represented in Figure 3-2, assuming that the volume of each moiety remains equal. L_1 (the length) is equal to the sum of all the diameters of the monosaccharides in the capsule, while L_0 (the width and depth) is represented by the diameter of the bigger monosaccharide in the chain. Hence, V_m for the oligosaccharides is the sum of the V_m values of the individual monomers.

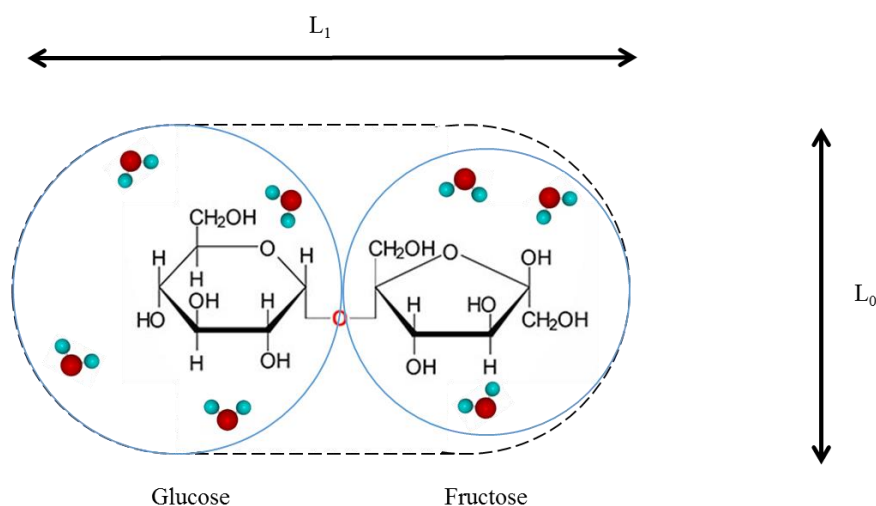


Figure 3-2. Representation of the sucrose molecule as a capsule composed by two spherical monomers, in which L_1 represents the length of the molecule and L_0 is the depth and the width of the molecule.

The structural considerations explained above are valid as long as an extended configuration for the chain is assumed. For disaccharides, this is true by definition. In the case of longer oligosaccharides, this assumption is not far from reality considering that these molecules tend to remain rigid and extended when they are in solution [20, 22, 23]. Almond et al. studied the structure of many oligosaccharides using molecular dynamics simulations and NMR measurements, and found that the interactions between the water molecules and the sugars result in tight and ordered conformations [23]. Later, they found that the presence of β linkages determine extended and relatively rigid structures that resulted in an end-to-end distance close to maximum [20, 22].

3.2.3 Fructooligosaccharides

Fructooligosaccharides are short chains of D-fructose units linked by $\beta(2-1)$ bonds that may carry a terminal $\alpha(1-2)$ linked D- glucose [24]. For modelling purposes this mixture of GF_n and F_n molecules can be classified according to their DP. Additionally, it is important to consider the peculiar behaviour of fructose. When fructose is in solution, its pyranose configuration (six-membered ring) is dominant [25]. However, when fructose is part of a chain, as it is the case in fructooligosaccharides, it assumes its furanose configuration (five-membered ring) [26]. Therefore, the volume of the hydrated fructose molecule in the oligosaccharide chain is smaller than its volume in its free form. The volume of this ‘chained fructose’ can be estimated by subtracting the volume of a hydrated glucose molecule from the hydrated volume of sucrose. Table 3-1 shows the estimated hydrated properties of some simple sugars used in this study.

Table 3-1. Hydration data of different sugars estimated according to Gharsallaoui et al. [21]. r_1 and r_0 represent the half-length and the radius of the spherical caps at the sides of the capsule-shaped molecule, respectively.

Molecule	Hydration number (n_H)	Molar volume (bare molecule) [$10^{-6} \text{ m}^3/\text{mol}$]	Molar volume (Hydrated molecule) [$10^{-6} \text{ m}^3/\text{mol}$]	r_1 [10^{-10} m]	r_0 [10^{-10} m]
Xylose	2.3[27]	98.7	139.8	3.81	3.81
Glucose	3.5[27]	118.1	174.8	4.11	4.11
Fructose	3.8[27]	118.0	179.2	4.14	4.14
Fructose in chain			128.3	3.70	3.70
Sucrose	5[21]	221.0	303	7.81	4.11
Raffinose			478	11.92	4.11

The dimensions of elongated molecules can be represented in three different ways: (1) the molecules can be considered to be spherical and the Stokes equation (Eq. 3.2) can be used to estimate their r_S ; (2) the molecules can be considered to be capsules and an average radius r_G according to Eq. 3.10 can be estimated in what we have called a Simplified Capsular approach; or (3) a Complete Capsular approach can be used, in which the molecular dimensions are represented by the two parameters that define a capsular geometry: r_1 and r_0 . Figure 3-3 shows the oligosaccharides' estimated dimensions using these 3 approaches based on the data in Table 3-1. Notice that all three approaches are equivalent for the case of monosaccharides, which can be regarded as spherical molecules. This means that considering molecular hydration in the solutes size improves the reliability of the approach since similar radii are calculated from diffusion and density data (r_S and r_G).

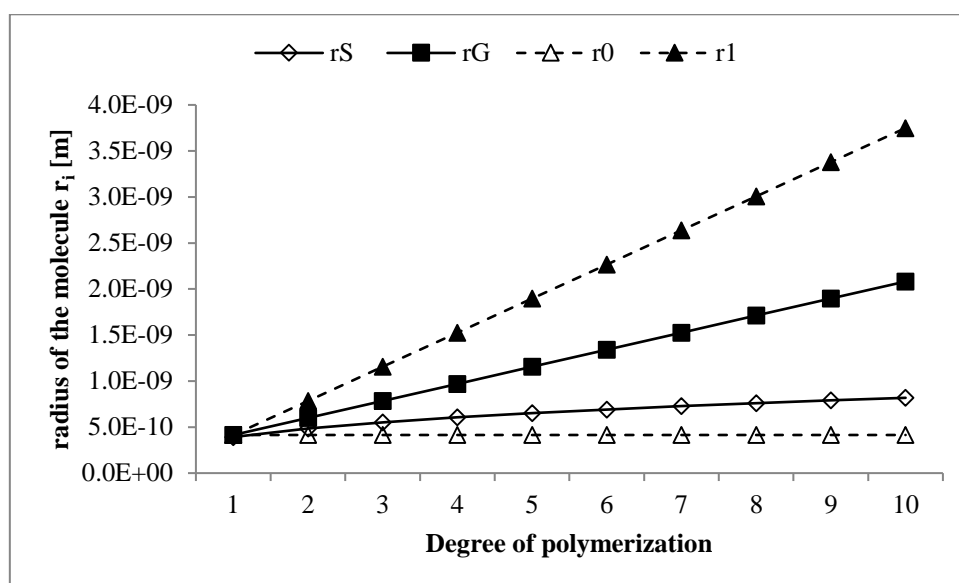


Figure 3-3. Radii of fructooligosaccharides as function of their degree of polymerization according to three different approaches: Spherical (r_S), Simplified Capsular (r_G) and Complete Capsular (r_1 , r_0). Only the symbols are produced by the calculations; lines were drawn to guide the eye.

3.2.4 Mass transfer outside the membrane

To estimate the mass transfer in the concentration polarization layer, the classic film model can be used (Eq. 3.11). In this way, an experimental Real Rejection (R) can already be calculated as shown in Eq. 3.12.

$$C_m = (C_r - C_p) \exp\left(\frac{J}{k}\right) + C_p \quad (3.11)$$

$$R = 1 - \frac{C_p}{C_m} \quad (3.12)$$

For very diluted solutions, where the osmotic pressure difference over the membrane can be neglected, the permeate flux (J) is a linear function of the pressure $|\Delta P|$, where the slope of this line is the membrane permeability (L_p) as shown in Eq. 3.13.

$$J = L_p |\Delta P| \quad (3.13)$$

The mass transfer coefficient k can be calculated using the Sherwood expression for spiral wound modules presented by Schock and Miquel[28]. They obtained this relation from experimental filtration data with different membranes, spacers and pressures, the Sherwood equation presented below can be considered to already contain suction effects due to the flux through the membrane [29].

$$k = \frac{Sh D}{d_h} \quad (3.14)$$

$$Sh = 0.065 Re^{0.875} Sc^{0.25} \quad (3.15)$$

$$Re = \frac{\rho_r v d_h}{\eta_r} \quad (3.16)$$

$$Sc = \frac{\eta_r}{\rho_r D} \quad (3.17)$$

To calculate the hydraulic diameter d_h and the cross-flow velocity v in spiral wound membranes, the procedure presented by Schock and Miquel can be used [28]. ρ_r and η_r stand for the density and the viscosity of the retentate. For diluted conditions, these values can be considered to be the same as for pure water. D is the bulk diffusion coefficient and can be calculated using the empirical relation proposed by Sano and Yamamoto in 1992 (Eq. 3.18, which links D_0 with the molecular weight of the sugar (Mw) [30].

$$D_0 = \frac{T}{9.5 \cdot 10^{13} Mw^{1/3} \eta_{H_2O}} \quad (3.18)$$

3.2.5 Mass transfer inside the membrane

While Φ represents the partitioning of a molecule at the interface of the membrane, the rejection represents the amount of solute that has been retained over the entire membrane thickness. To predict the rejection, the effect of the driving forces (pressure and concentration gradients) inside the membrane pore must be considered while taking into account the friction effect between the pore walls and the transient molecules. Bowen and Welfoot (2002) presented a modification of the SPM model that is briefly summarized as follows [5].

The flux of a component through the membrane (j) is the sum of the effect of convection, diffusion and pressure as shown in Eq. 3.19.

$$j = K_c CV - D_p \frac{dC}{dz} - \frac{CD_p}{RT} V_m \frac{dP}{dz} \quad (3.19)$$

The first term in Eq. 3.19 is the convection term in which K_c is the hindrance factor for convection, C is the local concentration and V is the solvent velocity inside the pore. The Hagen-Poiseuille relation describes the laminar flow of a liquid through a cylindrical tube, and can be used to estimate V as shown in Eq. 3.20, in which r_p represents the pore radius. Considering that $\Delta P = P_{per} - P_{ret}$, a negative sign should be included in this definition considering that ΔP is negative¹ in the direction of V .

$$V = \frac{r_p^2}{8\eta} \left(-\frac{\Delta P}{\Delta z} \right) = -\frac{r_p^2 \Delta P}{8\eta \Delta z} \quad (3.20)$$

The second term in Eq. 3.19 is the diffusion term, in which D_p is the diffusion coefficient inside the pore. To estimate it Eq. 3.21 can be used, in which the effect of the diffusion hindrance (K_d) and the increment in viscosity (η) due to the confinement of water is considered (Eq. 3.22). Here d is the thickness of the layer of water with increased viscosity that is estimated to be 0.28 nm.

$$D_p = K_d D \frac{\eta_0}{\eta} \quad (3.21)$$

$$\frac{\eta}{\eta_0} = 1 + 18 \left(\frac{d}{r_p} \right) - 9 \left(\frac{d}{r_p} \right)^2 \quad (3.22)$$

¹ This negative sign is mistakenly not considered in the original work of Bowen and Welfoot. This consideration affects the sign of 'Y' in Eq. 3.23.

Many authors do not agree with this viscosity correction since there is not a physical proof of the accuracy of this relation. It can even be argued that the effects of this constriction are already accounted for by the hindrance coefficients. Studies in molecular dynamics do show that there is an effect on the water structure to constriction but the validity of Eq. 3.22 is certainly not yet proven [31-34]. Later on, however, it will be evident that this correction is irrelevant in the transport of neutral molecules because it cancels out in the definition of the Péclet number (Eq. 3.25), and its contribution in other terms is negligible.

The third term of Eq. 3.19 is the pressure effect in the transport. This is commonly the least important effect in membrane filtration processes. The V_m values can be calculated according to section 3.2.2.

After linearizing $\frac{dP}{dz}$ in Eq. 3.19, it can be rearranged and integrated over the thickness of the membrane, using the following boundary conditions: $z = 0, C = C_m\phi$ and $z = \Delta Z, C = C_p\phi$. Rearranging the terms and defining a new variable Y (Eq. 3.23), an expression for the Porewise Real Rejection $R_{(r)}$ can be obtained (Eq. 3.24) as function of a modified version of the Péclet number Pe' (Eq. 3.25).

$$Y = -\frac{D_p}{RT} V_m \frac{8\eta}{r_p^2} \quad (3.23)$$

$$R_{(r)} = 1 - \frac{(K_c - Y)\phi}{1 - [1 - (K_c - Y)\phi]\exp(-Pe')} \quad (3.24)$$

$$Pe' = -\frac{(K_c - Y)r_p^2}{8\eta D_p} \Delta P \quad (3.25)$$

Eq. 3.25 contains a negative sign which comes from the definition of V (Eq. 3.20). This sign cancels out with the negative value of ΔP , making Pe' a positive value. Additionally, the resulting value of Y is negative, which means that the effect of the pressure gradient on the transport of solutes is not opposed to convection as derived by Bowen and Welfoot [5], but goes in the same direction of the convective flow (Eq. 3.25).

$R_{(r)}$ is not the rejection of the whole membrane, but corresponds to one specific pore with pore radius r_p . To calculate the Overall Real Rejection R , the frequencies of the pore size distribution f_R should be considered as shown in Eq. 3.26 [35]. Here the effect of pore size on the viscosity inside the pore is also considered; however, its contribution is insignificant as the same consideration is made in the numerator and in the denominator.

$$R = \frac{\int_0^\infty \frac{f_R(r)r^4 R(r)}{\eta(r)} dr}{\int_0^\infty \frac{f_R(r)r^4}{\eta(r)} dr} \quad (3.26)$$

f_R can be calculated assuming a log normal distribution of the pore sizes as previously done in other NF and UF studies [5, 36-39]. As it is shown in Eq. 3.27, f_R is defined by two parameters: the mean radius r^* and the standard deviation σ . These two parameters can be estimated using data of R vs pressure obtained from experiments.

$$f_R(r) = \frac{1}{r\sqrt{2\pi b}} \exp\left\{-\frac{\left[\ln(r/r^*) + \frac{b}{2}\right]^2}{2b}\right\} \quad (3.27)$$

$$\text{where } b = \ln\left[1.0 + \left(\frac{\sigma^*}{r^*}\right)^2\right]$$

3.2.6 Hindrance Coefficients

The hindrance to diffusion and convection originates from the combinations of particle – wall hydrodynamic interactions and steric restrictions [40]. For non-spherical molecules these interactions (drag and lag coefficients) are functions not only of position and molecular size, but also of orientation. This represent a challenge since all orientations must be averaged at all radial positions. Although the mathematical formulation is not complex, the information required is enormous [41].

Recently, Agasanapura et al. used computational fluid dynamics based on a centerline approximation to assess the convective hindrance in the filtration of capsular particles [19]. They found experimentally and with their model that convective hindrance was only relevant for small capsular particles ($\lambda < 0.4$) with small aspect ratio (closer to a sphere). For bigger molecules, the steric restrictions that limit the allowed positions and orientations dominate over the hydrodynamic particle-pore wall interactions, making the molecule travel at the average flow velocity [19]. Based on these findings and considering that the pore size of the NF membrane is in the same order of magnitude as r_s of the sugars, K_c values become necessary only for molecules with DP lower than three. For molecules with a DP of three or higher, $K_c = 1$ can be considered. The following expression for K_c can be used considering $\lambda = r_G/r_p$ [40].

$$K_c = \frac{1 + 3.867\lambda - 1.907\lambda^2 - 0.834\lambda^3}{1 + 1.867\lambda - 0.741\lambda^2} \quad (3.28)$$

In the case of the calculation of K_d for non-spherical molecules, to the best of our knowledge nothing concrete has been achieved yet. Even the assumption that rotational Brownian motion is sufficient to ensure complete randomness of solute orientation is uncertain. Randomness can only be assured when the rotational diffusivity of the solute is higher than the vorticity of the velocity field in the pore [41]. There are some theoretical studies that calculate the hindrances for polymer coils in cylindrical pores, by considering these macromolecules to be solvent-permeable bodies determining a permeability distribution across the pore [42]; however, in our case it does not seem appropriate to approximate rigid molecules to porous bodies. We believe instead that is safer to make use of the available theory for rigid spheres as done by other researchers when investigating the transport of elongated molecules [13, 43]. An expression for K_d applicable to any λ value from 0 to 1 can be obtained from the work of Bungay and Brenner (1973) [44]. Calculating λ using r_s ensures consistency with the fact that Stokes' law was considered in the estimation of the drag force by Bungay and Brenner [44, 45].

$$K_d(\lambda) = \frac{6\pi}{K_t(\lambda)} \quad (3.29)$$

$$K_t(\lambda) = \frac{9}{4}\pi^2\sqrt{2} (1 - \lambda)^{-\frac{5}{2}} \left[1 + \sum_{n=1}^2 a_n (1 - \lambda)^n \right] + \sum_{n=0}^4 a_{n+3} \lambda^n$$

$$a_1 = -1.2167, a_2 = 1.533, a_3 = -22.5083, a_4 = -5.6117, a_5 = -0.3363,$$

$$a_6 = -1.216, a_7 = 1.647$$

3.3 MATERIALS AND METHODS

3.3.1 Chemicals

Demineralised water was used in every experiment. In the case of the simple sugars, xylose was purchased from Merck KGaA (Darmstadt, Germany) and glucose, fructose, sucrose and raffinose pentahydrate were purchased from Sigma-Aldrich (Munich-Germany). The fructooligosaccharides (FOS) mixture Frutalose[®] L85 (batch: 8554908001) was kindly provided by Sensus (Roosendaal, Netherlands). This mixture is a viscous, clear syrup with a

concentration of 75% w/w, composed by mono, di and oligo-saccharides up to a DP of 10. Its composition on dry basis is shown in Table 3-2.

Table 3-2. Composition of fructooligosaccharides mixture (Frutalose® L85) on dry basis

Component	% (w/w)
DP1	6.1
DP2	7.6
DP3	28.8
DP4	22.5
DP5	16.9
DP6	12.2
DP7	5.2
DP8*	0.3
DP9*	0.4
DP10*	0.2

* Molecules that were not considered in the mathematical modelling.

Although the DP of the oligosaccharide mixture ranged from 1 to 10, only data up to DP7 was considered for the calculations and modelling since the concentrations of the higher DP molecules were too small to be measured accurately.

3.3.2 Membrane

A thin film composite (thin polyamide layer deposited on top of polysulfone porous layer), spiral wound GE membrane (GE Osmonics, Sterlitech, Kent – WA, United States) was used for all the experiments. This NF membrane was chosen mainly due to its appropriate MWCO and its good resistance to high temperatures as shown in Table 3-3. The experiments were performed in a pilot scale filtration system that included heat exchangers in the feed tank and in the recirculation loop of the retentate. The flow, temperature and pressure of both retentate and permeate streams were monitored by computer (DDE software from Labview).

Table 3-3. Specifications of GE membrane

Membrane specifications	GE
Model	1812C-34D
Type	Spiral wound
Manufacturer	General Electric
Membrane material	TFM
MWCO (declared by manufacturer)	1000 Da
Membrane area	0.32 m ²
Permeability at 45° C*	7.06 x 10 ⁻¹² m/(Pa s)
Spacer height*	8.60 x 10 ⁻⁴ m
Spacer porosity*	0.93
Maximum temperature	50°C

* Membrane characteristics measured in our lab.

3.3.3 Estimation of pore size distribution

The pore size distribution of the GE membrane was determined by estimating the parameters r^* and σ . These two parameters were fitted making use of the equations presented in section 3.2.4 and 3.2.5 and experimental rejection data obtained from filtration experiments with oligosaccharides. During this experiments, a very diluted aqueous solution (0.5% w/w) of Fructose[®] L85 was used as feed to avoid osmotic pressure effects. The retentate and the permeate streams were recycled back to the feed tank, and once the system reached steady state (constant permeate flux), samples were taken from both streams simultaneously. This operation was repeated at many pressures (2.5 – 20 bar). All runs were performed at 45°C to mimic industrial conditions and avoid microbial growth. The retentate recirculation flow was 150 L/h with a crossflow velocity of 0.088 m/s in the membrane module.

Using the collected data and process parameters, experimental R values for each molecule were calculated with Eqs. (3.11) - 3.18). As a result, 7 experimental curves of R vs Pressure (one for each DP), can be obtained. r^* and σ were fitted using all these curves simultaneously, considering that even when the sizes of the molecules were different, the pore size distribution is the same because all the experiments were performed with the same GE membrane. The sizes of the molecules were calculated according to the three different approaches for the calculation

of the species radii presented in section 3.2.1: (1) Spherical (r_S), (2) Simplified Capsular (r_G) and (3) Complete Capsular (r_1, r_0). In each case, modelled R was obtained by solving the Eqs. (3.21)- (3.29). After an iterative procedure, it was determined which values for the parameters r^* and σ produce the best description.

3.3.4 Analytical methods

The concentration of simple sugars was measured using High Performance Liquid Chromatography. A Shodex column KS-806 was used at 80°C with MilliQ water as eluent at a flow rate of 1mL/min. The detection was performed with a RI detector (Shodex R9-101). For the oligosaccharides mixture, an Ion Exchange Chromatography technique was used based on the method of Campbel et al. (1997) [24]. The Dionex column Carbopac PA-100, 250 x4.6mm + guard was utilized at 20°C. Three eluents were used: Demineralised water, 0.25M NaOH and 0.65M NaOAc at a flow rate of 1mL/min. The detection was performed with an electrochemical detector (Dionex ED-40, range 500 nC, pulse train 2).

3.3.5 Computational analysis

MATLAB R2015b was used for all the calculations. For the simultaneous fitting of two parameters the function 'lsqcurvefit' was used. This function solves nonlinear curve-fitting problems in least squares sense using the 'trust-region-reflective' algorithm. For the resolution of Eqs. 3.7, 3.8 and 3.26, the expressions were numerically integrated using the function 'integral'.

3.4 RESULTS AND DISCUSSION

3.4.1 Calculation of the partition coefficient

Only neutral molecules (sugars) were used as solutes in this study and it was assumed that no interaction occurred between the solutes and the membrane; consequently, the partitioning of these molecules in the membrane is determined solely by steric effects. The shape and size of the FOS molecules were estimated according to three different approaches: (1) Using the Stokes equation, in which the hydrodynamic radius (r_S) is calculated assuming an spherical molecular shape; (2) using the Simplified Capsular approach in which an average radius (r_G) is calculated; and (3) using the Complete Capsular approach considering 2 dimensions to represent this capsular shape (r_1, r_0).

Figure 3-4 shows the Φ values for all FOS molecules considering a hypothetical pore radius of 2 nm. As described by Giddings et al., the Φ values calculated using r_G were very similar to those calculated using the Complete Capsular approach (r_1, r_0). Conversely, Φ values calculated with r_S were consistently higher than the ones obtained with the other two methods. This was expected considering the fact that, for the FOS molecules, r_S was smaller than r_G (Figure 3-3). In the case of the DP1 sugar, since it is a spherical molecule, a similar Φ was obtained with all the approaches.

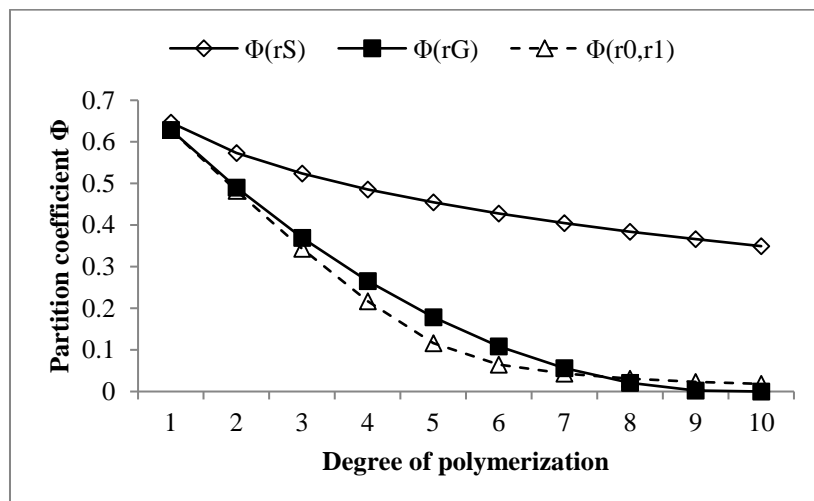


Figure 3-4. Partition coefficients for fructooligosaccharides with a degree of polymerization up to 10. Three approaches were used with respect to the molecular shape and size estimation: Spherical (r_S), Simplified Capsular (r_G) and Complete Capsular (r_0, r_1). The pore radius used in this calculation was 2 nm. Only the symbols are produced by the calculations; lines were drawn to guide the eye.

r_G is a good empirical approximation that simplifies the calculation of Φ greatly. It produces slightly higher values than the Complete Capsular approach when r_G/r_p is between 0.4 and 0.6, and slightly lower values when Φ is close to zero. This curious similarity between these two methods was assessed in Figure 3-5, in which Φ is illustrated as the ratio between the area available for the centre of the molecule in the pore and the total pore area. The calculations for this figure were made considering a DP4 molecule entering a pore of $r_p=2$ nm.

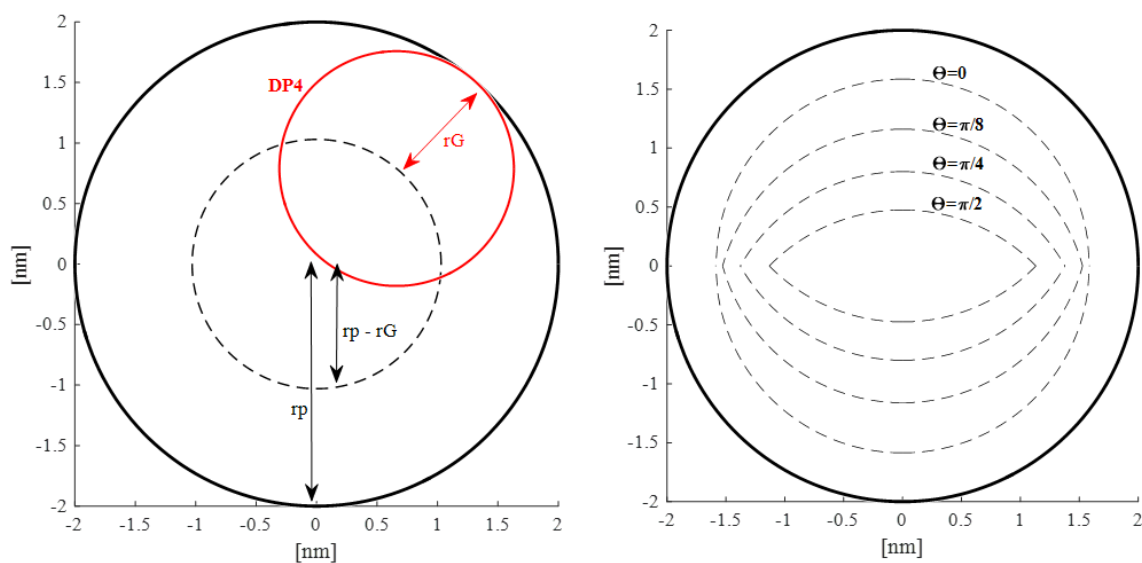


Figure 3-5. Comparison between the Simplified Capsular (left) and the Complete Capsular (right) approaches for the Φ calculation of a DP4 molecule in a pore with a 2 nm radius. Left: The area surrounded by the dashed line is the area available for the centre of the spherical molecule of radius r_G . Right: The area surrounded by the dashed lines represent the available area for the centre of a capsular molecule at different orientation angles θ .

Figure 3-5 (left) illustrates the calculation of Φ according to the Simplified Capsular approach in which r_G is used to represent the molecular size (Eq. 3.10). The area surrounded by the dashed line is the area available for the centre of the spherical molecule of radius r_G , while the area outside this line is the area that is excluded due to steric effects with the wall. The ratio between the available area and the total pore area is equal to Φ . Molecular orientation here is not relevant, since the molecule is considered spherical for the Φ calculation. It is clear that as soon as r_p is equal or smaller than r_G , Φ becomes zero, which means that the molecule is totally excluded from the pore. Likewise, the Φ calculation when the Complete Capsular approach is used is represented in Figure 3-5 (right), in which dashed lines surround the available area for the centre of capsular molecules at specific orientation angles θ . The ratios between these areas with the total pore area are equivalent to local partition coefficients φ'' as represented in Eq. 3.5, while the global partition coefficient Φ is the configuration-space average of these local values (Eq. 3.3). As expected, when the axis of the pore and that of the capsule are aligned ($\theta = 0$), φ'' is the highest for a given molecule since its projected area in the pore plane is the smallest possible. As consequence, the available area for the molecule is then the greatest possible,

resulting in a lower probability to touch the wall compared with other orientations. As θ increases, the projected area becomes larger, decreasing the available area for the molecule and its ϕ'' value. This explains the difference between both methods when Φ is close to zero in Figure 3-4. With the Simplified Capsular approach, as soon as a r_G is equal to r_p , Φ becomes zero, while in reality some molecular orientations still allow the entrance of the molecule in the pore when the axis of the pore and the molecule are aligned ($\theta \rightarrow 0$). This latter situation is adequately represented by the Complete Capsular approach. By using this method, it can be verified that for capsular molecules of similar volume, the greater the aspect ratio, the lower Φ , being the spherical conformation always the more compact, so the one with the highest Φ value.

3.4.2 Pore size distribution estimation

The pore size distribution of the GE membrane was estimated by using the model presented in sections 3.2.4 -3.2.6 to fit two parameters (r^* and σ) to experimental rejection data. This operation was repeated using the three different methods for the molecular size and shape estimation according to section 3.2.1.

In the case of the Simplified and Complete Capsular approaches, the fitting procedure worked fine and the model output matches the experimental measurements as shown in Figure 3-6. At low pressures, nevertheless, in the range where diffusion is an important driving force, the modelled rejection was systematically higher than the experimental data. For these two approaches the modelled rejection reached a plateau at lower pressures than the experimental data, meaning that the diffusion mechanism is underestimated in the model. We believe that the way how K_d was calculated (using r_s) slightly overestimates the effect of diffusion hindrance, producing K_d values lower than real, which result in higher rejections. An observation that supports this explanation is the better agreement between the model and the measurements for the DP1 molecules, which actually have a r_s radius. In the case of the oligosaccharides (elongated molecules), their orientation influences their interaction with the pore wall, thus K_d would be a complex function of r_1 , r_0 and r_p . It is also expected that K_d would be lower for longer chains, as its movement inside the pore is more limited.

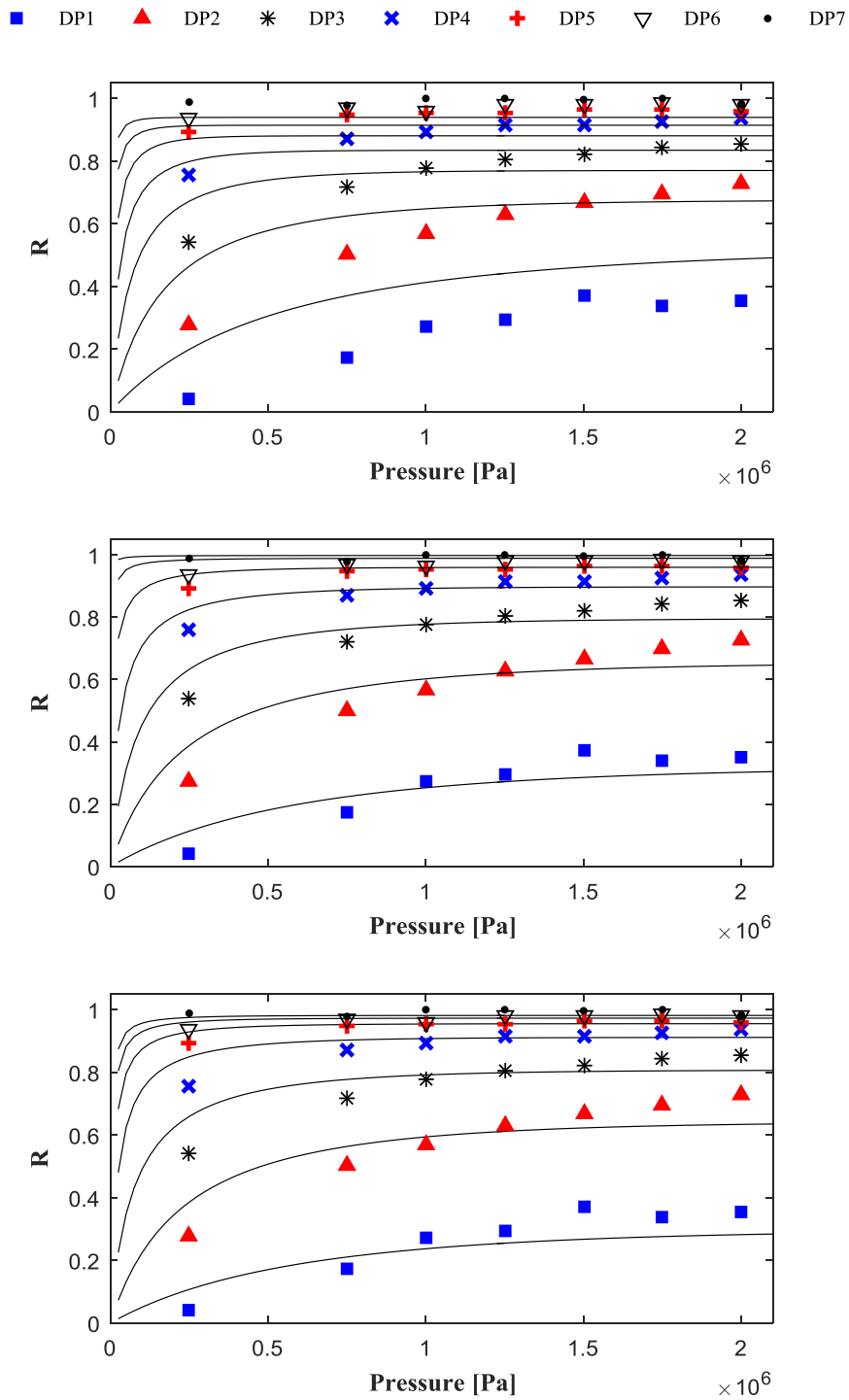


Figure 3-6. FOS rejections according to the Spherical (top), Simplified Capsular (middle) and Complete Capsular (bottom) approaches. The fitting procedures in all cases were done with the same experimental data, represented by symbols. Lines represent the output of the model using the estimated parameters for each case (see Table 3-4).

In the case of the Spherical approach, the resulting fit is not accurate for low and high rejection values as it is shown in the Figure 3-6 (top). The r_s values of DP1 to DP7 molecules scarcely differ from each other (Figure 3-3), resulting in a relatively narrow spectrum of rejections compared with the experimental results. Somewhat similar results were obtained by Nakao and Kimura when estimating the pore size of a UF membrane using different solutes [46]. They found that a linear polymer (PEG#4000) gave inconsistent results (too large pore size) when considering its r_s in the model. We are proving here that by considering the right solute shape, a unique pore size distribution can be estimated from rejection data, regardless the size of the solute molecules. Some authors argue that different solutes result in different pore sizes due to the tortuosity of the membrane. In our case, it was not necessary to incorporate more parameters to obtain a good description of the rejection data.

Table 3-4 shows the results of the parameter estimation procedure. It was found that the results obtained using the Simplified and Complete Capsular approaches were consistent with each other, while the Spherical approach resulted in a pore size distribution with a much lower r^* value. This was expected considering that r_s was much smaller than r_G and r_1 (Figure 3-3). Additionally, the effectiveness of the fitting, reflected in the sum of the squares of the errors E , was much better for the Simplified and Complete Capsular approaches.

Table 3-4. Comparison of the parameter estimation results for the pore size distribution of the GE membrane.

Method	Estimated parameters [nm]		E	Accuracy	
	r^*	σ		$s_{r^*} (CV_{r^*})$	$s_{\sigma} (CV_{\sigma})$
Spherical	0.94	0.010	0.366	0.10 (0.11)	3.78 ($\gg 1$)
Simplified Capsular	1.29	0.17	0.082	0.09 (0.07)	0.07 (0.41)
Complete Capsular	1.31	0.21	0.097	0.07 (0.05)	0.11 (0.52)

r^* = Mean radius, σ = Std. deviation of the pore size distribution, E = Sum of the square of the errors, s = Std. deviation of the estimated parameters, CV = Coefficient of variation.

To evaluate the accuracy of the non-linear fitting, also indicated as the estimation uncertainty, the standard deviation (s) of the estimated parameters was calculated for all three approaches

(Table 3-4) [47]. Likewise, the coefficient of variation (CV), which is the ratio of the standard deviation to the estimated parameter, was calculated in every case.

For the spherical approach, it was found that the s_σ value was higher than the estimated σ , which means that σ for this approach cannot be accurately estimated. For the other 2 approaches (Simplified and Complete Capsular), the CV values were much lower. In general, the fitting procedure allowed an easier and more accurate estimation of r^* than σ . Nevertheless, the estimated σ values for the Simplified and Complete Capsular approach were found acceptable as their CV was not excessively high.

Since it is a non-linear fitting, confidence intervals cannot be used [47]. Instead, Draper and Smith suggest to define a confidence region, delimited with contour lines of equal E , that can be viewed as ‘equally likely’ [48]. As example, we show in Figure 3-7 these contour lines for the case of the Simplified Capsular approach, in which a correlation between the parameters can be seen. This means that during the parameters estimation, a change in one parameter can be partially compensated by a change in the other parameter. In our case, an increase in σ can be compensated by a decrease in r^* and vice versa. Under these circumstances, it is critical to use solutes with a size comparable to that of the pore (as done in this study), to make their rejection more sensitive to changes in the parameters that define the pore size distribution of the membrane. A plot similar to Figure 3-7 was also obtained for the Complete Capsular approach.

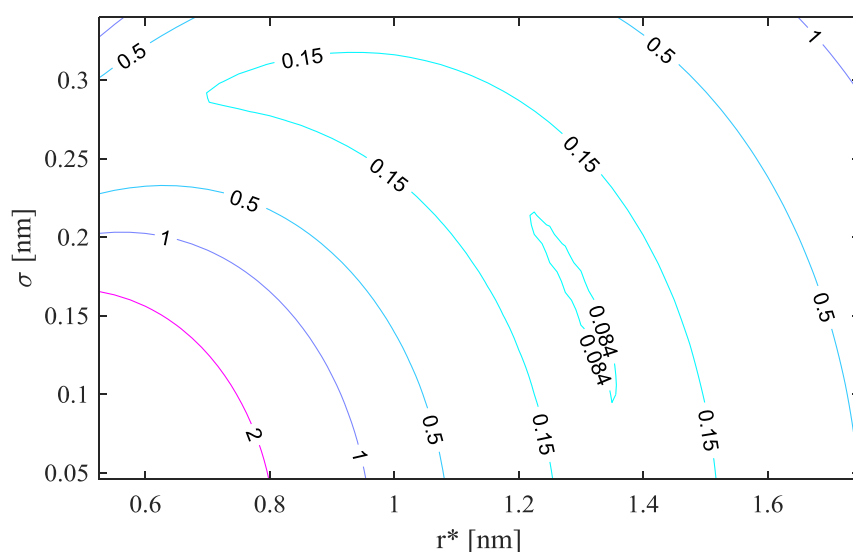


Figure 3-7. Contour plot of the sum of the squares of the errors (E) as function of the two estimated parameters: r^* and σ . Results belong to the Simplified Capsular approach.

The estimation of pore size distributions using rejection data has the disadvantage that rejection depends on r^4 (Eq. 3.26). This dependency means that the pore size estimation is very sensitive to few larger pores. Thus, sometimes diffusive data is preferred, because then the dependency is only on r^2 . Nevertheless, realistic pore size distributions were obtained using the Simplified and the Complete Capsular approaches. While these results are consistent with each other; the computer resources for the calculation were much higher for the Complete Capsular approach, which resulted in a slightly wider (higher σ value) pore size distribution as it is shown in Figure 3-8.

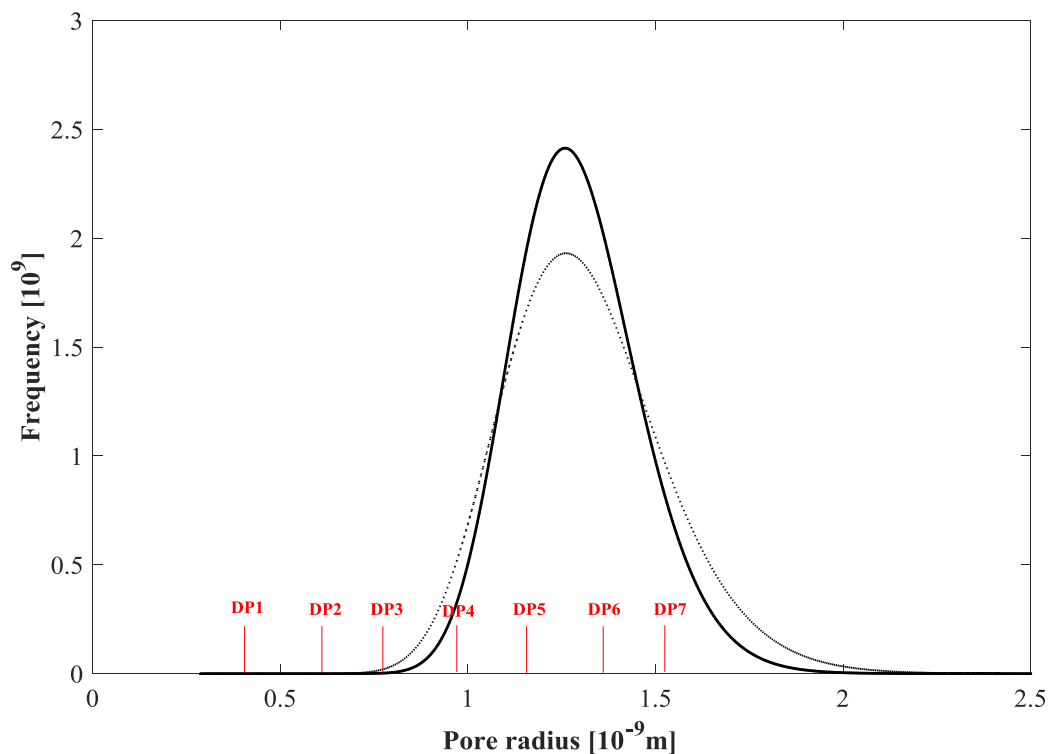


Figure 3-8. Pore size distribution estimated according to the Simplified Capsular (continuous line) and the Complete Capsular (dotted line) approaches. r_G values of the oligosaccharide molecules are shown in the x axis.

Figure 3-8 shows that the size of the pores of the GE membrane are in the same order of magnitude as the r_G of the FOS molecules. This demonstrates how critical a good estimation of the pore size distribution is for this type of purification processes. Even when the r_G values for DP6 and DP7 molecules are smaller than a fraction of pores in the membrane, the rejection for these molecules is practically 1 because the few molecules that enter the pore are slowed down

by the hindrance inside the pore. Frequently, these steric and hydrodynamic interactions inside the pore are not included in characterization studies, in which only data at limiting conditions (high flux) is considered for the fitting of the pore size distribution. The drawback of this method is the small number of degrees of freedom (number of measurements – number of estimated parameters), which might make the estimation statistically insignificant. Additionally, considering that Φ is still relevant at limiting conditions, the molecular shape considerations should not be neglected in this type of studies.

3.4.3 Model validation

To check the validity of the model, the estimated pore size distributions were utilized to predict the rejection of different sugars in a new set of experiments using the same GE membrane. Single diluted solutions (0.2% w/w) of raffinose, sucrose, and xylose were utilized as feed at 45°C with a crossflow velocity of 0.088 m/s. Their dimensions were estimated as explained in previous sections. Using the estimated values for r^* and σ , the R values for these sugars were predicted and compared with experimental data. Figure 3-9 shows the comparison between the predicted rejections calculated using all three approaches and the experimental measurements.

In the case of the Simplified and Complete Capsular Approach, the accuracy of the predictions is good, although both methods tend to slightly underestimate the rejection of raffinose. This might be due to inaccuracies in the size estimation of raffinose since we assumed that two of its monomers, glucose and galactose, have the same size. In the case of xylose, the difference in the predictions is entirely due to the different pore size distribution used with each method. Both methods are equivalent in this case because xylose is a monomer and is considered a sphere, thus $r_1 = r_0 = r_G$. Since the Complete Capsular approach resulted in a wider pore size distribution and considering that bigger pores have a greater effect in the rejection, the predicted rejection for xylose is slightly lower than the one calculated with the Simplified Capsular approach. For bigger molecules (sucrose and raffinose) this trend changed and the rejection predictions of the Complete Capsular approach became higher than that of the Simplified Capsular approach. This is expected considering that in this range of λ values, Φ are slightly smaller when calculated using the Complete Capsular approach.

The Spherical approach overestimates the rejection of xylose and greatly underestimates the rejection of raffinose. As expected, the prediction cannot cover the entire spectrum of rejections due to the relatively small difference in the r_3 of the sugars. In the case of xylose, even when

all three approaches are similar for spherical molecules, the prediction of the Spherical approach is the worst due to the incorrect pore size distribution obtained in the previous section.

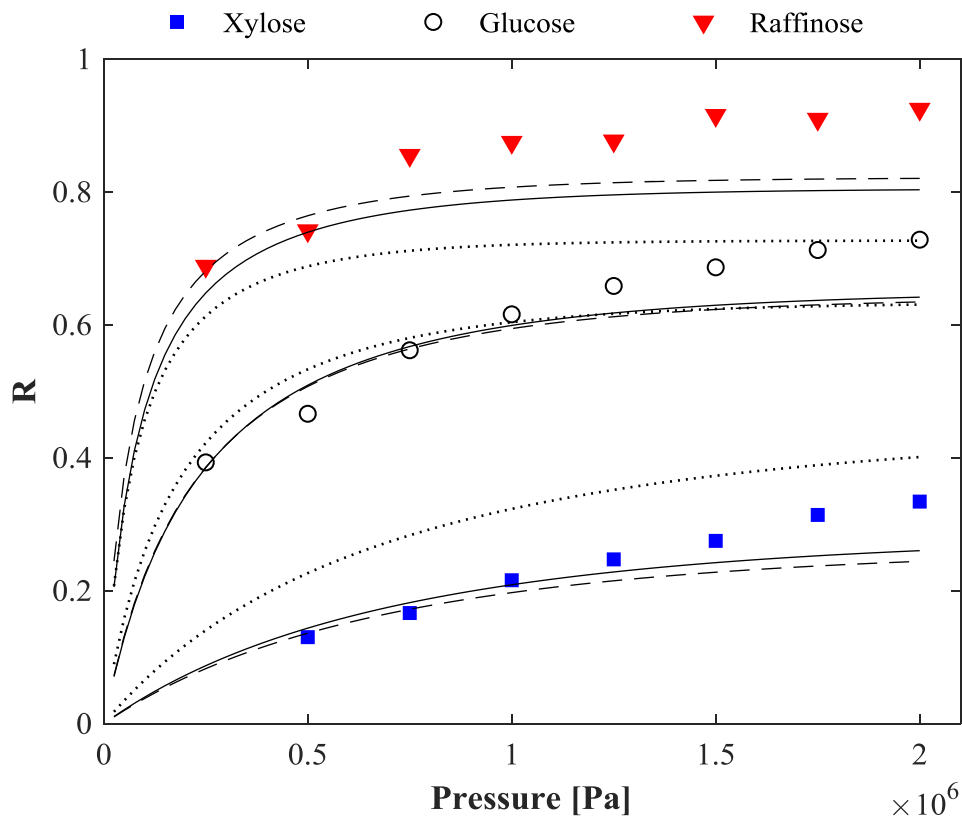


Figure 3-9 Comparison of the R predictions using the Spherical (dotted lines), Simplified Capsular (continuous lines) and the Complete Capsular (dashed lines) approaches. The pore size distributions used here were the ones obtained previously with each method (shown in Table 3-4).

3.5 CONCLUSIONS

The nanofiltration of rigid elongated molecules was assessed for modelling purposes. Three different strategies for the representation of the molecular size were evaluated: Spherical approach, Simplified Capsular approach and Complete Capsular approach. It was demonstrated that considering elongated molecules to be capsule-shaped gives better predictions of the rejection of rigid neutral molecules such as oligosaccharides.

The capsular shape is preferred over other geometries because it can be represented by only two parameters, making the calculation of its partition in cylindrical pores straightforward. In

addition, the capsule dimensions of oligomers can be easily inferred from the dimensions their monomers in the case of rigid-chain molecules.

Both the Simplified and Complete Capsular approaches satisfactorily predicted the rejection of sugars of different sizes at different pressures. Due to its simplicity and lower computing power demand, we suggest to use the Simplified Capsular approach for pore size estimation and rejection prediction, unless higher accuracy is needed (especially at high R values); in that case, we suggest to use the Complete Capsular approach.

A proper method for the calculation of the diffusion hindrance inside the pore (K_d) remains as a challenge for elongated molecules. In this study, this parameter was roughly estimated using an spherical approximation for the shape of the molecule. It was observed that the effect of K_d is relevant at low pressures in the range where diffusion is a significant transport mechanism inside the pores.

ACKNOWLEDGEMENTS

This work was carried out as part of a project of the Institute for Sustainable Process Technology, The Netherlands: project number CM-20-05.

NOMENCLATURE

C	Concentration [mol/m ³]
C_c	Correlation coefficient [dimensionless]
Cov	Covariance matrix [m ²]
D	Diffusion coefficient [m ² /s]
D_p	Diffusion coefficient inside the pore [m ² /s]
d	Diameter of the water molecule [m]
d_h	Hydraulic diameter [m]
E	Sum of the squares of the errors [dimensionless]
f_R	Frequency [dimensionless]
J	Permeate flux [m/s]
Jac	Jacobian Matrix [m ⁻¹]
K_c	Hindrance coefficient for convection [dimensionless]
K_d	Hindrance coefficient for diffusion [dimensionless]
k	Mass transfer coefficient [m/s]
k_B	Boltzmann constant [J/K]
L_p	Permeability
L_1	Length of the capsular molecule [m]
L_0	Width and depth of the capsular molecule [m]
MW	Molecular weight [g/mol]
N	Number of measurements [dimensionless]
n_H	Hydration number [dimensionless]

n_p	Number of estimated parameters [dimensionless]
P	Pressure [Pa]
p	Position [m]
q	Probability of no intersection with pore walls [dimensionless]
R	Real rejection Eqs. 3.12 and 3.26
R	Gas constant [J/(K mol)] Eqs. 3.19 and 3.23
Re	Reynolds number [dimensionless]
r_G	Average radius according to the Simplified Capsular approach [m]
r_i	Radius of molecule i [m]
r_p	Radius of the pore [m]
r_S	Stokes' radius [m]
r_1	Half of the capsular length [m]
r_0	Radius of the caps of the capsule [m]
r^*	Mean radius [m]
\hat{r}_p	Radius of the pore for the infinitely thin rod approximation [m]
\hat{r}_1	Half of the length of the rod for the infinitely thin rod approximation [m]
Sc	Schmidt number [dimensionless]
Sh	Sherwood number [dimensionless]
T	Temperature [K]
V	Pore wise flow velocity [m/s]
V_m	Molar volume [m ³ /mol]
v	Cross flow velocity [m/s]

Greek letters

η	Viscosity [Pa s]
θ	Angle between the axis of the capsular molecule and the axis of the pore [rad]
λ	Ratio between the molecular and pore radii [dimensionless]
ρ	Density [Kg/m ³]
σ	standard deviation of the pore size distribution [m]
Φ	Global partition coefficient [dimensionless]
φ'	Local partition coefficient as function of position [dimensionless]
φ''	Local partition coefficient as function of orientation [dimensionless]
ψ	Orientation [rad]

REFERENCES

- [1] R. Baker, *Membrane Technology and Applications* 2nd ed., Wiley, California, USA, 2004.
- [2] O. Kedem, A. Katchalsky, Thermodynamic analysis of the permeability of biological membranes to non-electrolytes, *Biochim. Biophys. Acta*, 27 (1958) 229-246.
- [3] K. Spiegler, O. Kedem, Thermodynamics of hyperfiltration (reverse osmosis): criteria for efficient membranes, *Desalination*, 1 (1966) 311-326.
- [4] W.R. Bowen, A.W. Mohammad, Characterization and Prediction of Nanofiltration Membrane Performance—A General Assessment, *Chem. Eng. Res. Des.*, 76 (1998) 885-893.
- [5] W.R. Bowen, J.S. Welfoot, Modelling the performance of membrane nanofiltration—critical assessment and model development, *Chem. Eng. Sci.*, 57 (2002) 1121-1137.
- [6] V. Silva, P. Prádanos, L. Palacio, J.I. Calvo, A. Hernández, Relevance of hindrance factors and hydrodynamic pressure gradient in the modelization of the transport of neutral solutes across nanofiltration membranes, *Chem. Eng. J.*, 149 (2009) 78-86.
- [7] B. Van der Bruggen, J. Schaep, D. Wilms, C. Vandecasteele, Influence of molecular size, polarity and charge on the retention of organic molecules by nanofiltration, *J. Membr. Sci.*, 156 (1999) 29-41.
- [8] V.N. Tsvetkov, Molecular structure and physical properties of rigid chain polymers in solutions. Review, *Polymer Science U.S.S.R.*, 25 (1983) 1815-1835.
- [9] T. Norisuye, M. Motowoka, H. Fujita, Wormlike Chains Near the Rod Limit: Translational Friction Coefficient, *Macromolecules*, 12 (1979) 320-323.
- [10] I. Teraoka, K.H. Langley, F.E. Karasz, Reptation dynamics of semirigid polymers in porous media, *Macromolecules*, 25 (1992) 6106-6112.
- [11] B. Van der Bruggen, C. Vandecasteele, Modelling of the retention of uncharged molecules with nanofiltration, *Water Res.*, 36 (2002) 1360-1368.
- [12] Y. Kiso, K. Muroshige, T. Oguchi, M. Hirose, T. Ohara, T. Shintani, Pore radius estimation based on organic solute molecular shape and effects of pressure on pore radius for a reverse osmosis membrane, *J. Membr. Sci.*, 369 (2011) 290-298.
- [13] Y. Kiso, K. Muroshige, T. Oguchi, T. Yamada, M. Hhirose, T. Ohara, T. Shintani, Effect of molecular shape on rejection of uncharged organic compounds by nanofiltration membranes and on calculated pore radii, *J. Membr. Sci.*, 358 (2010) 101-113.
- [14] J.L.C. Santos, P. de Beukelaar, I.F.J. Vankelecom, S. Velizarov, J.G. Crespo, Effect of solute geometry and orientation on the rejection of uncharged compounds by nanofiltration, *Sep. Purif. Technol.*, 50 (2006) 122-131.

- [15] F. Vinther, M. Pinelo, M. Brøns, G. Jonsson, A.S. Meyer, Statistical modelling of the interplay between solute shape and rejection in porous membranes, *Sep. Purif. Technol.*, 89 (2012) 261-269.
- [16] J.C. Giddings, E. Kucera, C.P. Russell, M.N. Myers, Statistical theory for the equilibrium distribution of rigid molecules in inert porous networks. Exclusion chromatography, *The Journal of Physical Chemistry*, 72 (1968) 4397-4408.
- [17] E.M. Renkin, Filtration, diffusion, and molecular sieving through porous cellulose membranes, *The Journal of general physiology*, 38 (1954) 225-243.
- [18] W. Sutherland, LXXV. A dynamical theory of diffusion for non-electrolytes and the molecular mass of albumin, *The London, Edinburgh, and Dublin Philosophical Magazine and Journal of Science*, 9 (1905) 781-785.
- [19] B. Agasanapura, R.E. Baltus, C. Tanneru, S. Chellam, Membrane rejection of nonspherical particles: Modeling and experiment, *AIChE J.*, 59 (2013) 3863-3873.
- [20] A. Almond, Towards understanding the interaction between oligosaccharides and water molecules, *Carbohydr. Res.*, 340 (2005) 907-920.
- [21] A. Gharsallaoui, B. Rogé, J. Génotelle, M. Mathlouthi, Relationships between hydration number, water activity and density of aqueous sugar solutions, *Food Chem.*, 106 (2008) 1443-1453.
- [22] A. Almond, A. Brass, J.K. Sheehan, Oligosaccharides as Model Systems for Understanding Water–Biopolymer Interaction: Hydrated Dynamics of a Hyaluronan Decamer, *The Journal of Physical Chemistry B*, 104 (2000) 5634-5640.
- [23] A. Almond, B.O. Petersen, J.Ø. Duus, Oligosaccharides Implicated in Recognition Are Predicted to Have Relatively Ordered Structures, *Biochemistry*, 43 (2004) 5853-5863.
- [24] J.M. Campbell, L.L. Bauer, G.C. Fahey, A.J.C.L. Hogarth, B.W. Wolf, D.E. Hunter, Selected Fructooligosaccharide (1-Kestose, Nystose, and 1F- β -Fructofuranosylnystose) Composition of Foods and Feeds, *J. Agric. Food. Chem.*, 45 (1997) 3076-3082.
- [25] G. Lelong, W.S. Howells, J.W. Brady, C. Talón, D.L. Price, M.-L. Saboungi, Translational and rotational dynamics of monosaccharide solutions, *The Journal of Physical Chemistry B*, 113 (2009) 13079-13085.
- [26] W.H. Brown, T. Poon, T. Poon, *Introduction to organic chemistry*, John Wiley & Sons, 2014.
- [27] H. Shiio, Ultrasonic interferometer measurements of the amount of bound water. Saccharides, *J. Am. Chem. Soc.*, 80 (1958) 70-73.

- [28] G. Schock, A. Miquel, Mass transfer and pressure loss in spiral wound modules, *Desalination*, 64 (1987) 339-352.
- [29] V. Geraldes, A.M. Brites Alves, Computer program for simulation of mass transport in nanofiltration membranes, *J. Membr. Sci.*, 321 (2008) 172-182.
- [30] Y. Sano, S. Yamamoto, Mutual Diffusion Coefficient of Aqueous Sugar Solutions, *J. Chem. Eng. Jpn.*, 26 (1993) 633-636.
- [31] I. Brovchenko, A. Geiger, A. Oleinikova, D. Paschek, Phase coexistence and dynamic properties of water in nanopores, *The European Physical Journal E*, 12 (2003) 69-76.
- [32] P. Hirunsit, P.B. Balbuena, Effects of Confinement on Water Structure and Dynamics: A Molecular Simulation Study, *The Journal of Physical Chemistry C*, 111 (2007) 1709-1715.
- [33] A.I. Kolesnikov, J.-M. Zanotti, C.-K. Loong, P. Thiyagarajan, A.P. Moravsky, R.O. Loutfy, C.J. Burnham, Anomalously Soft Dynamics of Water in a Nanotube: A Revelation of Nanoscale Confinement, *Phys. Rev. Lett.*, 93 (2004) 035503.
- [34] R. Mancinelli, The effect of confinement on water structure, *J. Phys.: Condens. Matter*, 22 (2010) 404213.
- [35] W.R. Bowen, J.S. Welfoot, Modelling of membrane nanofiltration—pore size distribution effects, *Chem. Eng. Sci.*, 57 (2002) 1393-1407.
- [36] P. Aimar, M. Meireles, V. Sanchez, A contribution to the translation of retention curves into pore size distributions for sieving membranes, *J. Membr. Sci.*, 54 (1990) 321-338.
- [37] N. García-Martín, V. Silva, F. Carmona, L. Palacio, A. Hernández, P. Prádanos, Pore size analysis from retention of neutral solutes through nanofiltration membranes. The contribution of concentration–polarization, *Desalination*, 344 (2014) 1-11.
- [38] S. Mochizuki, A.L. Zydney, Theoretical analysis of pore size distribution effects on membrane transport, *J. Membr. Sci.*, 82 (1993) 211-227.
- [39] A.L. Zydney, P. Aimar, M. Meireles, J.M. Pimbley, G. Belfort, Use of the log-normal probability density function to analyze membrane pore size distributions: functional forms and discrepancies, *J. Membr. Sci.*, 91 (1994) 293-298.
- [40] P. Dechadilok, W.M. Deen, Hindrance Factors for Diffusion and Convection in Pores, *Industrial & Engineering Chemistry Research*, 45 (2006) 6953-6959.
- [41] J.L. Anderson, J.A. Quinn, Restricted Transport in Small Pores: A Model for Steric Exclusion and Hindered Particle Motion, *Biophys. J.*, 14 (1974) 130-150.
- [42] M. G. Davidson, W. M. Deen, Hydrodynamic theory for the hindered transport of flexible macromolecules in porous membranes, *J. Membr. Sci.*, 35 (1988) 167-192.

- [43] V. Silva, P. Prádanos, L. Palacio, A. Hernández, Alternative pore hindrance factors: What one should be used for nanofiltration modelization?, *Desalination*, 245 (2009) 606-613.
- [44] P.M. Bungay, H. Brenner, The motion of a closely-fitting sphere in a fluid-filled tube, *Int. J. Multiphase Flow*, 1 (1973) 25-56.
- [45] W. Deen, Hindered transport of large molecules in liquid-filled pores, *AIChE J.*, 33 (1987) 1409-1425.
- [46] S.-I. Nakao, S. Kimura, ANALYSIS OF SOLUTES REJECTION IN ULTRAFILTRATION, *J. Chem. Eng. Jpn.*, 14 (1981) 32-37.
- [47] K.J. Keesman, *System identification: an introduction*, Springer Science & Business Media, 2011.
- [48] N.R. Draper, H. Smith, *Applied Regression Analysis*, Wiley, New York, 1966.

Chapter 4

Nanofiltration of concentrated oligosaccharide solutions – hydration and pore size distribution effects

This chapter is based on:

Victor Aguirre Montesdeoca, Anja E. M. Janssen, R. M. Boom , A. Van der Padt.
“Nanofiltration of concentrated oligosaccharide solutions – hydration and pore size distribution effects” *Submitted for publication.*

ABSTRACT

The effects of high concentration in the nanofiltration of a solution of oligosaccharides were investigated both experimentally and using a mass transfer model based on the Maxwell-Stefan equations. At high concentrations, negative retentions were found for the smaller sugars, which cannot be ascribed to effects of ionic interaction or membrane adsorption or fouling. Instead, the behaviour could be quantitatively described by incorporating the effects of the thermodynamic non-ideality of the solutions, and the effects of the pore size distribution. Experiments were performed to validate the model, using as feed an oligosaccharide mixture with a concentration up to a 35% w/w. The model predictions allows the identification of an optimum feed concentration for the purification of the oligosaccharides. The results show that nanofiltration of sugars can be well described and predicted, when taking into account the relevant thermodynamic interactions and the membrane pore size distribution.

4.1 INTRODUCTION

Nanofiltration (NF) applications are not restricted to water treatment, NF is increasingly used in the food and biotechnology industry for purification and concentration of streams. Its main advantages are its simplicity, low costs and eco-efficiency [1]. In order to seize this potential, a complete understanding of the involved mechanisms is required, becoming essential a mathematical representation of the process for proper design, control and optimization.

Various models have been derived to describe NF. They are often based on simplified considerations such as single solute mixtures and diluted conditions, with the Steric Pore Model and the Kedem-Katchalsky equations being the most common ones [2, 3]. Food streams, however, are complex non-ideal multicomponent solutions that frequently do not comply with the simplifications considered in the aforementioned models. Therefore, more rigorous considerations are needed for the development of a more realistic representation of the NF of complex food streams.

The combination of the multicomponent nature of food streams and the high solute concentration determines physicochemical interactions that make the system thermodynamically non-ideal [4]. In general, these interactions can be classified into three types: Interactions with the membrane, interactions between different solute molecules and interactions between solutes and solvent molecules. Many studies about the interactions with the membrane can be found in literature especially for separation of ionic solutions. The membrane charge is here normally used as a fitting parameter that depends on the nature and concentration of the solutes inside the membrane [2, 5, 6]. The other two types of interactions have received less attention and are often neglected by authors even when modelling systems at high concentrations [7, 8].

Only few filtration studies can be found in literature in which the effect of different solutes on each other is assessed. Van Oers et al. (1997) described the decrease in PEG rejection when combined with dextran in comparison with the rejection of PEG as single solute [9]. During these experiments, these authors even obtained negative rejection values for PEG under some specific conditions. Likewise, Bargeman et al. (2005) and Luo (2011) showed a decrease in the rejection of glucose when NaCl was added in the feed mixture [6, 10]. This influence of the solutes on each other rejection is not necessarily due to a direct interaction between solutes, but may also be caused by interactions between solutes and solvent, which in case of aqueous streams, can be ascribed to hydration [11, 12]. The hydration phenomena has a direct influence

on the effective size of the solute molecules and on the amount of free water in the system [11, 12]. In a recent study, we assessed the impact of hydration on the size of sugar molecules and on their permeation at diluted conditions [13]. At high concentrations, the effects of hydration on the system thermodynamics are expected to be larger [4].

We here therefore assess the effect of high concentrations on the performance of multicomponent NF systems. We develop a mathematical model based on the Maxwell Stefan Equations to account for the diffusive coupling effects between solutes in the concentration polarization layer. Experimental data is obtained using a fructooligosaccharides mixture with a range of polymerization degrees from 1 to 7 as feed, from which we aim to remove the mono- and disaccharides. All components of the mixture and the membrane are neutral, thus electrical interactions are ruled out of this study.

4.2 THEORETICAL ASPECTS

Membrane systems can be envisaged as two phases in equilibrium: the liquid phase and the membrane. The liquid phase includes the concentration polarization layer just in front of the membrane, in which the concentration of solutes is the highest and the system is thermodynamically non-ideal. Inside the membrane, the concentration is lower, and mass transfer may be assumed to take place through non-uniform cylindrical pores [2]. The concentration polarization layer and the membrane can be considered to be at thermodynamic equilibrium at the membrane interface.

4.2.1 Transport in the concentration polarization layer

In a multicomponent system, the pressure exerted over the system generates a flux of components (mostly water and small solutes) towards the permeate side of the membrane. As consequence, the concentration of the solutes, which are partially or totally retained by the membrane, increases at the membrane surface. This phenomenon is known as polarization and in diluted systems can be represented by the film model (Eq.4.1), which is derived from a solute mass balance over the thickness of the concentration polarization layer.

$$\frac{C_w - C_p}{C_b - C_p} = \exp\left(\frac{J}{k}\right), \quad (4.1)$$

in which J is the total flux through the membrane (mostly water), k is the mass transfer coefficient and C_w , C_b and C_p are the concentrations at the membrane surface, in the bulk of the retentate and in the permeate, respectively.

When the system is concentrated, the film model cannot be used anymore as it considers the solute fluxes to be independent of each other. In concentrated systems, diffusional coupling takes place and the transport of one solute is influenced by that of other solutes. Consequently, the so-called Maxwell-Stefan equations are much more suitable for concentrated multicomponent mixtures [14, 15]. These equations can be envisaged as a force balance in which the driving force exerted on a species is counteracted by the friction with all the other species present in the system. In this approach cross effects between components are considered, and thermodynamic considerations that account for the non-ideality can also be incorporated into the equations. Taylor and Krishna made a complete description of the Maxwell Stefan equations and their application [16].

A convenient way to present the Maxwell Stefan equations is shown in Eq. 4.2, in which the force balance in the concentration polarization layer for molecule i is described. Thus, the molecular diffusion in this layer can be represented by a set of $m - 1$ equations, m being the number of components (including water as component m). The left side of the equation represents the driving forces for solute i and the term at the right side represents the friction forces working over solute i . It is important to realize that the driving forces are expressed with the chemical potential gradient ($\nabla\mu_i$) and pressure gradient (∇P). x represents the solutes mole fraction, \bar{v} the molar volumes of the hydrated molecules and u are their linear velocities. \mathfrak{D}_{ij} is the Maxwell Stefan cross diffusion coefficient between species i and j [16].

$$x_i \left(\frac{1}{RT} \nabla_{T,P} \mu_i + \frac{\bar{v}_i}{RT} \nabla P \right) = - \sum_{\substack{j=1 \\ j \neq i}}^m \frac{x_i x_j (u_i - u_j)}{\mathfrak{D}_{ij}} \quad (4.2)$$

The chemical potential gradient has been worked out in Eq. 4.3 and it is shown that the mole fraction gradient of every solute has an effect on the driving force of molecule i . Additionally, the term containing the pressure gradient has been removed because the pressure is constant in the concentration polarization layer ($\nabla P = 0$). At the right side, the friction term has been adapted to molar fluxes (N), considering that $N_i = C_T x_i u_i$, in which C_T is the total molar concentration.

$$\sum_{j=1}^{m-1} \left(\delta_{ij} + x_i \frac{\partial \ln \gamma_i}{\partial x_j} \right)_{T,P} \frac{dx_j}{dz} = \sum_{\substack{j=1 \\ j \neq i}}^m \frac{(x_i N_j - x_j N_i)}{C_T \mathfrak{D}_{ij}} \quad (4.3)$$

The term inside brackets in the left side of Eq. 4.3 is known as the thermodynamic factor (Γ_{ij}), in which δ_{ij} is the Kronecker delta. Γ_{ij} is a function of the change in the solute activity coefficient γ_i and represents the interaction between species i and j . For ideal systems $\Gamma_{ij} = 0$ when $i \neq j$, meaning that no interaction takes place between species, and $\Gamma_{ij} = 1$ when $i = j$. Hence, in ideal systems, the driving force of molecule i is its own molar fraction gradient $\frac{dx_i}{dz}$ as shown in Eq. 4.4.

$$\sum_{j=1}^{m-1} \Gamma_{ij} \frac{dx_j}{dz} = \sum_{\substack{j=1 \\ j \neq i}}^m \frac{(x_i N_j - x_j N_i)}{C_T \mathfrak{D}_{ij}} \quad (4.4)$$

Kooijman and Taylor (1991) presented a relation (Eq. 4.5) to estimate the Maxwell-Stefan cross diffusion coefficients (\mathfrak{D}_{ij}) based on easily measurable binary diffusion coefficients (\mathfrak{D}_{im})[17]. The accuracy of this relation was found to be superior to other relations found in the literature; they were assessed in the work of Liu et al. using Equilibrium Molecular Dynamics simulations [18].

$$\mathfrak{D}_{ij}^{x_m \rightarrow 1} = \sqrt{\mathfrak{D}_{im}^{x_m \rightarrow 1} \mathfrak{D}_{jm}^{x_m \rightarrow 1}} \quad (4.5)$$

It is important to notice that even for aqueous concentrated systems, the molar fraction of component m (water) is still close to 1 due to the great difference in molecular weight between solutes and water. Therefore, $\mathfrak{D}_{im}^{x_m \rightarrow 1}$ is similar to the mutual diffusion (Fick) coefficient under diluted conditions D_i^∞ , which can be easily found in literature.

In order to numerically solve the Maxwell-Stefan equations, a uniform concentration polarization layer thickness (δ) should be considered for all the diffusing components. Depending on the system, the diffusivity of the fastest or the slowest species can be used in the calculation of the Sherwood number as described in Eqs. (4.6) – (4.9)[14].

$$\delta = \frac{d_h}{Sh} \quad (4.6)$$

$$Sh = 0.065 Re^{0.875} Sc_i^{0.25} \quad (4.7)$$

$$Re = \frac{\rho_r v d_h}{\eta_r} \quad (4.8)$$

$$Sc_i = \frac{\eta_r}{\rho_r D_i} \quad (4.9)$$

To calculate the hydraulic diameter d_h and the cross-flow velocity v in spiral wound membranes, the procedure presented by Schock and Miquel can be used [19]. ρ_r and η_r stand for the density and the viscosity of the retentate. D_i^∞ can be calculated using the empirical relation proposed by Sano and Yamamoto in 1992 (Eq. 4.10), which links D_i^∞ with the molecular weight of the sugar (Mw_i) [20].

$$D_i^\infty = \frac{T}{9.5 \cdot 10^{13} Mw_i^{1/3} \eta_{H2O}} \quad (4.10)$$

The viscosity in any part of the system can be calculated based on the composition of the mixture. Chirife et al. presented a simple viscosity relation (Eq.4.11) to calculate the viscosity of sugar solutions using the average molar mass of the mixture (Mw_{av}) and a parameter E . Parameter E can be calculated from a linear relation as it was done in a previous study [21] [22].

$$\eta = \eta_{H2O} \exp\left(E \sum_{i=1}^{m-1} x_i\right) \quad (4.11)$$

$$E = 0.162 Mw_{av} - 9.842$$

4.2.1.1 Thermodynamic non-idealities (Hydration).

It has been repeatedly described in literature that the non-idealities in concentrated sugar solutions up to 60° Brix can be explained by just considering the hydration effect on the solutes [11, 23, 24]. During hydration, sugars bind water molecules, ‘removing’ them from the solvent. As consequence of this reduction in the effective number of molecules, the activity coefficient of the solutes in the mixture increases. This is also known as “salting out effect”, and is commonly used to precipitate proteins by adding salts in a protein solution; the activity of the protein increases until it goes above its maximum solubility [25].

The activity coefficients (γ_i) of a solute can be related to its hydration by using Eq. 4.12, which is derived in detail in appendix A1. Here, h_f represents the hydration number of each segment of the oligosaccharides; s_i represents the number of segments (monomers) in the oligosaccharide chain. The fraction x_{seg} is the number (moles) of segments in the solution, divided by the overall number of moles (which makes it somewhat different from a mole fraction).

$$\gamma = \frac{1}{1 - h_f x_{seg}} \quad (4.12)$$

$$x_{seg} = \sum_{i=1}^{m-1} x_i s_i$$

The obtained value for γ holds for all the solutes in the mixture because all of them are influenced by the hydration effect in the same manner. In other words, sugar species with different degree of polymerization bind different numbers of water molecules, but the total number of bound water molecules affects the thermodynamics of all the components to the same extent. By taking the derivative with respect to x_{seg} , the following expression can be obtained.

$$\frac{\partial \ln \gamma}{\partial x_{seg}} = \frac{h_f}{1 - h_f x_{seg}} \quad (4.13)$$

The equation above can be used to modify the definition of the thermodynamic factor Γ_{ij} as it was defined in Eq. 4.3.

$$\Gamma_{ij} = \delta_{ij} + s_j \frac{\partial \ln \gamma_i}{\partial x_{seg}} x_i \quad (4.14)$$

Although C_T is usually considered constant in the Maxwell Stefan equations, when the polarization is high, C_T may differ significantly over the thickness of the concentration polarization layer. Eq.4.15 has been derived to estimate C_T using the local molar fractions. At the right hand side of the equation, the first term represents the volume occupied by all the hydrated sugars ($m - 1$ components) for 1 mol of mixture. The second term is the volume of the ‘non-removed’ (free) water for 1 mol of mixture. \bar{v}_i stands for the hydrated molar volume of the sugars and \bar{v}_m is the molar volume of water.

$$\frac{1}{C_T} = \sum_{i=1}^{m-1} x_i \bar{v}_i + \left(1 - \sum_{i=1}^{m-1} x_i - \sum_{i=1}^{m-1} x_i s_i h_f \right) \bar{v}_m \quad (4.15)$$

4.2.2 Interface

The concentration inside the pores is lower than on the outside due to the existence of an excluded volume adjacent to the pore walls that is not accessible to the centre of the incoming molecules [26]. This defines a partition with the membrane (φ) that, under diluted conditions, is exclusively dependent on the geometries of the pore and of the transient molecule. For spherical molecules and cylindrical pores, φ can be derived using Eq. 4.16 [27, 28]. Here r_i is

the radius of the transient molecule, which is normally represented by the Stokes radius when the molecule is spherical. In this case, since oligosaccharides molecules are elongated, an averaged radius r_G based on a capsular shape will be calculated; this approach is explained in detail in our previous study [29].

$$\varphi_i = \left(1 - \frac{r_i}{r_{pore}}\right)^2 \quad (4.16)$$

Under steady state conditions, local thermodynamic equilibrium is assumed to exist at the membrane interface. Hence, the chemical potential for each species is the same at the membrane surface (w) and just inside the pore ($'$) as represented in Eq. 4.17.

$$\mu_i^w = \mu_i' \quad (4.17)$$

$$RT \ln a_i^w = RT \ln a_i'$$

$$a_i^w = a_i'$$

$$x_i^w \gamma_i^w = x_i' \gamma_i'$$

These also apply to the other side of the membrane at the interface with the permeate stream (p). Consequently, the membrane can be regarded as a different phase, in which, due to the excluded volume near the pore wall, the solutes have a higher activity coefficient than in the surrounding aqueous phases and, therefore, a lower molar fraction. Thus, φ can also be defined as the ratio between the activity coefficients at both sides of the interface (Eq.4.18). Under diluted conditions, the value for the activity coefficient inside the pore γ_i' can be estimated from φ as shown in Eq. 4.19.

$$x_i^w \left(\frac{\gamma_i^w}{\gamma_i'}\right) = x_i' \quad (4.18)$$

$$\varphi_i = \left(\frac{\gamma_i^w}{\gamma_i'}\right); \text{ diluted } \gamma_i^w \approx 1 \therefore \gamma_i' = \frac{1}{\varphi_i} \quad (4.19)$$

Many studies have reported that at concentrated conditions, the partitioning of a molecule in a non-adsorbing porous interface is not constant, but concentration-dependent [26, 30]. Even when solute molecules do not attract or repel each other, two mechanisms can still produce a change in the partitioning. The first mechanism is related with the fact that molecules always interact due to their mutual impenetrability. This short-range ordering effect gets more pronounced inside the pores due to the constriction [26, 31, 32]. The second mechanism refers to the interaction of the solutes with the solvent and its effect on the thermodynamics of the system. This last effect, in contrast, is more pronounced outside the membrane, where the

concentration of solutes is higher, determining a higher value for γ_i^w than γ_i^p in the permeate [24]. Considering the fact that the membrane rejects most of the solutes, the solution inside the pores is assumed to be diluted. Therefore, only the second mechanism is considered in this study. As consequence, unlike in diluted conditions, partition coefficients in concentrated conditions are expected to be different at both membrane interfaces.

4.2.3 Transport inside the membrane pores

The transport inside the NF membrane is analysed porewise, assuming that pores are straight and cylindrical. The model should take into account the effect of osmotic pressure and the effect of high concentrations on the partition coefficients. Since the solution inside the pores is considered to be diluted, non-idealities and cross effects between solutes can be neglected. Therefore, γ_i' is constant, and hence $\partial \ln \gamma_i' / \partial \ln x_i$ is zero, so $\Gamma_i = 1$. The resulting binary Maxwell-Stefan Equation between species i and m (water) derived from Eq. 4.2 gets simplified as follows:

$$\frac{dx}{dz} + \frac{x_i \bar{v}_i}{RT} \frac{dP}{dz} = - \frac{x_i x_m (u_i - u_m)}{\mathfrak{D}_{im}} \quad (4.20)$$

We can work out Eq. 4.20 further by considering that at these conditions $x_m \approx 1$. \mathfrak{D}_{im} should be corrected to calculate an effective diffusivity inside the pore $D_{p,i}$. Likewise, the solution velocity (approximated here to water velocity u_m) should also be corrected with a convection hindrance factor K_c to consider the flow inside the pore.

$$x_i u_i = K_c x_i u_m - D_{p,i} \frac{dx_i}{dz} - D_{p,i} \frac{x_i \bar{v}_i}{RT} \frac{dP}{dz} \quad (4.21)$$

Due to the principle of mass conservation, the flux of solutes inside the pore is similar to the flux of solutes in the permeate just outside the pore, thus: $C_T x_i u_i = C_{Tp} x_{p,i} u_p$. Assuming that $C_T \approx C_{Tp}$, and considering that the velocity of species i in the permeate (just outside the pore) is similar to that of water ($u_p = u_m = u$), we obtain:

$$x_{p,i} u = K_{c,i} x_i u - D_{p,i} \frac{dx_i}{dz} - D_{p,i} \frac{x_i \bar{v}_i}{RT} \frac{dP}{dz} \quad (4.22)$$

At the right side of the Eq. 4.22, the first term represent the transport due to convection, in which x_i is the local molar fraction and u is the solution velocity. u can be estimated using the Hagen-Poiseuille relation (Eq. 4.23). This relation describes convection of a liquid through a

cylindrical tube with laminar flow. Here, r represents the pore radius and dP_e is the effective pressure over the pore. A negative sign should be included in this definition considering that ΔP_e is negative in the direction of u (see Figure 4-1B).

$$u = \frac{r^2}{8\eta} \left(-\frac{dP_e}{dz} \right) = -\frac{r^2 \Delta P_e}{8\eta \Delta z} \quad (4.23)$$

The second term in Eq. 4.22 is the diffusion term, in which D_p is the diffusion coefficient inside the pore. To estimate it, Eq. 4.24 can be used, in which the effect of the diffusion hindrance (K_d) and the increment in viscosity due to the confinement of water is considered (Eq. 4.25). Here d is the thickness of the layer of water with increased viscosity that is estimated to be 0.28 nm.

$$D_{p,i} = K_{d,i} D_i^\infty \frac{\eta}{\eta_0} \quad (4.24)$$

$$\frac{\eta}{\eta_0} = 1 + 18 \left(\frac{d}{r} \right) - 9 \left(\frac{d}{r} \right)^2 \quad (4.25)$$

The third term of Eq. 4.22 is the pressure effect in the transport. Under diluted conditions, this is for the solutes ($i \neq m$) the least important transport mechanism in membrane filtration processes.

The meaning and relevance of the hindrance factors (K_c and K_d) were reviewed by Deen (1987) [34]. The chosen expressions to calculate these hindrance coefficients must be applicable to any λ value from 0 to 1 ($\lambda = r_i/r_{pore}$). This is critical when taking into account pore size distributions in the model. The expression for K_c can be taken from Dechadilok and Deen (2006) [35] and the equation for K_d can be obtained from the work of Bungay and Brenner (1973) [36]. Eqs. 4.26 and 4.27 were developed for spherical solutes; in the case of elongated molecules (as in this study), K_c can be considered equal to 1 for molecules bigger than DP3 [37], and K_d can only be roughly estimated using the Stokes radius (r_s) as done in our previous study [29].

$$K_c = W(\lambda)/\varphi \quad (4.26)$$

$$W(\lambda) = (1 - \lambda)^2 \left(\frac{1 + 3.867\lambda - 1.907\lambda^2 - 0.834\lambda^3}{1 + 1.867\lambda - 0.741\lambda^2} \right)$$

$$K_d = \frac{6\pi}{K_t} \quad (4.27)$$

$$K_t = \frac{9}{4} \pi^2 \sqrt{2} (1 - \lambda)^{-\frac{5}{2}} \left[1 + \sum_{n=1}^2 a_n (1 - \lambda)^n \right] + \sum_{n=0}^4 a_{n+3} \lambda^n$$

$$a_1 = -\frac{73}{60}, a_2 = \frac{77.293}{50.400}, a_3 = -22.5083, a_4 = -5.6117, a_5 = -0.3363,$$

$$a_6 = -1.216, a_7 = 1.647$$

To solve Eq. 4.22 a procedure similar to the one of Bowen and Welfoot with the Steric Pore Model was followed [2, 33]. Thus, after linearizing $\frac{dP}{dz}$ in Eq. 4.22, an expression for $\frac{dx_i}{dz}$ can be obtained (Eq. 4.28). Here a new variable Y_i , which is considered constant along the thickness of the membrane, has been defined. Y represents the contribution of the pressure gradient in the transport of each solute.

$$\frac{dx_i}{dz} = \frac{u}{D_{p,i}} [(K_{c,i} - Y_i)x_i - x_{p,i}] \quad (4.28)$$

$$Y_i = \frac{D_{p,i} \bar{v}_i}{RT V} \frac{dP}{dz} = -\frac{8\eta D_{p,i} \bar{v}_i}{RT r^2} \frac{\Delta P}{\Delta P_e} \quad (4.29)$$

It is important to emphasize that under concentrated conditions $\Delta P \neq \Delta P_e$, because ΔP_e is a function of the osmotic pressure (Π), which counteracts the effect of ΔP as shown in Eq. 4.30 and in Figure 4-1. Thus, on the one hand, the solutes transport due to the pressure gradient ΔP is constant, while on the other hand, the convective transport of solutes is affected by the osmotic pressure generated due to the difference in the concentration of solutes at both sides of the membrane. Therefore, it is expected that the importance of the three different transport mechanisms inside the membrane changes depending on the feed concentration (Π_w and Π_p being the osmotic value on the feed side on the membrane surface and on the permeate side, respectively).

$$\Delta P_e = \Delta P - \Delta \Pi = \Delta P - (\Pi_w - \Pi_p) \quad (4.30)$$

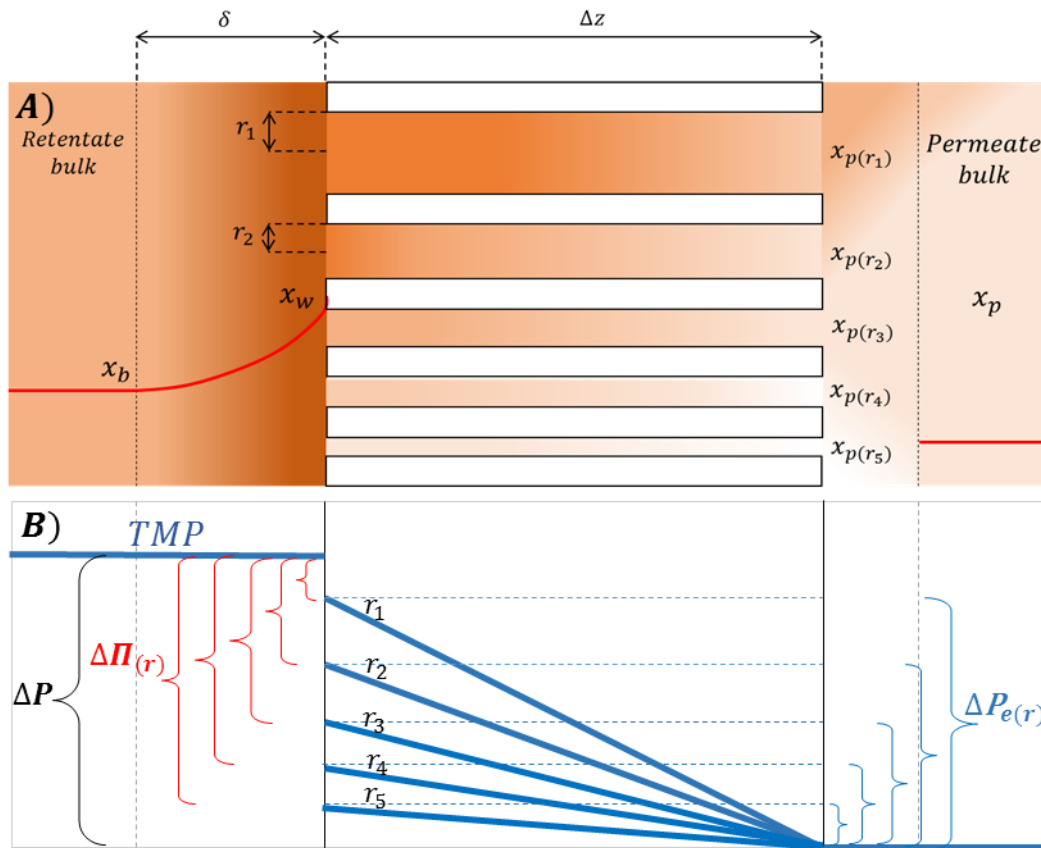


Figure 4-1. Schematic representation of the solute concentration (A) and the pressure profiles (B) over the NF system as described by the model. Both figures show the variables for different pore sizes.

As shown in Figure 4-1, the analysis presented here is for one particular pore, so independency between pores is assumed. At the permeate side of the pores, different compositions are expected depending on the pore diameter and, consequently, different osmotic pressure differences are generated over pores with different diameters. Larger osmotic pressure difference originates over smaller pores, resulting in a lower effective pressure.

To calculate $\Delta\Pi$, it is necessary to know the composition at the membrane and permeate sides of every pore size. These compositions yield the water activity (a_{H_2O}) using Eq. 4.31, which has been derived in detail in the appendix section (A2). The osmotic pressure compared to pure water Π can then be calculated using Eq. 4.32 [25].

$$a_{H_2O} = \frac{x_{H_2O} - hx_{seg}}{1 - hx_{seg}} \quad (4.31)$$

$$\Pi = -\frac{RT}{\bar{v}_{H_2O}} \ln a_{H_2O} \quad (4.32)$$

x_i can be integrated (from Eq. 4.1) over the thickness of the membrane using the boundary conditions given in Eq. 4.33, in which two different partition coefficients are defined. They depend on the activity coefficients at both sides of each interface as shown in Eq. 4.19. Additionally, a modified version of the Péclet number Pe'_i has been used in the derivation to group some variables (Eq. 4.34). As a result, an expression for the porewise permeate mole fraction $x_{i,p(r)}$ can be obtained (Eq. 4.35).

$$x_0 = \varphi_{w,i} x_{w,i} \quad (4.33)$$

$$x_{end} = \varphi_{p,i} x_{p,i}$$

$$Pe'_i = \frac{V}{D_{p,i}} \Delta z (K_{c,i} - Y_i) = -\frac{r^2 \Delta P_e}{8\eta D_{p,i}} (K_{c,i} - Y_i) \quad (4.34)$$

$$x_{i,p(r)} = \frac{(K_{c,i(r)} - Y_{i(r)}) \varphi_{w,i} x_{w,i} \exp(Pe'_{i(r)})}{(K_{c,i(r)} - Y_{i(r)}) \varphi_{p,i(r)} - 1 + \exp(Pe'_{i(r)})} \quad (4.35)$$

$x_{p,i(r)}$ is not the mole fraction of i in the permeate stream, but corresponds to the mole fraction of i just outside the membrane, at the permeate side, for only one specific pore size r as it is sketched in Figure 4-1A. This implies that the values of many variables of the model depend on the pore size. To calculate the overall concentration of i in the permeate stream $C_{p,i}$, the frequencies of the pore size distribution f_R should be considered as shown in Eq. 4.36 [33].

$$C_{p,i} = \frac{\int_0^\infty \frac{f_R(r) r^4 C_{T,p(r)} x_{p,i(r)} \Delta P_{e(r)}}{\eta(r)} dr}{\int_0^\infty \frac{f_R(r) r^4 \Delta P_{e(r)}}{\eta(r)} dr} \quad (4.36)$$

As it is shown in Eq. 4.37, f_R is defined, assuming a log normal distribution, by two parameters: the mean radius r^* and the standard deviation σ .

$$f_{R(r)} = \frac{1}{r\sqrt{2\pi b}} \exp\left\{-\frac{\left[\ln(r/r^*) + \frac{b}{2}\right]^2}{2b}\right\} \quad (4.37)$$

$$\text{where } b = \ln \left[1.0 + \left(\frac{\sigma^*}{r^*} \right)^2 \right]$$

4.2.4 Flux calculation

As can be seen in Eq.4.3, to solve x_i along the concentration polarization layer, the solute fluxes (N_i) must be known. An extra relationship, known as ‘bootstrap’, linking the fluxes and the molar fractions, is needed to solve the system of Maxwell-Stefan Equations [16]. Eq. 4.38 can be used for this purpose.

$$N_i = x_{i,p} N_T \quad (4.38)$$

To calculate the total molar flux (N_T), Eq. 4.39 can be used, for which the value of the total volumetric flux (J_v) is needed. As shown in Eq.4.40, J_v cannot be calculated in advance because it is a strong function of the pore-dependent effective pressure $\Delta P_{e(r)}$. As consequence, an iterative procedure is required to solve J_v starting from an educated guess.

$$N_T = J_v C_{T,p} \quad (4.39)$$

$$J_v = P_n \pi \int_0^\infty f_{R(r)} V_{(r)} r^2 dr = \left(\frac{P_n}{\Delta z} \right) \frac{\pi}{8} \int_0^\infty \frac{f_{R(r)} r^4 \Delta P_{e(r)}}{\eta(r)} dr \quad (4.40)$$

J_v also depends on two unknown parameters: The number of pores per square meter of membrane surface area (P_n) and the thickness of the active layer of the membrane (Δz) [33]. Nevertheless, these two parameters can be conveniently lumped in one: $\frac{P_n}{\Delta z}$. This is a geometric parameter (constant) of the membrane that, when the membrane pore size distribution is known, can be calculated from experimental data using the pure water flux.

4.3 MATERIALS AND METHODS

4.3.1 Chemicals

Demineralised water was used in every experiment. The fructo-oligosaccharides mixture Frutalose® L85 (batch: 8554908001) was kindly provided by Sensus (Roosendaal, The Netherlands). This mixture is a viscous, clear syrup with a concentration of 75°Brix, composed of mono, di and oligo-saccharides with DP of up to 10. Its composition on dry basis is shown in Table 3-2.

Table 4-1. Composition on dry basis of fructooligosaccharides mixture (Frutalose® L85) and other properties of the sugars at 45°C.

Component	% [w/w]	D_i^∞ [$10^{-10} \text{ m}^2/\text{s}$]	\bar{v}_i ($10^{-4} \text{ m}^3/\text{mol}$)	r_G^* (10^{-10} m)
DP1	6.1	10.05	1.79	4.14
DP2	7.6	8.13	3.03	5.99
DP3	28.8	7.16	4.36	7.85
DP4	22.5	6.53	5.64	9.70
DP5	16.9	6.08	6.92	11.55
DP6	12.2	5.73	8.20	13.40
DP7	5.9	5.45	9.49	15.26

* average radius calculated according to our previous study [29], DP = Degree of polymerization

4.3.2 Membrane

A thin film composite (thin polyamide layer deposited on top of polysulfone porous layer), spiral wound GE membrane (GE Osmonics, Sterlitech, Kent – WA, United States) was used for all the experiments. The pore size distribution of this nanofiltration membrane was determined in our previous study [29], and the lumped parameter $\frac{P_n}{\Delta z}$ was estimated to be 1.53×10^{13} pores/ m^3 using Eq. 4.40. These, among other membrane specifications, are shown in Table 3-3. The experiments were performed in a pilot scale filtration system that included heat exchangers in the feed tank and in the recirculation loop of the retentate. The flow, temperature, brix and pressure of both retentate and permeate streams were monitored by computer (using DDE software from Labview).

Table 4-2. Specifications of GE nanofiltration membrane

Membrane specifications	GE
Model	1812C-34D
Type	Spiral wound
Manufacturer	General Electric
Membrane material	TFM
MWCO (declared by manufacturer)	1000 Da
Membrane area	0.32 m ²
Spacer height*	8.60 x 10 ⁻⁴ m
Spacer porosity*	0.93
Maximum temperature	50°C
Pore size distribution [29]*	$r^*=1.29\text{nm}$, $\sigma=0.17$
$P_n/\Delta Z^*$	1.53x10 ¹³ pores/m ³

*Membrane characteristics measured in our lab.

4.3.3 Experiments at high concentrations

Experiments using the fructooligosaccharides mixture at different concentrations (0.5% - 35% w/w) were performed using the GE membrane. The retentate and permeate streams were recycled back to the feed tank, and once the system reached steady state (constant permeate flux and Brix), samples were taken from both streams simultaneously. Table 4-A summarizes the process conditions for all the experiments. All runs were performed at 45°C to mimic industrial conditions and to avoid microbial growth. The retentate recirculation flow was 150 L/h with a crossflow velocity of 0.088 m/s in the membrane module.

Table 4-3. Experimental process conditions

Concentration %(w/w)	Pressure [bar]
0.5%	2.5, 7.5, 10, 12.5, 15, 17.5, 20.
5%	8, 12, 16, 20, 24.
10%	20.
20%	10, 12, 14, 16, 18, 20, 22.
25%	12, 14, 16, 18, 20, 22.
30%	20.
35%	16, 20, 24

4.3.4 Model assumptions

The complexity of the multicomponent concentrated system was alleviated by key assumptions that enable the resolution of the model.

- In the concentration polarization layer, a uniform layer thickness (δ) was used for the integration of the molar fraction of all the solutes. As the concentration profiles of larger solutes are steeper than those of small solutes, modelling the transport of the larger solutes is more sensitive to δ . Therefore, δ was calculated (Eqs. 4.6 to 4.9) using the diffusivity of the largest solute in our mixture (DP7).
- Since inside the membrane the concentration of solutes is low (most of them are retained by the membrane), the value calculated for γ'_i using Eq. 4.19 was considered constant along the length of the pores. In other words, only the excluded volume due to the pore wall was considered in the calculation of γ'_i , while the effects of hydration were neglected. Conversely, the values of γ_i^w and γ_i^p were calculated considering the effect of hydration according to their local composition using Eq. 4.12.
- The concentrations of the solutes just before the membrane $C_{w,i}$ were assumed similar for all pore sizes, as sketched in Figure 4-1. Transversal diffusion and even convection over the membrane surface ensure that local differences are evened out. The effect of different pore sizes is reflected only in the mole fraction inside the pores $x_{i(r)}$ and in the permeate just outside the pore $x_{p,i(r)}$.

4.3.5 Prediction of the permeate flux and permeate concentrations (algorithm)

The model was created using the equations given in section 4.2 and the aforementioned assumptions. The model inputs are the process conditions (solute concentrations in the retentate and the applied TMP), the membrane pore size distribution and the structural membrane parameter $\frac{P_n}{\Delta z}$ (Eq. 4.40). Figure 4-2 shows the algorithm for the resolution of the model.

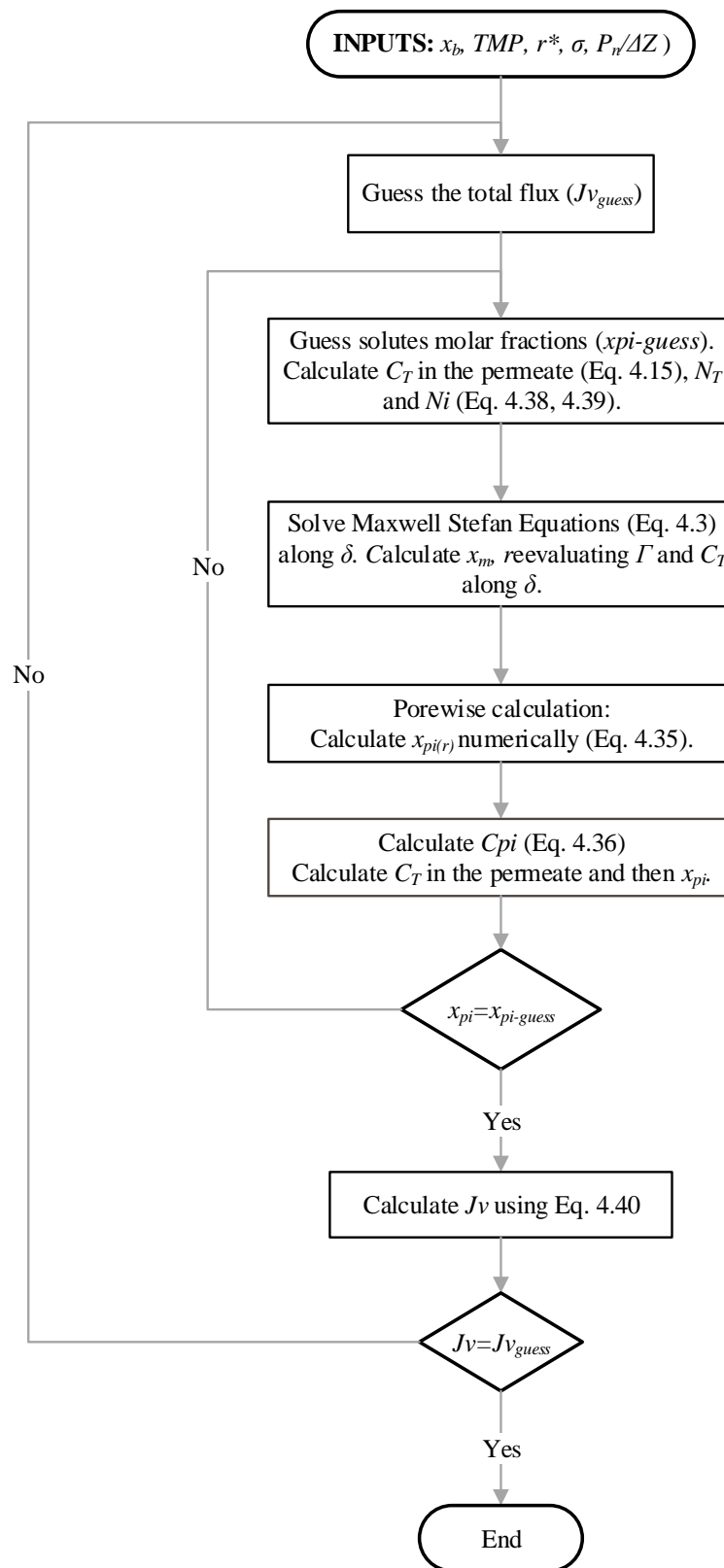


Figure 4-2. Algorithm for the resolution of the multicomponent model for concentrated conditions.

4.3.6 Analytical methods

The concentration of the different sugars in the oligosaccharides mixture was measured using ion exchange chromatography, using a method based on the study of Campbel et al. (1997) [38]. The Dionex column Carbopac PA-100, 250 x4.6mm + guard was employed at 20°C. Three eluents were used: Demineralised water, 0.25M NaOH and 0.65M NaOAc at a flow rate of 1mL/min. The detection was performed with an electrochemical detector (Dionex ED-40, range 500 nC, pulse train 2).

4.3.7 Computational analysis

MATLAB R2017b was used for all the calculations. Numerical integrations were performed using the function 'integral'. The numerical procedure to find J_v and x_{pi} was done with the function 'fsolve', which is a solver for systems of non-linear equations that uses the 'trust-region-dogleg' algorithm. To solve the Maxwell Stefan equations, the function ode15i was used, which allows to solve systems of implicit differential equations.

4.4 RESULTS AND DISCUSSION

Experiments with the oligosaccharide mixture up to a feed concentration of 35% (w/w) were performed at different TMPs. It was found that, for each pressure, the rejection of all the solutes decreased (especially DP1-2) as the concentration in the feed increased. At feed concentration of 20% w/w and higher, negative rejections were observed for DP1 sugars. Figure 4-3 shows a comparison of the observed rejection as a function of applied TMP at different feed concentrations. One can observe that up to a concentration of 25%, the decrease in the rejection of solutes was more notorious for the smaller molecules DP1 and DP2, represented in red in Figure 4-3. At 35%, there was a pronounced decrease in the rejection of the bigger molecules of the mixture, while the rejection of DP1 molecules remained stable. The complete experimental rejection data can be found in the appendix (A3).

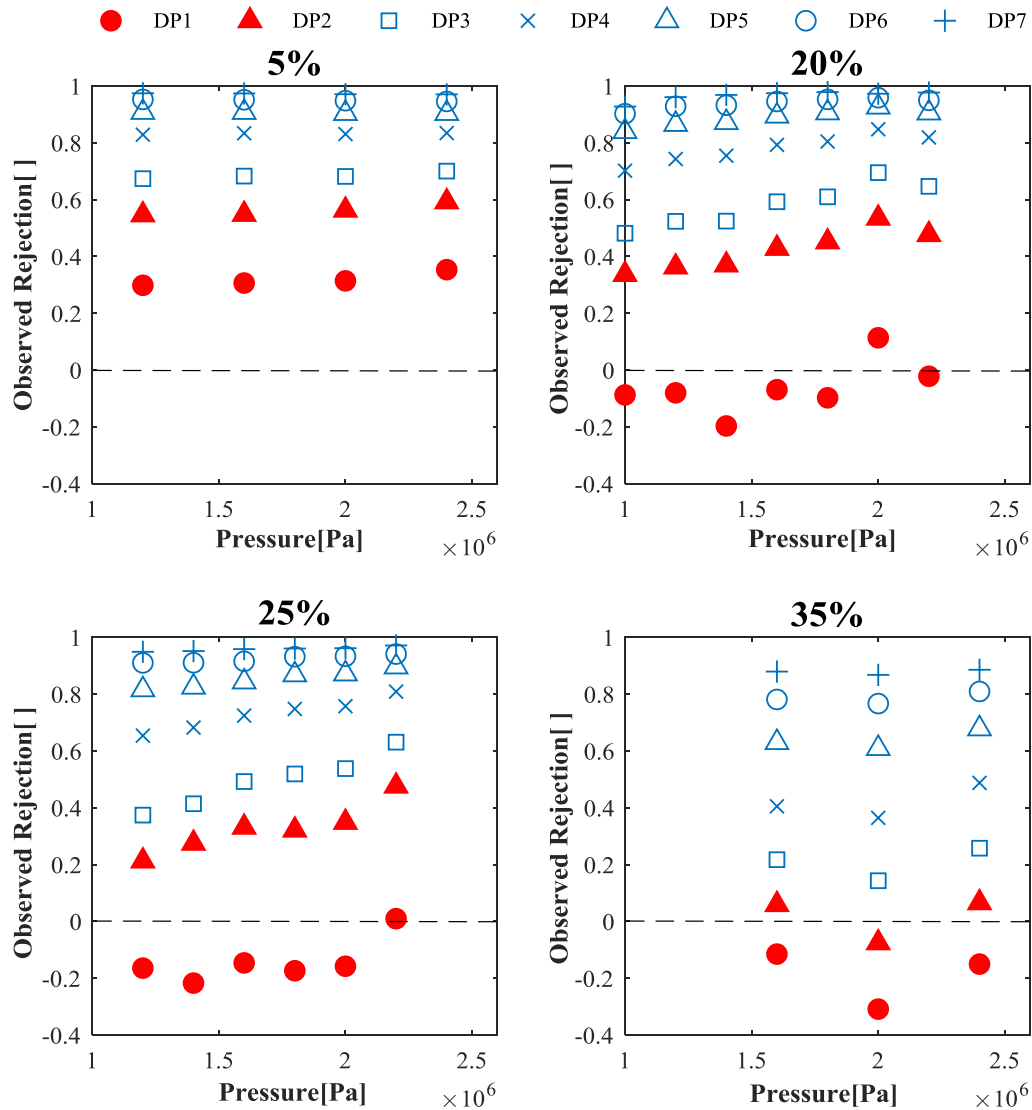


Figure 4-3. Observed rejection as function of pressure for nanofiltration experiments at feed concentrations 5, 20, 25 and 35% w/w. The rest of the process conditions were similar in all experiments (crossflow velocity =0.088m/s, $T=45^{\circ}\text{C}$). The concentration units used for the calculation of rejection were g/Kg.

The observation of negative rejections has been ascribed to different effects [9, 39].

- (1) Negative rejections have been linked by some authors to selective ionic transport and electrical interactions with the membrane [40]. In our case, we can rule out the possibility of electrical interactions because only neutral solutes are used in this study.
- (2) Likewise, we consider membrane adsorption and fouling unlikely due to the flux stability over time, which is supported by the complete recovery of the original water permeability after a short rinsing step.

(3) We also made sure that the reduction in rejection was not produced merely by the decrease in permeate flux at high concentrations. By comparing experiments with similar permeate flux one can observe that the reduction in hydrodynamic drag, produced by the permeate flux decrease, cannot explain the magnitude of the reduction in rejections. Lower fluxes cannot possibly explain the negative rejections obtained for the DP1 molecules.

We therefore conclude that the thermodynamics of our system, specified for each particular pore size is required to explain our observations.

As described in sections 4.2.1-4.2.3, hydration effects and a porewise representation of the conditions inside the membrane were incorporated in our model. The comparison between the permeate concentrations predicted by our model and the measurements from experiments, under different process conditions, is shown in Figure 4-4. The match is quite satisfactory, becoming less accurate only at very high permeate concentrations. Further discussion on the relevant mechanisms that make these predictions possible is presented in the next sections.

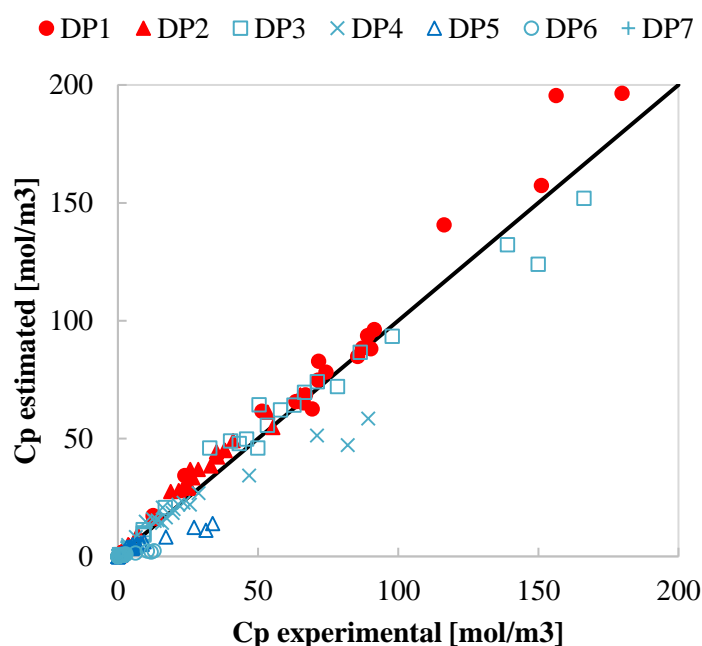


Figure 4-4. Comparison between estimated and experimental data on permeate concentration.

4.4.1 Thermodynamic effects

At the sugar concentrations used in this study, hydration is the most relevant thermodynamic phenomenon [11, 23, 24]. The strong interaction between the hydroxyl groups of the sugar molecules and water molecules ‘removes’ free water from the solution, increasing the chemical

activity (a) of the water. Therefore, less water is available for other solutes, which also increases their activity. This translates to an increase in the activity coefficient, considering that $a_i = x_i \gamma_i$. Since the hydration of all sugar segments is assumed to be the same, as was discussed in section 4.2.1.1, the value of the activity coefficient of all solutes has to be the same.

Figure 4-5 shows the results obtained by solving the Maxwell Stefan Equations in the concentration polarization layer, in which the activity coefficient increases along the layer thickness due to the increment in the concentration of solutes. The value of γ increases from 1.13 to 1.18 over a layer thickness of $56 \mu\text{m}$. It is important to notice that γ is not equal to 1 at the point $\delta=0$ since the effect of hydration is already relevant at the concentration in the bulk of the retentate ($\approx 25\% \text{w/w}$).

The resulting increase in the activities of the solutes enhances the diffusion of the solutes back towards the bulk of the retentate. Consequently, if we would have neglected this effect, the estimates of the solute fluxes would have been too high.

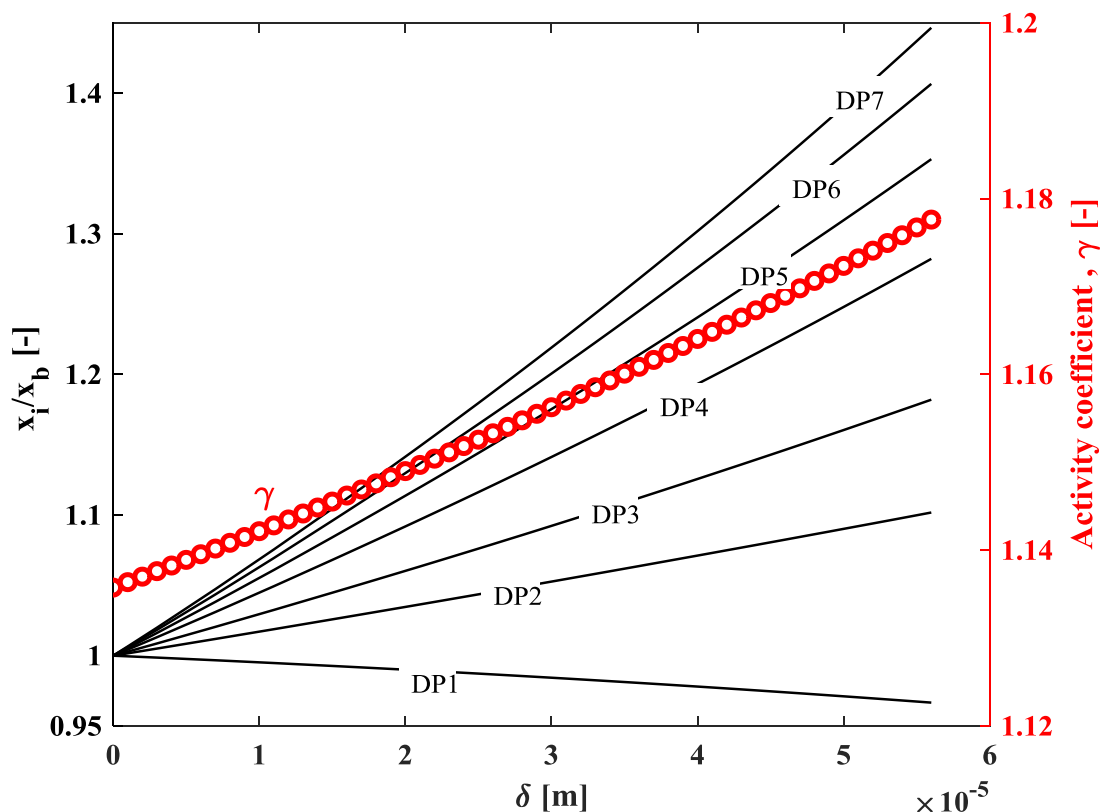


Figure 4-5. Concentration profiles and solutes activity coefficient along the thickness of the concentration polarization layer. Prediction corresponds to the following process conditions: 25% w/w and $\text{TMP} = 20 \text{ bar}$.

The effect of hydration becomes more important at the membrane interface, which is relevant for the partitioning of the solutes and thus for the rejections. As shown in Eq.4.17, at local thermodynamic equilibrium, the activity of the solutes at both sides of the interface must be the same ($x_i^w \gamma^w = x_i' \gamma_i'$). Since the concentration of solutes inside the pores of the membrane is low, γ_i' remains constant and not affected by the 'external conditions'. As consequence, an increment of γ^w causes an increment in x_i' , and thus a higher partition coefficient. As γ^w is the same for all the solutes, this increment of the partition is proportionally similar for all the solutes. Nevertheless, the increment it is larger for the smaller solutes since they have a lower activity coefficient γ_i' inside the pores (see Eq.4.19). Figure 4-6 shows how the partition coefficient of a DP1 molecule depends on the feed concentration and on the pore size. The effect of high concentration is more notorious in the larger pores because there γ_i' is lower. We must keep in mind, however, that the solute concentration in these pores is larger than in the smaller pores, and therefore our assumption of a constant γ' in these larger pores is less accurate at concentrated conditions [26, 30].

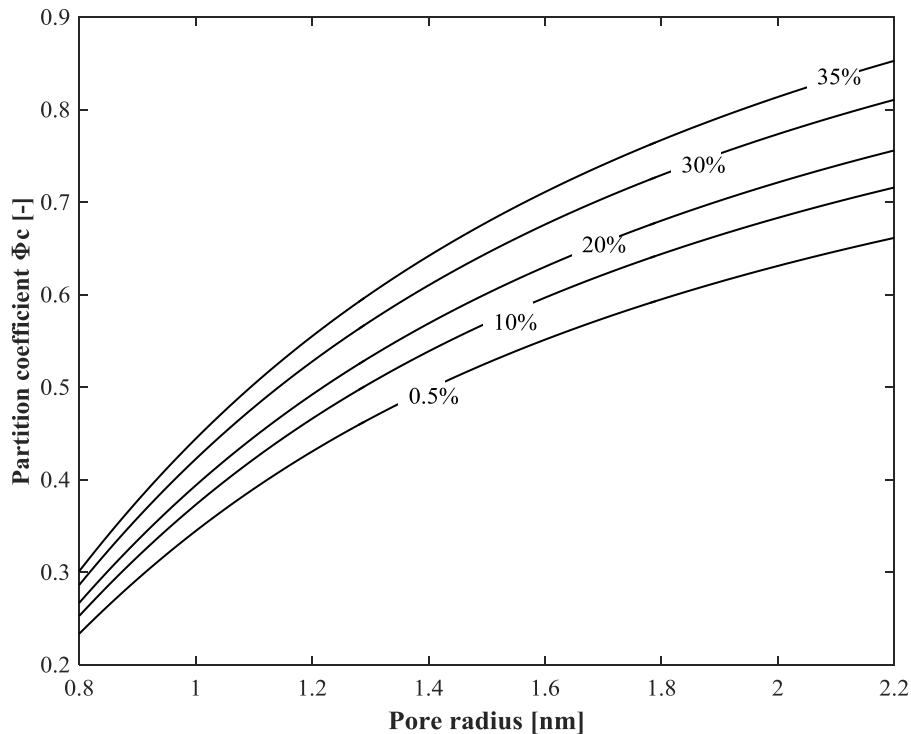


Figure 4-6. Partition coefficient of DP1 molecules as a function of pore size for different retentate concentrations. These prediction were generated by our model using a TMP of 20 bar.

By using our model, activities and molar fractions can be calculated at any point in the system. These two variables for a DP1 molecule were compared under diluted and concentrated conditions (Figure 4-7). In the case of a diluted feed, the activity and the molar fractions have the same value, since it is thermodynamically ideal ($\gamma \approx 1$ in the feed and permeate). Thus, there is no interaction between the solutes due to hydration, and the solute fluxes are independent of each other.

On the other hand, at high concentrations, because of the hydration phenomena, the activity increases, reaching its maximum at the membrane surface (at the retentate side). Under these conditions, something noteworthy occurs in the concentration polarization layer: The molar fraction and the activity gradient for DP1 have different sign. This is only possible because of the presence of other solutes that bind water, thus making water less available near the membrane. Darken and other authors have reported this type of situations in complete different of systems (e.g. diffusion of carbon in austenite bars) [41-43]. They agreed in the importance of considering the chemical potential gradient as the truly driving force for diffusion.

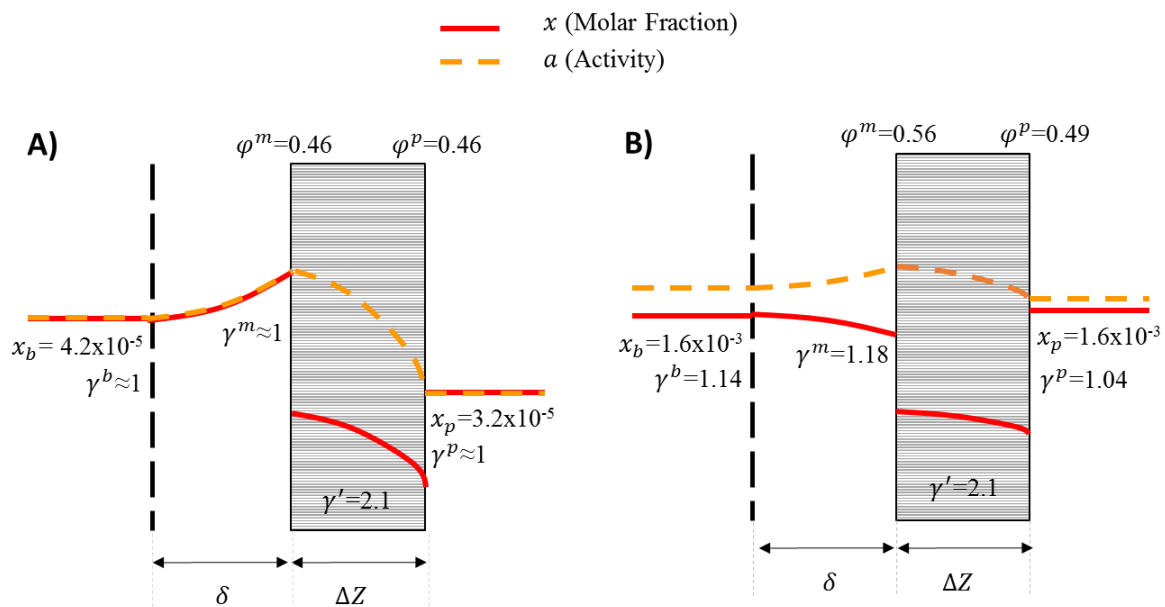


Figure 4-7. Concentration and activity profiles for DP1 over the nanofiltration system at diluted (A) and concentrated conditions (B). The feed concentration in was 0.5% w/w in A and 35% w/w in B. The rest of the process parameters were similar (TMP=20 bar, 45°C).

At concentrated conditions, the partition coefficients are different at both sides of the membrane. Since γ^w is higher than γ^p , and γ' is constant, a higher φ value originates at the membrane interface that is in contact with the concentrated phase. Additionally, the molar fractions of DP1 were similar in the retentate and permeate, determining a rejection of zero. The same rejection calculated with concentration units g/Kg was around -0.3 due to the difference in C_T in the permeate and retentate stream. Finally, it is also remarkable in Figure 4-7 the different way how the concentration profiles evolve along the membrane, even when, for modelling purposes, no thermodynamic considerations were made inside the membrane pores. This is discussed further in the next sections.

4.4.2 Pore size distribution effects.

Apart from the hydration effects, the model allows us to analyse the effects of the pore size distribution in concentrated systems. Figure 4-6 illustrates that some variables inside the model vary depending on the pore size. This brings up the question about the importance of the distribution of pore sizes under concentrated conditions.

Figure 4-8 shows the pore size distribution based on the volumetric flux through the pores. This calculation was made using a $\frac{P_n}{\Delta z}$ value of 1.53×10^{13} pores/m³, which we estimated from flux measurements using pure water. The overall flux decreases as the concentration of the feed goes up. This decrease is, however, not similar for every pore size, but more prominent for smaller pores because the difference in osmotic pressure over these pores is larger than that over bigger pores, as illustrated in Figure 4-1. Therefore, the shape of the distribution get slightly skewed to the left, increasing the importance of the transport through the biggest pores.

The volumetric flux (J_v) is a very strong function of the pore radius (Eq.4.40), which means that the big pores are dominant in the overall separation. This can also be seen by comparing the mean radius under different circumstances. The mean radius r^* , based on the number of pores (frequencies), is 1.29 nm. For the same membrane the mean radius based on the volumetric flux is 1.39 nm at a retentate concentration of 0.5% and 1.46 nm at 35% w/w. Therefore, under concentrated conditions, the transport through the bigger pores becomes even more important, which causes the rejection of all solutes to decrease since the larger pores impose less size exclusion.

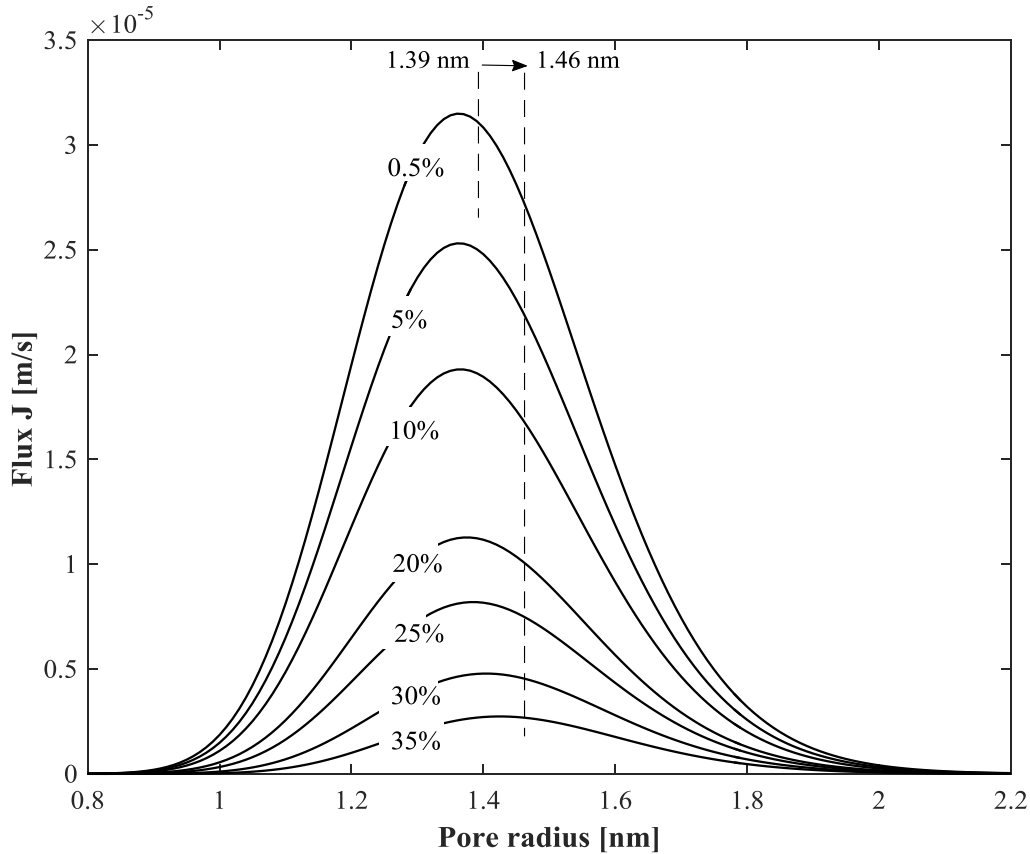


Figure 4-8. Pore size distribution based on the porewise volumetric flux at a TMP of 20 bar. Dashed lines represent the mean pore size for the distributions at a feed concentration of 0.5% and 35% w/w.

The predictions for J_v were calculated by integrating the porewise volumetric flux curves (Eq. 4.40), such as the ones shown in Figure 4-8. A very good match between the experimental data and predictions were found for all the performed experiments (Figure 4-9). As expected, higher accuracy was obtained at diluted conditions where the effects of osmotic pressure and increased viscosity are still not relevant. At higher concentrations, the model tends to slightly overestimate the flux, probably due to the small overestimation of the permeate concentrations (Figure 4-4), which increases the effective pressure over the membrane. Consequently, even better predictions may be attained if hydration effects inside the membrane would be considered. These effects would increase the value of γ'_i , reducing the concentration of solutes inside the membrane and in the permeate.

It was not experimentally feasible to perform experiments at retentate concentrations higher than 35% w/w with a TMP of 20 bar since the obtained fluxes were too small to be accurately measured. Similarly, model-wise, it was not possible to obtain predictions at higher

concentrations since the obtained porewise volumetric fluxes were negative for narrow pore sizes and convergence was not attained using our algorithm.

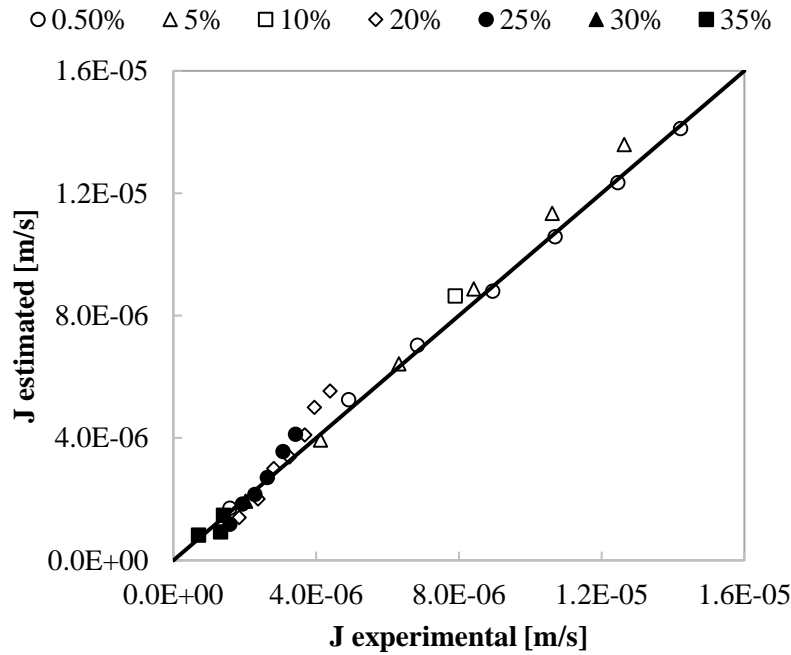


Figure 4-9. Comparison between experimental and modelled volumetric flux J_v at different experimental conditions.

In addition to estimating C_p and J_v , we can use our model to estimate the membrane porosity (ε). By assuming an active layer thickness (ΔZ) of $1\mu\text{m}$, which is often found in literature [1, 2], the number of pores (P_n) can be estimated from the $\frac{P_n}{\Delta Z}$ value. ε can then be calculated using P_n and the frequencies of the pore size distribution, as follows:

$$\varepsilon = P_n \pi \int_0^{\infty} f_{R(r)} r^2 dr \quad (4.41)$$

The obtained value for ε was 0.026, which is in the same order of magnitude as other reported values [1, 2]. This demonstrates the physical relevance and consistency of our model. It also indicates that the assumption of independency among pores is likely to be true with such small porosity.

4.4.3 Transport mechanisms inside the pores

The relative importance of the solute transport mechanisms inside the membrane depends on the solutes concentration. Eq.4.22 shows that at diluted conditions, convection and diffusion

are the main transport mechanisms, while the effect of TMP over the solutes is small and often neglected [2, 44]. However, at concentrated conditions, the reduction of the effective pressure due to the osmotic pressure, reduces the convection through the pores. As consequence, the solute transport driven by the gradients in the system (concentration and pressure) becomes more important. It is important to notice that even when the effective pressure over the system has diminished, the TMP, which is the pressure driving force over the solutes, remained the same.

Figure 4-10 shows the effects of high feed concentrations on the concentration profiles inside the membrane pores. Normalized profiles are shown with and without considering the effect of the pressure gradient on the solute concentrations. Under diluted conditions, the effect of including pressure is small and all but negligible; however under concentrated conditions it becomes quite important, increasing the transport of solutes towards the permeate. This is in line with the observations by Van Oers et al., who considered the reduction in the rejection of PEG3400 in the presence of dextran more related to the TMP than to the permeate flux [9].

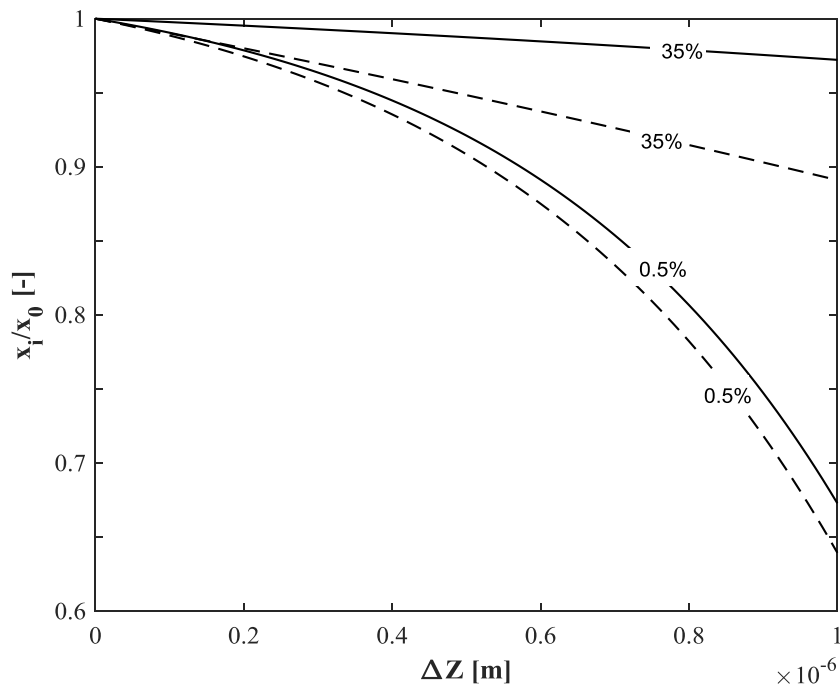


Figure 4-10. Normalized concentration profiles along the pore length for DP1 molecules under diluted and concentrated retentate conditions. The shown profiles correspond to a pore with $r_p=1.29$ nm using $TMP=20$ bar. Continuous lines represent the complete model and the dashed lines correspond to the model without the contribution of the pressure gradient ($Y=0$ in Eq.4.28).

As previously discussed, larger feed concentrations reduce the importance of convective flow for solute rejections, relative to the effects of diffusion (concentration gradient) and pressure (pressure gradient – see equation 4.22). The importance of the pressure gradient is co-determined by the product of the diffusion coefficient and the molar volume of the solute, $D_{p,i}\bar{v}_i$, which depends both on the pore size (exclusion) and on the molecular weight of the solute. While the bulk diffusion coefficient increases only slightly on the molecular weight, it decreases strongly when the size of the solute come in the range of the pore size, due to exclusion effects. Combined with the effect of the molar volume \bar{v}_i , which is roughly proportional to the molecular weight, we see that $D_{p,i}\bar{v}_i$ increases with the molecular weight in larger pores (due to \bar{v}_i), but decreases with the molecular weight in small pores (due to the exclusion factor $K_{d,i}$) (Figure 4-11).

This explains the observed changes in the solutes rejection in Figure 4-3. At moderate concentrations (20-25% w/w), the rejection of DP1 molecules is markedly lower than with dilute concentrations, with almost no difference in the rejection of the biggest molecules (DP6-7). On the other hand, at high concentrations (35% w/w), the mean pore size shifts towards the right, and the rejection of DP1 molecules decreases slightly, while that of the biggest molecules decreases more strongly.

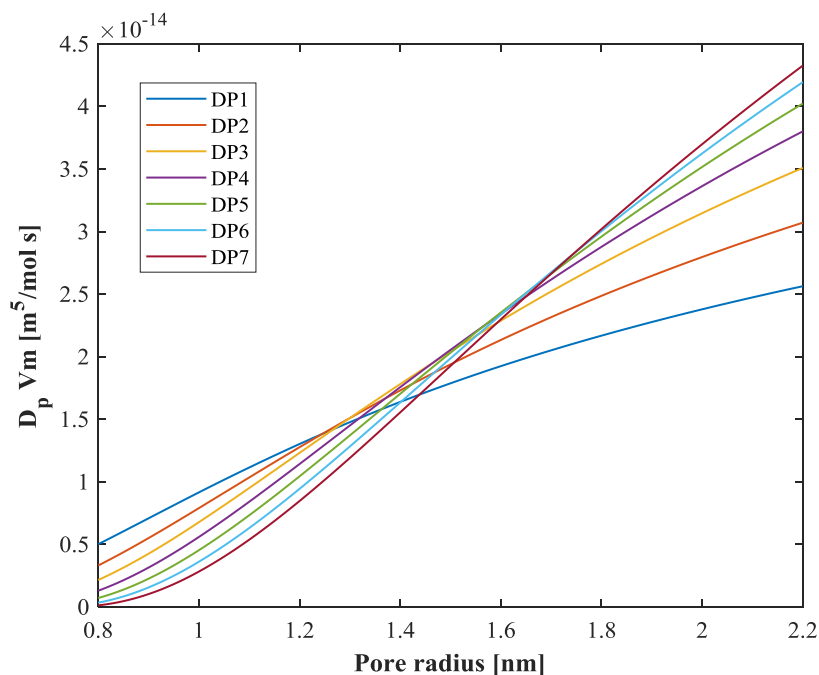


Figure 4-11. Product of D_p and V_m for all solutes at different pore radii. Values were estimated considering a retentate concentration of 25% w/w and TMP=20 bar.

4.4.4 Process optimization

The observed changes in rejection for the different sugars suggest that there is a feed concentration that gives the highest purity of DP1-2 molecules in the permeate. This optimum concentration was identified in Figure 4-12(top), in which the purity of the DP1-2 molecules in the permeate stream is shown as function of the feed concentration. Likewise, the mass flux of these two molecules was included in the figure to complete the analysis of the dependence of the efficiency of the process on feed concentration.

The maxima of these variables (purity and flux) were found at a retentate concentration of 20% w/w. Interestingly, the enhancing effect in the transport of large molecules due to the pressure gradient at very high concentrations, resulted in a marked decrease in the permeate purity of DP1-2. Figure 4-12 (bottom) shows the reduction in the rejection of the molecules as the concentration in the retentate increases. For the small molecules (DP1-DP2), it is evident that the decrease in the rejection is steeper up to a concentration of 30%w/w, at which the slope of the rejection curve becomes less negative. In the case of the bigger molecules, the reduction in rejection becomes significant at a concentration of 20% w/w, and from then decreases quickly with concentration. One should notice that the position of the optimum depends strongly on the membrane, since all results depends very strongly on the pore size and size distribution.

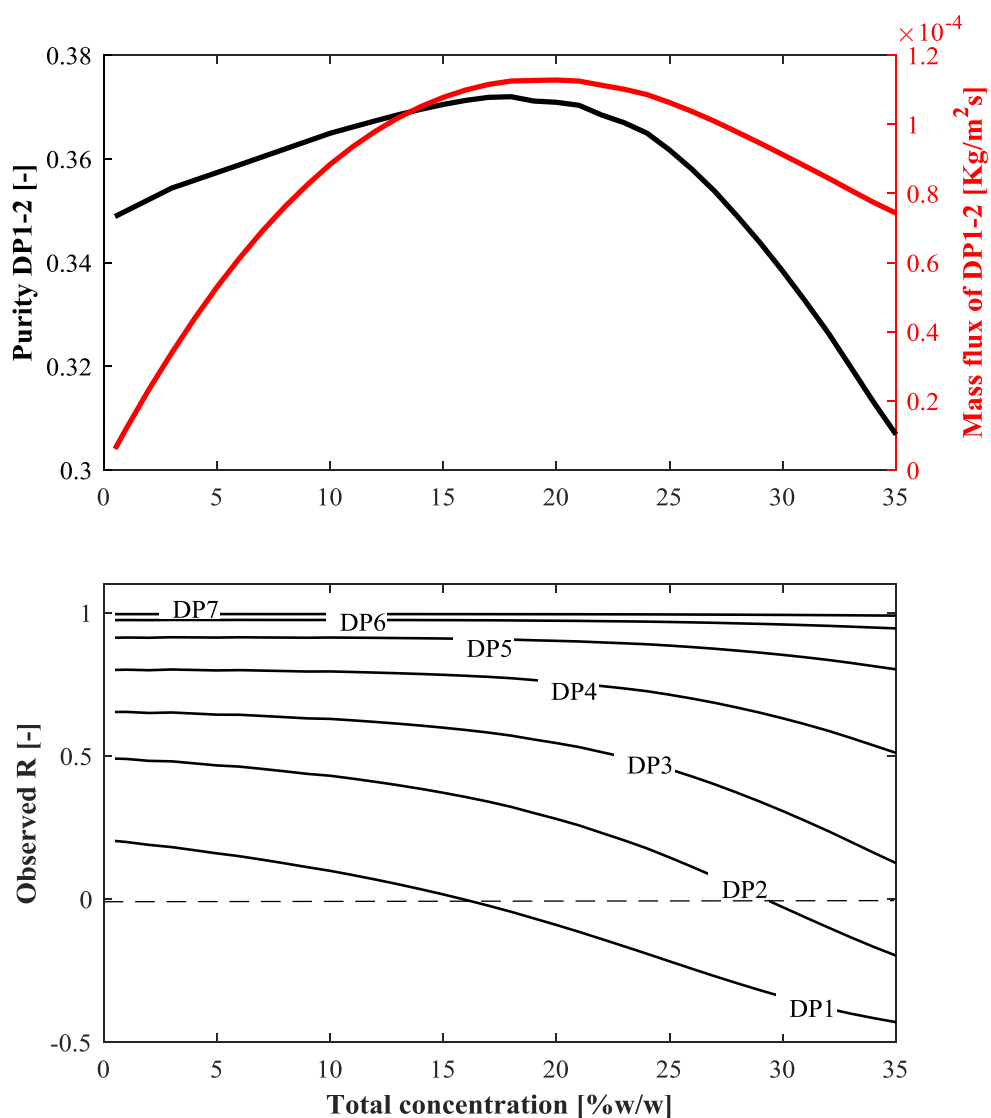


Figure 4-12. Model estimations of Purity (black line) and mass flux (red line) of DP1-2 molecules as function of feed concentration (top). Model predictions of the observed rejection for all solutes as function of feed concentration (bottom).

4.5 CONCLUSIONS

The effect of high solutes concentration in nanofiltration was studied using a mixture of oligosaccharides with a feed concentration up to 35% w/w. A model was created that included the non-ideality of concentrated sugar solutions and the effects of the pore size distribution.

The rejection of all solutes decreased as the concentration in the feed increased. For the smallest solutes negative retentions were observed. The reasons of such behaviour are not because of ionic interaction or membrane adsorption or fouling, but are caused by the non-ideality of

concentrated sugar solutions. Due to hydration, the activity coefficient of the solutes increases at high concentrations. This influences the driving force for diffusion in the concentration polarization layer. At the membrane interface, having at local equilibrium one concentrated phase (retentate) and one diluted phase (membrane), enhances the relative transport of small solutes inside the membrane.

The transport through smaller and larger pores is affected differently under concentrated conditions. The difference in the osmotic pressure is larger over narrower pores than over larger pores. As consequence, higher concentrations reduce more strongly the flux through smaller pores, increasing the importance of the transport through the larger pores.

Solute transport due to the pressure gradient, normally neglected in most of the studies, becomes important at high concentrations, at which convection transport is lowered due to the osmotic pressure effects. Under these conditions, the slope of the concentration profiles inside the membrane become less negative, decreasing the solutes rejection.

The results show that for a particular membrane, there is an optimum concentration for obtaining the highest purity of small sugars in the permeate. For the investigated GE1812C-34D membrane, this optimum is around 20% w/w.

ACKNOWLEDGEMENTS

This work was carried out as part of a project of the Institute for Sustainable Process Technology, The Netherlands: project number CM-20-05.

NOMENCLATURE

a	Chemical activity [dimensionless]
C	Concentration [mol/m ³]
C_T	Total molar concentration [mol/m ³]
D	Mutual Diffusion coefficient [m ² /s]
D_p	Diffusion coefficient inside the pore [m ² /s]
d	Diameter of the water molecule [m]
d_h	Hydraulic diameter [m]
f_R	Frequency [dimensionless]
h_f	Hydration number for fructose [dimensionless]
J	Volumetric flux [m/s]
K_c	Hindrance coefficient for convection [dimensionless]
K_d	Hindrance coefficient for diffusion [dimensionless]
k	Mass transfer coefficient [m/s]
M_w	Molecular weight [g/mol]
m	Number of components (including water as component m) [dimensionless]
N	Molar flux [mol/(m ² s)]
n_H	Hydration number [dimensionless]
P	Transmembrane Pressure [Pa]
P_e	Effective Pressure [Pa]
P_n	Total number of pores per area of membrane [m ⁻²]
Pe	Péclet number [dimensionless]

R	Gas constant [J/(K mol)]
Re	Reynolds number [dimensionless]
r_G	Average radius according to the Simplified Capsular approach [m]
r_i	Radius of molecule i [m]
r_p	Radius of the pore [m]
r_S	Stokes' radius [m]
r^*	Mean radius [m]
Sc	Schmidt number [dimensionless]
Sh	Sherwood number [dimensionless]
s	Number of segments per solute [dimensionless]
T	Temperature [K]
u	Linear velocities [m/s]
\bar{v}	Molar volume [m ³ /mol]
v	Cross flow velocity [m/s]
w	Membrane surface
Y	Variable that contains the contribution of the pressure gradient [dimensionless]
x	Molar fraction [dimensionless]

Greek letters

δ_{ij}	Kronecker delta operator [dimensionless]
ΔZ	Membrane thickness [m]
\mathfrak{D}	Maxwell-Stefan diffusion coefficient [m ² /s]

Γ	Thermodynamic factor [dimensionless]
Π	Osmotic Pressure [Pa]
γ	Activity coefficient [dimensionless]
δ	Concentration polarization layer thickness [m]
η	Viscosity [Pa s]
λ	Ratio between the molecular and pore radii [dimensionless]
μ	Chemical Potential [J/mol]
ρ	Density [Kg/m ³]
σ	standard deviation of the pore size distribution [m]
φ	Partition coefficient [dimensionless]

APPENDICES

A.1 Calculation of activity coefficient (γ) from hydration numbers.

The chemical activity (a) is interpreted as an effective molar fraction. Thus, the activity of solute i in a mixture with other solutes and water results in:

$$a_i = \frac{n_i}{\left(\sum_{j=1}^m n_j\right) - n_{hyd}} \quad (4.A1)$$

where n is the number of moles, the term in brackets represent the sum of moles of all the components in the mixture and n_{hyd} is the number of water moles bound to the solutes. Then, If we divide every term by the total number of moles (the term in brackets), we obtain:

$$a_i = \frac{x_i}{1 - \frac{n_{hyd}}{\left(\sum_{j=1}^m n_j\right)}} \quad (4.A2)$$

The activity coefficients γ are interpreted according to Henry's law. Therefore, the reference state is the solute with only solvent molecules in its surrounding, and the next relations hold:

$$\gamma_i \rightarrow 1 \text{ as } x_i \rightarrow 0 \text{ (solutes)} \quad (4.A3)$$

$$\gamma_m \rightarrow 1 \text{ as } x_m \rightarrow 1 \text{ (solvent)} \quad (4.A4)$$

Considering the aforementioned definitions, the activity coefficient for solute i is:

$$\gamma_i = \frac{a_i}{x_i} = \frac{\frac{x_i}{1 - \frac{n_{hyd}}{\left(\sum_{j=1}^m n_j\right)}}}{x_i} = \frac{1}{1 - \frac{n_{hyd}}{\left(\sum_{j=1}^m n_j\right)}} \quad (4.A5)$$

n_{hyd} represents the number of moles of water in the hydration layers of all the sugar molecules in the mixture. Assuming that the segments (fructose in the case of fructooligosaccharides) of each type of sugar behave in a similar way we can generalize in the following way:

$$n_{hyd} = h_f n_{seg} \quad (4.A6)$$

$$n_{seg} = \sum_{i=k}^{m-1} n_k S_k \quad (4.A7)$$

Where h_f is the hydration number of one segment (in our case fructose) and s is the degree of polymerization of each type of sugar (number of segments). We postulate that h_f is constant for all segments, and is independent of s . Consequently:

$$x_{seg} = \frac{n_{seg}}{n_{total}} = \frac{n_{seg}}{\sum_{j=1}^m n_j} \quad (4.A8)$$

x_{seg} is not precisely a molar fraction because the total number of moles takes into account the complete sugars and not their segments. It is useful to simplify Eq. 4.A5 as follows:

$$\frac{n_{hyd}}{\sum_{j=1}^m n_j} = h_f x_{seg} \quad (4.A9)$$

$$\gamma = \frac{1}{1 - h_f x_{seg}} \quad (4.A10)$$

A.2 Calculation of water activity (a_w) from composition.

As done previously with the activity of i , water activity can also be represented as an effective molar fraction. For a system of $m-1$ solutes (j) and water, we obtain:

$$a_{H_2O} = \frac{n_{H_2O} - n_{hyd}}{\sum_{j=1}^m n_j - n_{hyd}} \quad (4.A11)$$

If we divide the numerator and denominator of Eq. 4.A11 by the total number of moles ($\sum_{j=1}^m n_j$), we obtain:

$$a_{H_2O} = \frac{\frac{n_{H_2O}}{\sum_{j=1}^m n_j} - \frac{n_{hyd}}{\sum_{j=1}^m n_j}}{1 - \frac{n_{hyd}}{\sum_{j=1}^m n_j}} \quad (4.A12)$$

Considering the definitions in Eqs. 4.A6 - 4.A8, we can simplify the expression above to:

$$a_{H_2O} = \frac{x_{H_2O} - h_f x_{seg}}{1 - h_f x_{seg}} \quad (4.A13)$$

Since a_i and a_{H_2O} are effective mole fractions, they should sum 1 all together:

$$\sum_{i=1}^{m-1} \frac{x_i}{1 - h_f x_{seg}} + \frac{x_{H_2O} - h_f x_{seg}}{1 - h_f x_{seg}} = \frac{\sum_{i=1}^{m-1} x_i + x_{H_2O} - h_f x_{seg}}{1 - h_f x_{seg}} = \frac{1 - h_f x_{seg}}{1 - h_f x_{seg}} = 1$$

A.3 Experimental data

Table 4-A1. Experimental concentrations for the retentate and permeate streams under different process conditions.

Feed Conc. [% w/w]	Pressure [bar]	Retentate [g/Kg]							Permeate [g/Kg]						
		DP1	DP2	DP3	DP4	DP5	DP6	DP7	DP1	DP2	DP3	DP4	DP5	DP6	DP7
0.5	2.5	0.41	0.26	1.04	0.94	0.74	0.53	0.22	0.43	0.19	0.50	0.24	0.09	0.04	0.00
0.5	7.5	0.41	0.27	1.05	0.96	0.77	0.53	0.21	0.35	0.15	0.35	0.16	0.05	0.02	0.01
0.5	10	0.42	0.27	1.09	1.00	0.79	0.58	0.23	0.33	0.14	0.32	0.15	0.05	0.03	0.00
0.5	12.5	0.43	0.30	1.12	1.03	0.82	0.58	0.26	0.33	0.14	0.31	0.14	0.06	0.02	0.00
0.5	15	0.44	0.28	1.14	1.05	0.83	0.59	0.25	0.32	0.13	0.31	0.15	0.06	0.02	0.00
0.5	17.5	0.43	0.29	1.15	1.07	0.83	0.59	0.27	0.33	0.13	0.31	0.15	0.06	0.01	0.00
0.5	20	0.42	0.28	1.14	1.08	0.85	0.62	0.29	0.32	0.12	0.30	0.14	0.08	0.03	0.01
5	8	3.46	2.91	14.16	13.28	10.14	7.70	3.51	2.24	1.29	4.59	2.42	0.99	0.38	0.09
5	12	3.40	2.90	14.11	13.29	10.18	7.81	3.52	2.39	1.32	4.60	2.28	0.94	0.37	0.09
5	16	3.44	2.96	14.33	13.65	10.42	7.95	3.59	2.38	1.34	4.55	2.27	0.97	0.39	0.09
5	20	3.41	3.02	14.18	13.58	10.33	7.91	3.63	2.34	1.32	4.52	2.30	1.00	0.41	0.11
5	24	3.50	3.04	14.94	14.35	10.96	8.41	3.85	2.26	1.24	4.48	2.38	1.06	0.46	0.11
10	20	6.66	5.61	27.62	26.52	20.15	15.63	7.02	4.23	2.36	8.38	4.22	1.84	0.77	0.19
20	10	11.78	14.15	54.06	41.87	32.03	22.79	9.77	12.81	9.39	28.03	12.49	5.14	2.23	0.71
20	12	11.46	13.79	54.31	42.58	32.62	23.71	10.17	12.37	8.79	25.88	10.95	4.41	1.70	0.40
20	14	10.05	13.31	51.03	41.25	31.61	22.46	9.60	12.03	8.39	24.28	10.13	4.07	1.53	0.30

20	16	10.90	14.38	54.92	43.81	33.20	24.08	10.34	11.65	8.22	22.39	9.09	3.52	1.32	0.27
20	18	10.50	14.26	54.08	43.27	34.35	24.57	11.88	11.53	7.83	21.11	8.47	3.25	1.16	0.26
20	20	10.17	13.49	52.83	42.37	33.96	24.84	11.16	9.01	6.28	16.12	6.46	2.52	1.03	0.31
20	22	10.85	13.72	55.64	44.30	34.55	24.77	10.95	11.09	7.18	19.67	8.02	3.28	1.26	0.25
25	12	13.35	16.85	65.77	52.20	39.80	29.34	13.31	15.55	13.27	41.17	18.08	7.35	2.65	0.68
25	14	12.65	17.13	63.90	51.02	38.64	28.13	12.22	15.40	12.42	37.44	16.22	6.78	2.52	0.59
25	16	13.32	17.14	67.25	53.71	40.94	29.51	12.87	15.27	11.46	34.15	14.81	6.43	2.50	0.54
25	18	12.77	17.08	66.55	54.28	41.72	30.31	12.96	14.99	11.60	32.02	13.70	5.51	2.07	0.51
25	20	12.72	16.63	65.51	52.28	39.59	28.75	12.63	14.73	10.84	30.28	12.68	5.10	1.92	0.49
25	22	12.54	16.26	66.34	53.68	40.07	28.92	12.22	12.42	8.52	24.50	10.27	4.18	1.71	0.35
30	20	17.98	15.34	73.07	68.91	52.61	40.62	18.30	19.48	12.09	45.85	28.99	13.18	5.79	1.51
35	16	21.80	17.96	86.26	82.04	62.63	48.13	22.01	24.31	16.90	67.53	48.81	23.20	10.53	2.66
35	20	21.86	18.29	86.40	82.72	63.08	48.41	22.14	28.61	19.67	74.04	52.58	24.70	11.30	2.93
35	24	22.06	17.64	85.09	83.28	62.95	49.17	22.34	25.38	16.49	63.18	42.68	20.29	9.38	2.56

REFERENCES

- [1] R. Baker, *Membrane Technology and Applications* 2nd ed., Wiley, California, USA, 2004.
- [2] W.R. Bowen, J.S. Welfoot, Modelling the performance of membrane nanofiltration—critical assessment and model development, *Chem. Eng. Sci.*, 57 (2002) 1121-1137.
- [3] O. Kedem, A. Katchalsky, Thermodynamic analysis of the permeability of biological membranes to non-electrolytes, *Biochim. Biophys. Acta*, 27 (1958) 229-246.
- [4] M.A.J.S. van Boekel, *Kinetic Modeling of Reactions In Foods*, CRC Press, 2008.
- [5] J. Straatsma, G. Bargeman, H.C. van der Horst, J.A. Wesselingh, Can nanofiltration be fully predicted by a model?, *J. Membr. Sci.*, 198 (2002) 273-284.
- [6] G. Bargeman, J.M. Vollenbroek, J. Straatsma, C.G.P.H. Schroën, R.M. Boom, Nanofiltration of multi-component feeds. Interactions between neutral and charged components and their effect on retention, *J. Membr. Sci.*, 247 (2005) 11-20.
- [7] R.C. Kuhn, F. Maugeri Filho, V. Silva, L. Palacio, A. Hernández, P. Prádanos, Mass transfer and transport during purification of fructooligosaccharides by nanofiltration, *J. Membr. Sci.*, 365 (2010) 356-365.
- [8] W. Li, J. Li, T. Chen, Z. Zhao, C. Chen, Study on nanofiltration for purifying fructooligosaccharides: II. Extended pore model, *J. Membr. Sci.*, 258 (2005) 8-15.
- [9] C.W. van Oers, M.A.G. Vorstman, R.v.d. Hout, P.J.A.M. Kerkhof, The influence of thermodynamic activity on the solute rejection in multicomponent systems, *J. Membr. Sci.*, 136 (1997) 71-87.
- [10] J. Luo, Y. Wan, Effect of highly concentrated salt on retention of organic solutes by nanofiltration polymeric membranes, *J. Membr. Sci.*, 372 (2011) 145-153.
- [11] R. A. Robinson, R. H. Stokes, *Activity coefficients in aqueous solutions of sucrose, mannitol and their mixtures at 25°*, 1961.
- [12] A.A. Hussain, S.K. Nataraj, M.E.E. Abashar, I.S. Al-Mutaz, T.M. Aminabhavi, Prediction of physical properties of nanofiltration membranes using experiment and theoretical models, *J. Membr. Sci.*, 310 (2008) 321-336.
- [13] J.B. V. Aguirre, A. Van der Padt, Anja E.M. Janssen, R. Boom, Nanofiltration of elongated molecules, *J. Membr. Sci.*, (2017).
- [14] J.A. Wesselingh, R. Krishna, *Mass Transfer in Multicomponent Mixtures*, VSSD, Delft, 2006.

- [15] S. Postel, S. Wessel, T. Keil, P. Eiselt, M. Wessling, Multicomponent mass transport in organic solvent nanofiltration with solvent mixtures, *J. Membr. Sci.*, 466 (2014) 361-369.
- [16] R. Taylor, R. Krishna, *Multicomponent Mass Transfer*, John Wiley & Sons, Inc, New York, 1993.
- [17] H.A. Kooijman, R. Taylor, Estimation of diffusion coefficients in multicomponent liquid systems, *Industrial & Engineering Chemistry Research*, 30 (1991) 1217-1222.
- [18] X. Liu, T.J.H. Vlugt, A. Bardow, Maxwell–Stefan diffusivities in liquid mixtures: Using molecular dynamics for testing model predictions, *Fluid Phase Equilib.*, 301 (2011) 110-117.
- [19] G. Schock, A. Miquel, Mass transfer and pressure loss in spiral wound modules, *Desalination*, 64 (1987) 339-352.
- [20] Y. Sano, S. Yamamoto, Mutual Diffusion Coefficient of Aqueous Sugar Solutions, *J. Chem. Eng. Jpn.*, 26 (1993) 633-636.
- [21] J. Chirife, M.P. Buera, A simple model for predicting the viscosity of sugar and oligosaccharide solutions, *J. Food Eng.*, 33 (1997) 221-226.
- [22] V. Aguirre Montesdeoca, A. Van der Padt, R.M. Boom, A.E.M. Janssen, Modelling of membrane cascades for the purification of oligosaccharides, *J. Membr. Sci.*, 520 (2016) 712-722.
- [23] G. Scatchard, THE HYDRATION OF SUCROSE IN WATER SOLUTION AS CALCULATED FROM VAPOR-PRESSURE MEASUREMENTS, *J. Am. Chem. Soc.*, 43 (1921) 2406-2418.
- [24] M.J. Blandamer, J.B.F.N. Engberts, P.T. Gleeson, J.C.R. Reis, Activity of water in aqueous systems; A frequently neglected property, *Chem. Soc. Rev.*, 34 (2005) 440-458.
- [25] P. Walstra, *Physical Chemistry of Foods*, Marcel Dekker Inc., New York, 2003.
- [26] E.D. Glandt, Distribution equilibrium between a bulk phase and small pores, *AIChE J.*, 27 (1981) 51-59.
- [27] E.M. Renkin, Filtration, diffusion, and molecular sieving through porous cellulose membranes, *The Journal of general physiology*, 38 (1954) 225-243.
- [28] J.C. Giddings, E. Kucera, C.P. Russell, M.N. Myers, Statistical theory for the equilibrium distribution of rigid molecules in inert porous networks. Exclusion chromatography, *The Journal of Physical Chemistry*, 72 (1968) 4397-4408.
- [29] V. Aguirre Montesdeoca, B. Jaap, A. Van der Padt, R.M. Boom, A.E.M. Janssen, Nanofiltration of non-spherical molecules (submitted), (2018).
- [30] B.D. Mitchell, W.M. Deen, Effect of concentration on the rejection coefficients of rigid macromolecules in track-etch membranes, *J. Colloid Interface Sci.*, 113 (1986) 132-142.

- [31] Y.-X. Yu, J. Wu, Structures of hard-sphere fluids from a modified fundamental-measure theory, *The Journal of Chemical Physics*, 117 (2002) 10156-10164.
- [32] Y.-X. Yu, J. Wu, Y.-X. Xin, G.-H. Gao, Structures and correlation functions of multicomponent and polydisperse hard-sphere mixtures from a density functional theory, *The Journal of Chemical Physics*, 121 (2004) 1535-1541.
- [33] W.R. Bowen, J.S. Welfoot, Modelling of membrane nanofiltration—pore size distribution effects, *Chem. Eng. Sci.*, 57 (2002) 1393-1407.
- [34] W. Deen, Hindered transport of large molecules in liquid-filled pores, *AIChE J.*, 33 (1987) 1409-1425.
- [35] P. Dechadilok, W.M. Deen, Hindrance Factors for Diffusion and Convection in Pores, *Industrial & Engineering Chemistry Research*, 45 (2006) 6953-6959.
- [36] P.M. Bungay, H. Brenner, The motion of a closely-fitting sphere in a fluid-filled tube, *Int. J. Multiphase Flow*, 1 (1973) 25-56.
- [37] B. Agasanapura, R.E. Baltus, C. Tanneru, S. Chellam, Membrane rejection of nonspherical particles: Modeling and experiment, *AIChE J.*, 59 (2013) 3863-3873.
- [38] J.M. Campbell, L.L. Bauer, G.C. Fahey, A.J.C.L. Hogarth, B.W. Wolf, D.E. Hunter, Selected Fructooligosaccharide (1-Kestose, Nystose, and 1F- β -Fructofuranosylnystose) Composition of Foods and Feeds, *J. Agric. Food. Chem.*, 45 (1997) 3076-3082.
- [39] A.K.H. D'Haese, I. De Leersnyder, P. Vermeir, A.R.D. Verliefde, On negative rejection of uncharged organic solutes in forward osmosis, *J. Membr. Sci.*, 548 (2018) 22-31.
- [40] A.E. Yaroshchuk, Negative rejection of ions in pressure-driven membrane processes, *Adv. Colloid Interface Sci.*, 139 (2008) 150-173.
- [41] L.S. Darken, Diffusion of carbon in austenite with a discontinuity in composition, *Trans. AIME.*, 180 (1949) 430-438.
- [42] R. Krishna, Uphill diffusion in multicomponent mixtures, *Chem. Soc. Rev.*, 44 (2015) 2812-2836.
- [43] R. Krishna, Diffusing uphill with James Clerk Maxwell and Josef Stefan, *Current Opinion in Chemical Engineering*, 12 (2016) 106-119.
- [44] S. Bandini, V. Morelli, Effect of temperature, pH and composition on nanofiltration of mono/disaccharides: Experiments and modeling assessment, *J. Membr. Sci.*, 533 (2017) 57-74.

Chapter 5

Modelling UF performance by integrating local (critical) fluxes along the membrane length.

This chapter is based on:

Victor Aguirre-Montesdeoca, Anja E. M. Janssen, A. Van der Padt, and R. M. Boom.
“Modelling UF performance by integrating local (critical) fluxes along the membrane length”
Submitted for publication

ABSTRACT

Despite the vast number of studies on the understanding and estimation of the permeate flux in ultrafiltration, most of them base their estimations on either one or another mechanism, without pointing out a clear 'bridge' between them. The aim of this paper is to assess these mechanisms on the prediction of the UF flux, using as feed a multicomponent mixture of BSA, NaCl and H₂O.

Maxwell-Stefan Equations expressed as function of the components' volume fractions were used for an easier consideration of the non-idealities of the system. These non-idealities (hydration, adsorption, electrical interactions and volume exclusion) were critical in the local fluxes calculation, for which an increase in the thickness of the boundary layer along the filtration channel was considered.

For partially fouled membranes, two sections of the membrane can be distinguished, in which the uncovered section is mostly influenced by the osmotic pressure of the system, while in the section covered with a gel, local critical fluxes, defined by the gel layer mechanism, are reached. The steady state values for the TMP and permeate flux were found to be the same whether the system was operated at constant pressure or at constant flux.

5.1 INTRODUCTION

The ultrafiltration of proteins is an important process in the food and biotechnology industry, it is generally used for purification and concentration purposes, in which the retentate (concentrate) is usually the stream with highest value. The main drawback of this process is the marked flux decline obtained over time. This decrease can be larger than one order of magnitude depending on the process conditions and protein concentration [1-4]. It has, therefore, been subject of intensive study over the last five decades and many models and theories have been developed to explain the mechanisms that lead to this flux decrease.

The most popular theory that explains this flux decrease during UF is the so-called gel layer model . It assumes that the surface of the membrane is completely covered by a layer of proteins, which have reached their maximum concentration and, as consequence, formed a gel [5, 6]. The gel increases the resistance of the membrane, lowering the permeate flux over time until it reaches a plateau. Theoretically, the flux at steady state can be calculated with a balance between convection and dispersive forces (back diffusion) in the concentration polarization layer. Nevertheless, Cohen and Probstein already in 1986 found out that the measured flux was much higher than the ‘theoretical’ one obtained with the aforementioned balance [7]. They speculated that the factor responsible for this effect might be related with the surface interaction between colloidal particles, a phenomenon related to the inherent charge of the macromolecules. Likewise, in order to predict the steady state flux of the system, other studies have considered phenomena such as: osmotic pressure [5, 8], shear induced diffusion [9], inertial migration [10], DLVO theory [11], etc. In 1995 Bowen and Jenner even developed a rigorous dynamic model that accounted for many types of long and short range interaction between charged colloids[12].

Most of the studies tend to base their predictions on either one or another model, without pointing out a clear integration between the different mechanisms to create a coherent mechanistic picture of the process. It has already been shown that the gel does not grow uniformly on top of the membrane. Due to varying boundary layer thickness, the gel first appears at the outlet of the filtration channel and then it grows towards the inlet [9, 13]. This means that under some conditions the membrane can be partially fouled and more than one mechanism can determine the resulting overall permeate flux as shown in Figure 5-1.

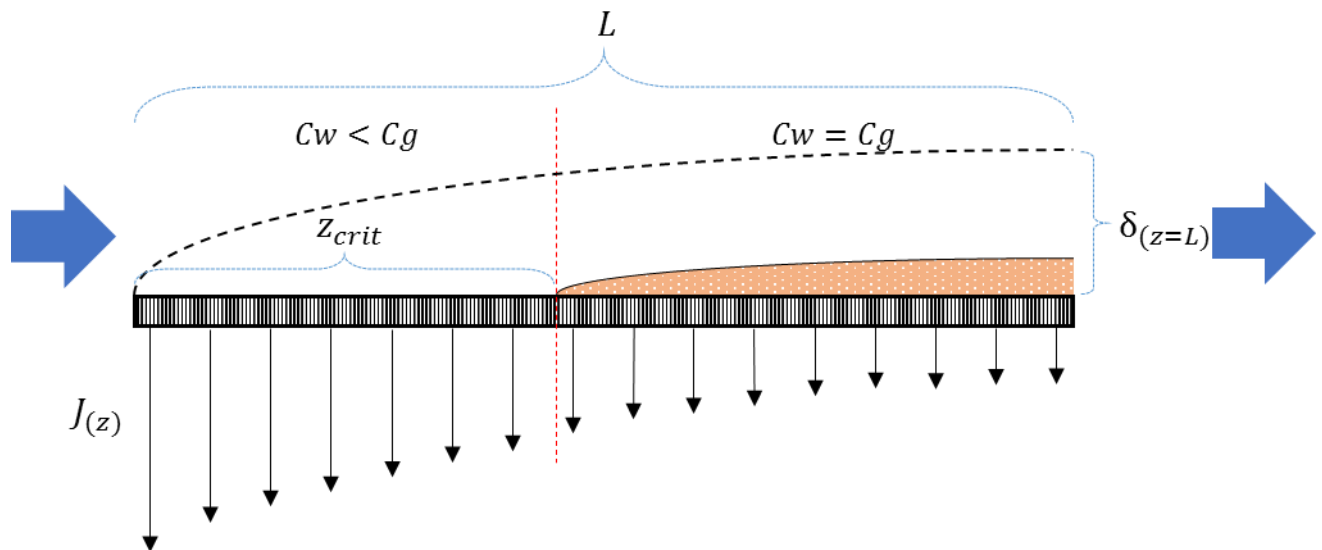


Figure 5-1. Representation of a flat membrane partially covered with gel and the resulting local fluxes $J(z)$. C_w stands for concentration of the protein at the membrane surface and C_g is the gel concentration. δ represents the growing boundary layer along the filtration channel of length L . z_{crit} is the distance from the inlet to the point where gel deposit appears.

The aim of this paper is to assess the mechanisms that determine the permeate flux in the ultrafiltration of protein solutions. Special attention is given to the effects of the electrical interactions between proteins and ions in the mixture. The model system chosen for this study was BSA, NaCl and water. We used a long filtration channel (length 1 m) to represent an actual filtration system, in which, due to a growing boundary layer down the channel, several flux limiting mechanism may occur. To facilitate the modelling of the system, we chose a membrane that completely rejects BSA but let the accompanying ions pass freely. The experimental results are compared with the predictions of a rigorous model built within the framework of the Maxwell-Stefan (M-S) equations.

5.2 THEORETICAL ASPECTS

5.2.1 Local critical fluxes

Before starting the analysis of the mechanisms behind flux reduction in UF, it is necessary to mention the definition of limiting and critical flux. The limiting flux is the maximum steady state permeate flux that can be achieved by increasing the transmembrane pressure in the system [6]. Figure 5-2 shows that at the limiting flux, increasing the pressure does not increase the

steady state flux. It is generally accepted that at these conditions the membrane is totally fouled and pressure increments lead to thickening of the gel layer at the membrane surface, resulting in the same steady state flux. The critical flux, on the other hand, is the flux below which no fouling occurs; in other words, it is the flux required to overcome particle repulsion; exceeding this flux leads to the coagulation of the protein on the surface [13, 14].

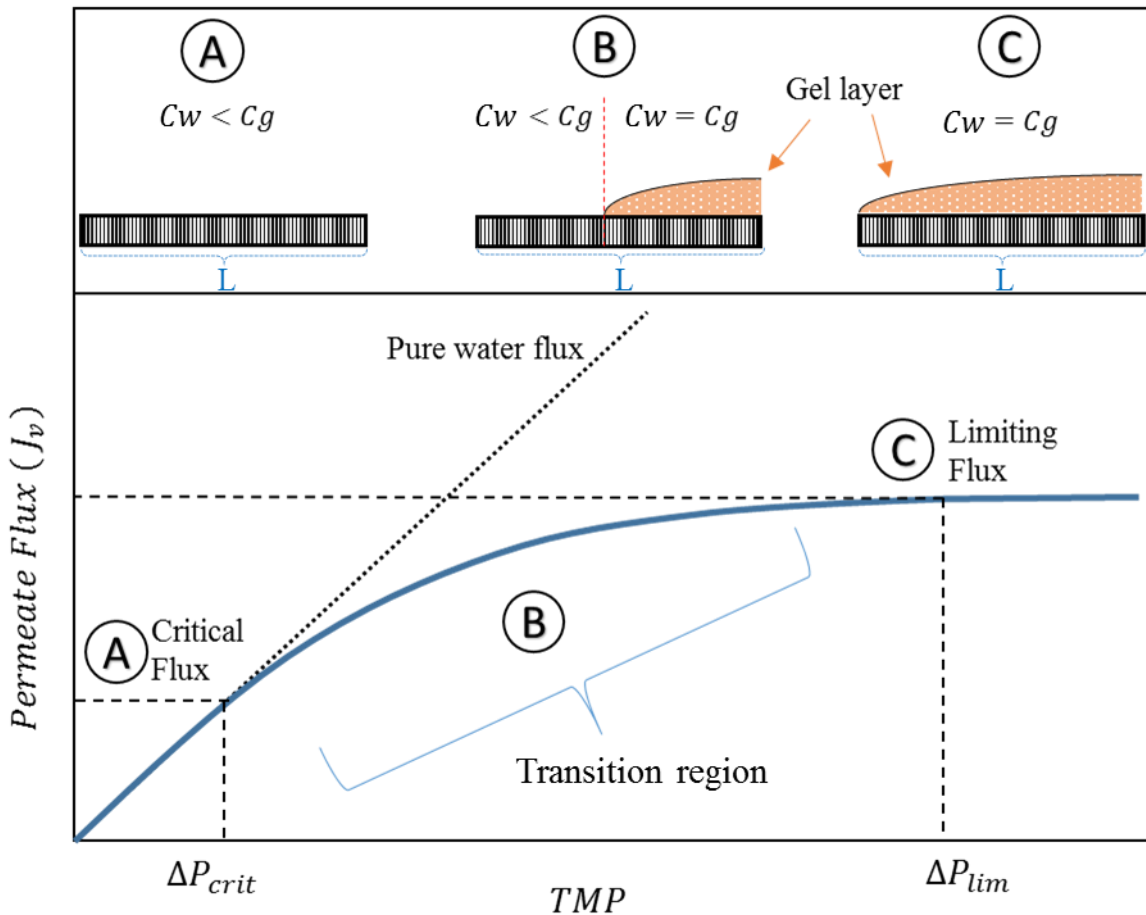


Figure 5-2. Permeate flux as function of transmembrane pressure (TMP) for the ultrafiltration of proteins. Region A represent membrane conditions below the critical flux, region B is the ‘transition region’ where the membrane is partially fouled, and region C represents the limiting conditions.

Bacchin et al. made an interesting connection between the limiting and critical concepts when they introduced the concept of ‘local critical fluxes’ [13]. As shown in Figure 5-1, these authors described a system with a growing boundary layer along the membrane length, in which fouling occurs first in the outlet and extends towards the module inlet depending on the TMP of the system. In this way, local critical fluxes will be different along the membrane, being lower at the outlet of the module than at the entrance. When working at sub-critical conditions, with a

pressure lower than ΔP_{crit} , the membrane remains clean without the formation of gel layer (Figure 5-2 region A). As the pressure increases, fouling starts appearing at the outlet of the membrane, showing that the critical flux has been exceeded. As the gel layer grows along the membrane, partially covering it, a non-linear dependency of the flux with respect to the pressure occurs (region B – Transition region). Finally, when the gel layer has covered the entire membrane length, the limiting flux is reached and the flux becomes independent of the pressure (region C).

It has been demonstrated that the concentration polarization in filtration systems can be represented using a stagnant film model, in which mass transfer is assumed to occur across a stagnant film of thickness δ [15]. In theory, local fluxes can be calculated as long as the local values for δ are known. Considering that a typical boundary layer for a laminar and developed flow follows a power law of 1/3, the next relation can be used in agreement with Davis and Sherwood [9]:

$$\delta_{(z)} = \delta_{(z=L)} \left(\frac{z}{L} \right)^{1/3} \quad (5.1)$$

in which z represents the position along the channel and L is its total length. The calculation of the total flux (J_v) for a system totally covered by protein gel can be done by integrating the local fluxes as shown in Eq. 5.2, where $J_{crit}(z)$ represent the local critical flux at every position z .

$$J_v = \frac{1}{L} \int_0^L J_{crit}(z) dz \quad (5.2)$$

When the TMP is higher than the pressure needed to reach the limiting flux (ΔP_{lim}), the permeate flux is totally influenced by the gel layer mechanism and Eq. 5.2 can be used. However, if $TMP < \Delta P_{lim}$ it could be that the membrane is partially fouled (region B in Figure 5-2) or not fouled at all (region A). In those cases, osmotic pressure influences the overall permeate flux. Therefore, if only a section of the membrane is fouled, more than one flux limiting mechanism is active. Therefore, both sections of the membrane should be analysed separately as shown in Eq. 5.3, in which z_{crit} is the distance from the inlet of the channel to the point at which the gel first appears (see Figure 5-1).

$$J_v = \frac{1}{L} \left(\int_0^{z_{crit}} J_{osmo}(z) dz + \int_{z_{crit}}^L J_{crit}(z) dz \right) \quad (5.3)$$

The calculation of the local fluxes with and without the presence of a gel layer (J_{crit} and J_{osmo}) needs to be performed considering all the driving forces and all the components of the system. Likewise, the thermodynamic non-idealities need to be included to account for the surface interaction between particles. Therefore, the M-S equations can be used to combine the aforementioned aspects in one single model.

5.2.2 Maxwell Stefan equations

During ultrafiltration, the concentration of the proteins increases in the concentration polarization layer, since they are retained by the membrane. This concentration profile, together with that of the ions determine a gradient in the electrochemical potential, which together with the chemical potential are the driving forces of the system. At steady state, the forces acting on the solutes balance out in the concentration polarization layer. In a non-ideal multicomponent system, the most appropriate approach to describe the forces in this layer is using the M-S equations. These equations can be envisaged as a force balance between the driving forces and the friction forces in the system [16].

A convenient way to present the M-S equations is shown in Eq. 5.4, in which the force balance in the concentration polarization layer for molecule i is described. The molecular diffusion in this layer can be represented by a set of $m - 1$ equations, being m the number of components (including water as component m). The term at the left hand side represents the driving forces for solute i and the one at the right represents the friction forces working over solute i . It is important to realize that the driving forces together are expressed as the electrochemical potential gradient ($\nabla\tilde{\mu}_i$). x represents the solutes mole fraction and u are their linear velocities. \mathfrak{D}_{ij} is the M-S cross diffusion coefficient between species i and j [16, 17].

$$-\frac{x_i}{RT}\nabla_{T,P}\tilde{\mu}_i = \sum_{\substack{j=1 \\ j \neq i}}^m \frac{(u_i - u_j)x_i x_j}{\mathfrak{D}_{ij}} \quad (5.4)$$

The electrochemical potential gradient can be split into the chemical ($\nabla\mu_i$) and the electrical potential gradients ($\nabla\Psi$) [16]. Furthermore, it is convenient to express the equations in terms of volume fractions (φ) instead of molar fractions because, as it is explained further in section 5.2.3, most of the non-idealities are functions of φ . Thus, considering:

$$x_i = \frac{\varphi_i}{\bar{V}_i C_T} \quad (5.5)$$

in which \bar{V}_i is the molar volume of i and C_T is the total molar concentration, we can obtain

$$-\frac{\varphi_i}{\bar{V}_i C_T RT} \nabla \mu_i - \frac{\varphi_i}{\bar{V}_i C_T} \frac{Z_i F}{RT} \nabla \Psi = \sum_{\substack{j=1 \\ j \neq i}}^m \frac{(u_i - u_j)}{\mathfrak{D}_{ij}} \frac{\varphi_i}{\bar{V}_i C_T} \frac{\varphi_j}{\bar{V}_j C_T} \quad (5.6)$$

in which Z_i is the charge of species i and F is the Faraday constant. Similarly, volume fluxes (J_i) and modified M-S diffusion coefficients (\mathfrak{D}_{ij}^V) can be defined using the following relations:

$$J_i = \varphi_i u_i \quad (5.7)$$

$$\mathfrak{D}_{ij}^V = \mathfrak{D}_{ij} \bar{V}_j C_T \quad (5.8)$$

Here, it is important to mention that under this definition the modified M-S diffusion coefficients obey the following symmetry in agreement with Onsager's reciprocal relations [18, 19]:

$$\mathfrak{D}_{ij} = \frac{\mathfrak{D}_{ij}^V}{\bar{V}_j C_T} = \mathfrak{D}_{ji} = \frac{\mathfrak{D}_{ji}^V}{\bar{V}_i C_T}; \quad \frac{\mathfrak{D}_{ij}^V}{\bar{V}_j} = \frac{\mathfrak{D}_{ji}^V}{\bar{V}_i}$$

By combining Eqs. 5.6, 5.7 and 5.8, many variables cancel out, resulting in a simpler relation [18, 19]:

$$\frac{\varphi_i}{RT} \nabla \mu_i + \frac{\varphi_i Z_i F}{RT} \nabla \Psi = \sum_{\substack{j=1 \\ j \neq i}}^m \frac{(J_j \varphi_i - J_i \varphi_j)}{\mathfrak{D}_{ij}^V} \quad (5.9)$$

If we consider that in UF the permeate flux is mostly water ($J_v \approx J_m$), and the volume fraction of water in the permeate is almost 1 ($\varphi_{m,p} \approx 1$). J_i for the ions can be related with J_v as shown in Eq. 5.10. This equation, known as 'bootstrap', let us link the fluxes with the concentrations in our system [17].

$$\frac{J_i}{J_m} = \frac{\varphi_{i,p}}{\varphi_{m,p}}$$

$$J_i = J_v \varphi_{i,p} \quad (5.10)$$

For a system with 4 components: BSA (1), Na⁺(2), Cl⁻(3) and H₂O (4), three equations equivalent to Eq.5.9 corresponding to component 1, 2 and 3 are needed. Additionally, the following condition is necessary to calculate the volume fractions for component 4:

$$\sum_{i=1}^m \varphi_i = 1 \quad (5.11)$$

5.2.3 Non-idealities

Several types of interactions occur between the components of the mixture. A summary is presented in Table 5-1. The relevance of these interactions is generally dependent on the concentration of the involved components in the mixture. Since the concentration of BSA increases greatly in the concentration polarization layer, most of the interactions become relevant and need to be considered to account for the thermodynamic non-ideality of the solution.

Table 5-1. Interactions between components of the feed mixture

	BSA	Na+	Cl-	H2O
BSA	Excluded volume	Electric coupling	Electric coupling Cl- ads. to BSA	Hydration
Na+	Electric coupling		Electric coupling	Hydration
Cl-	Electric coupling Cl- ads. to BSA	Electric coupling		Hydration

5.2.3.1 Hydration

Hydration of solutes is incorporated by using a ‘hydrated molar volume’ that includes the volume occupied by water in the hydration layer of the solute molecule. For BSA, density measurements showed that its specific volume is $0.051 \text{ m}^3/\text{mol}$, which remains relatively constant within a pH range of 4.9 – 8 [20]. Additionally, a single water monolayer ($0.028 \text{ m}^3/\text{mol BSA}$), corresponding to 0.4 g of water per g of BSA, is bound to the globular (spherical) protein, determining a total hydrated molar volume of $0.079 \text{ m}^3/\text{mol}$ [21, 22]. In the case of Na^+ and Cl^- , their hydrated molar volumes are calculated considering them to be spherical and using their corresponding Stokes radii, which already includes the water molecules that are bound to the ions.

This means that for the sake of simplicity in the calculations, the system is regarded as a mixture of hydrated (spherical) components and free water. \bar{V}_i is the hydrated molar volume of the

solutes and, consequently, the calculated φ values include the volume of the water bound to the solutes.

5.2.3.2 Electric coupling - Electroneutrality

In general, the electro-neutrality of a multi-component solution containing species with charge Z , relative to a hydrogen ion, can be expressed as:

$$\sum_i^{m-1} Z_i x_i = \sum_i^{m-1} Z_i \frac{\varphi_i}{V_i} = 0, \quad (5.12)$$

which should be included during the solution of the system of M-S Equations (Eqs. 5.9 and 5.11) to guarantee that in every position along the concentration polarization layer, the net charge remains zero.

5.2.3.3 Cl⁻ adsorption

The adsorption of Cl⁻ to BSA leads to an increase in the negative charge of BSA. In fact, Z_{BSA} is the result of the difference between the bound protons (νH^+) and bound Cl⁻ (νCl^-) in the surface of the BSA molecule, which strongly depends on the pH and ion strength of the solution [23]:

$$Z_{BSA} = \nu H^+ - \nu Cl^- \quad (5.13)$$

in which νH^+ is calculated according to Tanford model for H^+ equilibria in BSA [24] and νCl^- is calculated following the two site chloride binding model of Scatchard et al. [23].

5.2.3.4 Excluded volume

In the M-S approach, thermodynamic non-idealities are part of the driving forces of the system. Nevertheless, the aforementioned non-idealities are expressed in an implicit way within the model, without altering the driving forces terms in the calculation. In the case of the effect of the volume exclusion between BSA molecules, however, we do need to modify the chemical potential gradient term (Eq. 5.14), which should be worked out differently depending on the component of the mixture.

$$\frac{\varphi_i}{RT} \nabla \mu_i = \varphi_i \frac{d \ln a_i}{d \varphi_i} \frac{d \varphi_i}{dz} \quad (5.14)$$

The ‘excluded volume’ of a molecule is the volume that is inaccessible to other molecules due to the finite size of the first molecule. When these molecules are forced close together at high concentrations, the osmotic pressure of the solution increases due to the resulting ordering of the molecules which decreases their degree of freedom to move in free fluid space (entropy) [25].

Component 1: BSA

To consider the thermodynamic effect of the excluded volume by the BSA molecules, the system can be envisaged as a two-component system, in which only BSA (component 1) and water (component 4) coexist. As previously done by Noordman et al., by assuming that BSA has a spherical shape, the osmotic pressure (Π_{RS}) of this two-component system can be calculated using the Carnahan-Starling equation of state as shown in Eq. 5.15 and 5.16 [26].

$$\frac{PV}{n_1RT} = \frac{1 + \varphi_1 + \varphi_1^2 - \varphi_1^3}{(1 - \varphi_1)^3} \quad (5.15)$$

$$P = \Pi_{RS} = \frac{\varphi_1 RT}{\bar{V}_1} \left(\frac{1 + \varphi_1 + \varphi_1^2 - \varphi_1^3}{(1 - \varphi_1)^3} \right) \quad (5.16)$$

The activity of water is linked with the osmotic pressure in the following way.

$$\ln a_4 = \frac{-\bar{V}_4 \Pi}{RT} \quad (5.17)$$

Combining Eq. 5.16 and 5.17, we obtain:

$$\ln a_4 = -\frac{\bar{V}_4}{\bar{V}_1} \left(\frac{\varphi_1 + \varphi_1^2 + \varphi_1^3 - \varphi_1^4}{(1 - \varphi_1)^3} \right) \quad (5.18)$$

The derivative of $\ln a_4$ with respect to φ_1 can be obtained by applying the product and chain rules. The result is shown in Eq. 5.19.

$$\frac{d \ln a_4}{d \varphi_1} = -\frac{\bar{V}_4}{\bar{V}_1} \left(\frac{1 + 4\varphi_1 + 4\varphi_1^2 - 4\varphi_1^3 - \varphi_1^4}{(1 - \varphi_1)^4} \right) \quad (5.19)$$

To calculate the change in the activity of BSA from the change in water activity, the Gibbs-Duhem relation can be used.

$$SdT - VdP + \sum_{\substack{i=1 \\ i \neq 2,3}}^m n_i d\mu_i = 0 \quad (5.20)$$

Considering that T and P are constants in the concentration polarization layer, the following relation results for our ‘imaginary’ binary system:

$$RT \sum_{\substack{i=1 \\ i \neq 2,3}}^m n_i d\ln a_i = 0 \quad (5.21)$$

Which can be further simplified into:

$$n_1 d\ln a_1 = -n_4 d\ln a_4$$

$$\frac{\varphi_1}{\bar{V}_1} d\ln a_1 = -\frac{\varphi_4}{\bar{V}_4} d\ln a_4$$

$$\varphi_1 \frac{d\ln a_1}{d\varphi_1} = -\frac{\bar{V}_1}{\bar{V}_4} (1 - \varphi_1) \frac{d\ln a_4}{d\varphi_1} \quad (5.22)$$

Combining Eq. 5.22 with Eq. 5.19, we obtain:

$$\varphi_1 \frac{d\ln a_1}{d\varphi_1} = \frac{1 + 4\varphi_1 + 4\varphi_1^2 - 4\varphi_1^3 + \varphi_1^4}{(1 - \varphi_1)^3} \quad (5.23)$$

Eq. 5.23 represents the correction needed to account for the volume exclusion for component 1 (BSA). By multiplying the right hand side of Eq. 5.23 by the gradient of molar volume ($\frac{d\varphi_i}{dz}$), an expression equivalent to Eq. 5.14 is obtained, which should be used in the system of M-S Equations.

Component 2 and 3: Na⁺ and Cl⁻

At relatively high concentrations of ions in the solution, the ions activity coefficient can be considered constant along the concentration polarization layer [27, 28]. Therefore, Eq. 5.14 can be worked out in the following way for components 2 and 3.

$$\varphi_i \frac{d\ln a_i}{d\varphi_i} = \varphi_i \left(\frac{d\ln x_i}{d\varphi_i} + \frac{d\ln \gamma_i}{d\varphi_i} \right) \quad (5.24)$$

Combining this with Eq. 5.5 we obtain:

$$\varphi_i \left[\frac{d \ln \left(\frac{\varphi_i}{\bar{V}_i C_T} \right)}{d\varphi_i} + \frac{d \ln \gamma_i}{d\varphi_i} \right] = \varphi_i \left[\frac{\bar{V}_i C_T}{\varphi_i} \frac{d \left(\frac{\varphi_i}{\bar{V}_i C_T} \right)}{d\varphi_i} + \frac{d \ln \gamma_i}{d\varphi_i} \right] \quad (5.25)$$

C_T is hardly influenced by changes in the volume fraction of the ions, thus C_T can be taken out of the derivative together with \bar{V}_i , cancelling out these variables. Additionally, as stated before, the expected change in the volume fraction of ions does not significantly alter their activity coefficient.

$$\varphi_i \frac{d \ln a_i}{d\varphi_i} = \frac{\varphi_i}{\varphi_i} \frac{d\varphi_i}{d\varphi_i} + \varphi_i \frac{d \ln \gamma_i}{d\varphi_i} = 1 \quad \text{for } i = 2,3 \quad (5.26)$$

$$\varphi_i \frac{d \ln a_i}{d\varphi_i} \frac{d\varphi_i}{dz} = \frac{d\varphi_i}{dz} \quad \text{for } i = 2,3 \quad (5.27)$$

In reality, the activity coefficient of the ions are affected by the binding of water molecules to the solutes, and in the case of Cl^- , its activity coefficient is also affected by the adsorption of Cl^- to BSA. However, there is no need to account for these effects since they are already considered within the model: Water bound to the solutes is taken into account in their volume fraction and the adsorption of Cl^- to BSA is already considered when calculating the charge of BSA and the electroneutrality along the CP layer [29]. As consequence, Na^+ and Cl^- are considered thermodynamically ideal in the system and their activity coefficients are constant along the concentration polarization layer.

5.2.4 Equilibrium at the membrane interface

Local thermodynamic equilibrium is assumed at the membrane interface. Therefore, the chemical potential of every component at the membrane surface (μ_i^w) is similar to the chemical potential just inside the membrane pores (μ_i'). Considering that ions behave ideally, the chemical potentials can be described as functions of x_i as shown in Eq.5.29, in which the effect of the pressure in the potential is neglected. This expression allow us to relate the concentration of the ions at the permeate stream with that of the ions at membrane surface [30].

$$\mu_i^w = \mu_i' \quad (5.28)$$

$$RT \ln x_i^w + Z_i F \Psi^w = RT \ln x_i' + Z_i F \Psi' \quad \text{for } i = 2,3 \quad (5.29)$$

By summing the expression corresponding for $i=2$ and $i=3$, Eq. 5.30 can be obtained, which is equivalent to the Donnan equilibrium relation [31].

$$\ln x_2^w + \ln x_3^w = \ln x_2' + \ln x_3'$$

$$x_2^w x_3^w = x_2' x_3' \rightarrow x' = \sqrt{x_2^w x_3^w} \quad (5.30)$$

5.2.5 Diffusion coefficients

One of the advantages of the M-S diffusion coefficients is that they do not contain the thermodynamic non-idealities of the system; hence, they get less affected by changes in concentration than Fick diffusion coefficients. The binary diffusivities of Na^+ and Cl^- with water can be assumed constant. In the case of BSA, \mathfrak{D}_{14}^V changes depending on BSA concentration, and can be calculated using the following relation, which is derived in detail in the appendix section (A1).

$$\mathfrak{D}_{14}^V = D_{14}^0 \frac{0.21 + 0.79 \exp(-4.7\varphi_1)}{\frac{1 + 4\varphi_1 + 4\varphi_1^2 - 4\varphi_1^3 + \varphi_1^4}{(1 - \varphi_1)^3}} \quad (5.31)$$

Although the concentration of BSA can be very high in the concentration polarization layer ($\varphi_1^w \approx 0.55$), the system is still diluted in terms of molar fractions with x_4^w values of nearly 0.99. For this reason, the effect of the cross diffusivities between solutes is not too important in the final outcome [17]. The friction terms between BSA and the ions can be neglected in Eq. 5.9, while the cross diffusivities between ions (\mathfrak{D}_{23}) can be calculated using the following empirical relation, in which I stands for the ionic strength of the solution [17].

$$\mathfrak{D}_{23} = \mathfrak{D}_{32} = \frac{\mathfrak{D}_{24} + \mathfrak{D}_{34}}{2} \frac{I^{0.55}}{|Z_2 Z_3|^{2.3}} \quad (5.32)$$

$$I = 0.5 \sum_i Z_i^2 x_i$$

Note that the ion cross-diffusivity needs to be converted to modified diffusivities ($\mathfrak{D}_{23}^V, \mathfrak{D}_{32}^V$) using the relation in Eq. 5.8, before being used in the M-S Equation (Eq. 5.9).

5.2.6 Osmotic pressure

When the flux in a specific point along the length of the membrane is lower than the local critical flux, steady state is still achieved but the chemical and electrical potential gradients in

that point are not the maximal. Under these ‘local subcritical conditions’, change of phase for the proteins is not occurring because the gel concentration is not reached at the membrane surface. Therefore, the flux in that point is only influenced by the difference in the osmotic pressure across the membrane since it is assumed that no fouling occurs in the membrane surface at that specific point. Consequently, the local membrane permeability is considered unaltered.

Under these conditions, the concentration of the protein at the membrane surface becomes an unknown because it cannot be considered that $\varphi_1^w = \varphi_{gel}$. Thus, apart from the force balance represented by the M-S equations, an extra equation is needed. That extra equation is the flux relation derived from Darcy’s law (Eq.5.33).

$$J_{osmo} = L_p(\Delta P - \Delta \Pi) \quad (5.33)$$

The osmotic pressure difference ($\Delta \Pi$) in Eq.5.33 should be calculated using the real osmotic pressure of the system and not the one obtained in our ‘imaginary’ binary system from section 5.2.3.4. To do so, the contribution of the ions in the osmotic pressure should be included by using Eq. 5.34 and 5.35. A complete explanation of the derivation of these expressions is included in the Appendix section (A2).

$$\Pi = -\frac{RT}{\varphi_4} \left(\frac{\ln \gamma_4 \varphi_4}{\bar{V}_4} - \frac{\varphi_1}{\bar{V}_1} - \frac{\varphi_2}{\bar{V}_2} - \frac{\varphi_3}{\bar{V}_3} \right) \quad (5.34)$$

$$\ln \gamma_4 = \frac{\bar{V}_4 \varphi_1^4 - 3\varphi_1^2}{\bar{V}_1 (1 - \varphi_1)^3} \quad (5.35)$$

For the case of the permeate stream, in which no BSA is expected, the system is considered ideal, so $\ln \gamma_4 \approx 0$, and $\varphi_4 \approx 1$. As consequence, Eq. 5.34 reduces to the Van’t Hoff’s equation:

$$\Pi = -RT(-2C_{2,3}) \quad (5.36)$$

Where C stands for the concentration of the ions in mol/m³. The factor 2 originates from the fact that the concentration of both ions is the same in the permeate, and is commonly known as Van’t Hoff’s index.

Figure 5-3 shows the predictions obtained using Eq. 5.34 and 5.35 for a solution of BSA, NaCl and water at different pH and I=0.15M. Experimental values from Vilker et al. are also shown in Figure 5-3, where it can be seen that the accuracy of the prediction is good [8]. At high volume fractions, the excluded volume of BSA increases exponentially and becomes the most

important non-ideality in the system. Such behaviour is reflected in the steep rise in osmotic pressure as the system becomes more concentrated.

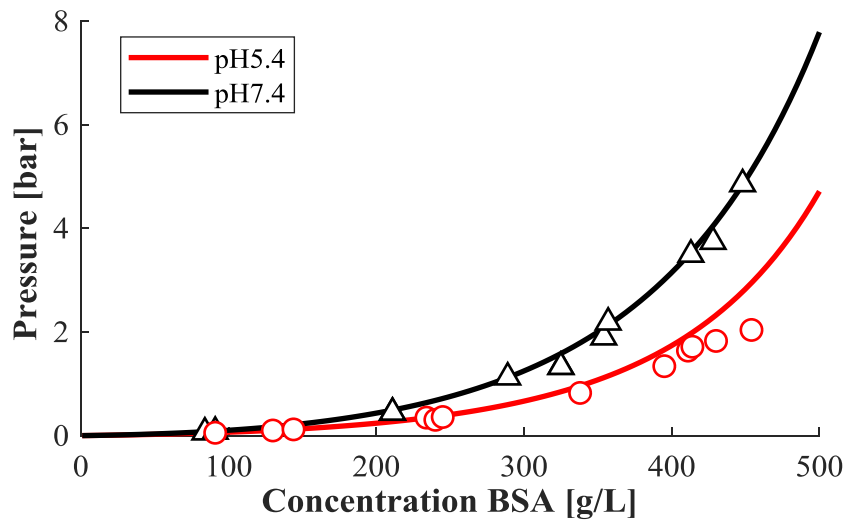


Figure 5-3. Osmotic pressure predictions (Eq.5.34) and measurements for BSA+NaCl+water solutions at $I=0.15M$. The measurements were taken from the work of Vilker et al [8].

5.3 MATERIALS AND METHODS

5.3.1 Chemicals

Milli-Q water® (ultrapure water) obtained from Millipak® 40 Express Filter with a pore size of $0.22 \mu m$ (Darmstadt, Germany) was used for all the experiments. Lyophilized bovine serum albumin powder with a purity $\geq 96\%$ was used to prepare the feed solutions. Likewise, NaCl with a purity $\geq 99\%$ was used to set the ionic strength of the solutions. NaOH and HCl with a purity $\geq 99\%$ were used to prepare solutions 2 M to adjust the pH of the BSA solutions. All these chemicals were bought from Sigma Aldrich (Steinheim, Germany). Table 5-2 shows the charge, diffusivity at diluted conditions, radius and hydrated molar volume of the solutes used in this study.

Table 5-2. Properties of the solutes used in this study

Component	Z_i	D_{i4}^∞	r_i	\bar{V}_i
	[]	[10^{-10} m ² /s]	[10^{-9} m]	[10^{-5} m ³ /mol]
BSA	Dependent on pH and I	0.61	3.14	7900
Na	+1	13.3	0.184	1.57
Cl	-1	20.3	0.121	0.45

5.3.2 Membranes and set up

Two types of UF flat sheet membranes were used during the experiments. Their pore size was such that complete rejection of BSA was assured while the rejection for NaCl was nearly 0 in the pH range 4.9 – 8. The first membrane was a GH thin film membrane with a MWCO of 2500 Da produced by GE Water & Process Technologies (Kent – United States), and the second one was a NP010 P polyether sulfone nanofiltration membrane with a MWCO \approx 3000 Da produced by Microdyn Nadir (Wiesbaden, Germany). Experiments with pure water showed that the average membrane permeabilities (L_p) of the membranes were 1.56×10^{-6} and 2.79×10^{-6} m/(s bar) for the GH and NP010P membrane respectively.

The rig consisted of a rectangular filtration channel with dimensions: 1000x50x7 mm, and included flow meters to measure crossflow and permeate flow, and sensors to monitor the temperature, electrical conductivity and pressure of the retentate and permeate streams. A double jacket in the feed tank allowed stabilization of the system at 25°C.

5.3.3 Experiments at constant pressure

0.5% w/w feed solutions of BSA at different ion strength and pH were used in this study. To prepare the solutions, BSA and Milli-Q water were combined and stirred for 45 minutes at 25°C. Then, the solutions were filtered with a Whatman® grade 50 filtration paper to remove aggregates and clumps. These feed solutions were adjusted to the desired ionic strength (0.03 and 0.15 M) using NaCl. The experiments were run at three different pH values (4.9, 5.8 and 7.2), which were reached by adding aliquots of 2M solutions of NaOH or HCl.

The filtration system was kept at 25 °C with a low crossflow flux of 0.056 m/s to assure laminar flow inside the channel. The filtration started using a TMP of 2 bar, switching to 6 and 8 bar after reaching steady state flux. At steady state, samples from the retentate and permeate were collected to measure the concentration of BSA and Cl⁻. For each new experiment a new previously soaked membrane (GH or NP010) was used.

5.3.4 Experiments at constant flux

For the experiments at constant flux, the process parameters (temperature and crossflow velocity) were similar as in the constant pressure experiments, but only the GH membrane was used. The pre-selected permeate flux was not altered during the experiment, and when the pressure reached a constant value, samples from retentate and permeate were collected. For each new experiment a new previously soaked membrane was used.

5.3.5 Analytical methods

High-performance liquid chromatography (HPLC) was used to measure the BSA concentration in the retentate and permeate streams. The analysis was done using a TSKGel G3000SWXL column (size: 300 x 7.8 mm) kept at a temperature of 30°C. A solution of 30% Acetonitrile in MilliQ with 0.1% trifluoroacetic acid was used as eluent at a flow rate of 1mL/s. UV detection at a wavelength of 214 nm was used to detect the protein.

For the NaCl determination, Cl⁻ was measured with Titralab AT1000 series from Hach (Tiel, Netherlands), which is an automated titration equipment that uses Mohr's method to measure the concentration of Cl⁻ ions by doing a titration with 0.1 M AgNO₃.

5.3.6 Computational Analysis

MATLAB R2017b was used for all the calculations. Integrations were performed using the function 'trapz', which uses the trapezoidal numerical integration method. To solve the M-S equations, the function 'ode15i' was used, which allows solving systems of implicit differential equations.

5.3.7 Algorithm

Under limiting conditions (region C in Figure 5-2), to calculate the steady state permeate flux, the solution of the system of M-S Equations described in Eq. 5.9 is necessary together with two extra conditions Eq. 5.11 and 5.12. The term including the chemical potential differences in Eq.

5.9 should be worked out for each solute considering Eqs. 5.14, 5.23 and 5.27. If the non-uniform nature of the boundary layer is considered (section 5.2.1), the overall permeate flux will be the outcome of the integration of the local fluxes, according to Eq. 5.2.

Since no suitable model for the calculation of the local mass transfer coefficients for BSA was found in literature, the parameter $\delta(z = L)$ was fitted to experimental flux data at limiting conditions. From the boundary layer theory, it is known that the boundary layer grows along the membrane axis with a proportionality of $(z/L)^{1/3}$. Therefore, with the value of $\delta_{(z=L)}$, the values of $\delta_{(z)}$ along the channel can be calculated, and consequently, the local critical fluxes along the membrane can also be obtained. The maximum protein concentration (gel concentration) was set to be $\phi_1^w = 0.55$ [12] and the observed rejection of ions was considered to be 0 regardless the process conditions.

When working at low pressures with $TMP < \Delta P_{lim}$ (region A or B in Figure 5-2) we calculate de critical distance z_{crit} , so we can distinguish two sections in the membrane: clean and fouled. To do so, we solve Eq. 5.33 considering a concentration of $\phi_1^w = 0.55$, and a distribution of ions according to Donnan equilibrium. The obtained flux is compared with the previously estimated local critical fluxes, and the point at which these two fluxes are similar will be z_{crit} . If the flux value calculated with Eq.5.33 is lower than all the critical fluxes along the membrane, then the membrane is completely clean and $z_{crit} = L$ (region A in Figure 5-2).

When the membrane is partially fouled (region B in Figure 5-2), from z_{crit} to $z = L$, the membrane is considered to be covered by gel; therefore, the local fluxes are the critical ones (J_{crit}). On the other hand, from $z = 0$ to z_{crit} , the membrane is not fouled, and the M-S Equations (Eq. 5.9, 5.11 and 5.12) should be solved once again to calculate the concentration of the solutes at the membrane surface and the corresponding local fluxes (J_{osmo}). To do so, the $\delta_{(z)}$ values previously calculated at limiting conditions can be used since they can be considered constant regardless the pressure of the system. Finally the overall permeate flux (J_v) is calculated taking into account the $J_{crit}(z)$ and $J_{osmo}(z)$ values as described in Eq.5.3. For different conditions in the feed (pH and I), the complete algorithm should be repeated (see Figure 5-4).

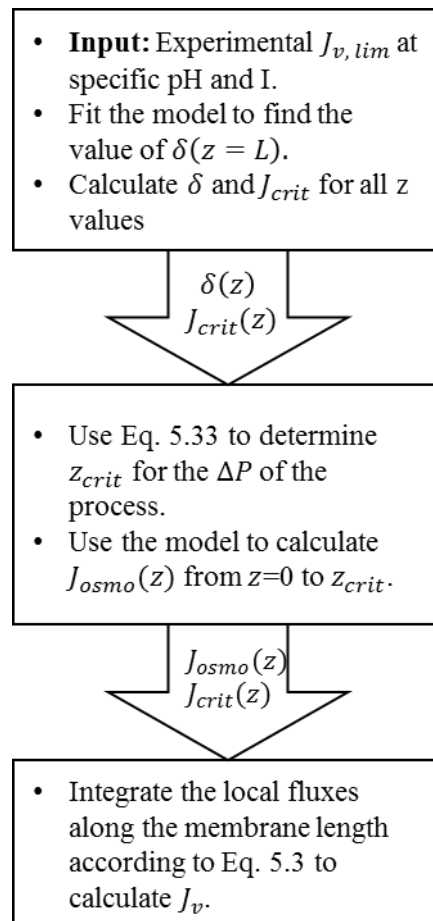


Figure 5-4. Scheme of the algorithm to calculate the overall permeate flux J_v at steady state. For different pressures, only the last two steps of this scheme should be repeated. For different physicochemical conditions the whole algorithm should be recalculated. In the case of constant flux experiments, an iterative procedure involving the last two steps is needed to determine the ΔP value that corresponds to the predefined J_v .

5.4 RESULTS AND DISCUSSION

5.4.1 Filtration at limiting conditions

Filtration experiments were performed at limiting conditions (region C in Figure 5-2) using feed solutions at different pH and ion strengths. These variations imply electrical interactions between solutes to different degrees, and consequently, different permeate fluxes at steady state. The mass transfer coefficient (k) and, consequently, the concentration polarization layer thickness were also expected to be different for every experiment. Therefore, the experimental

steady state fluxes were used to estimate this thickness at the outlet of the system ($\delta_{(z=L)}$). The results of this estimation are shown in Table 5-3.

Table 5-3. Estimated values for $\delta_{(z=L)}$ from experimental flux data at limiting conditions for different pH and ion strength. GH membrane was used during these experiments.

Feed Solution		Z_{BSA}	$J_{v\ lim} [10^{-6}\text{m/s}]$	$\delta_{(z=L)} [10^{-4}\text{m}]$
pH 4.9	$I=0.03\ \text{M}$	0	2.24	1.34
	$I=0.15\ \text{M}$	-2.4	2.36	1.28
pH 5.7	$I=0.03\ \text{M}$	-6.7	2.90	1.30
	$I=0.15\ \text{M}$	-11.2	2.76	1.24
pH 7.2	$I=0.03\ \text{M}$	-13.5	3.48	1.68
	$I=0.15\ \text{M}$	-18.8	3.05	1.37

While a higher pH and hence a larger Z_{BSA} value leads on average to larger values of $\delta_{(z=L)}$, an increase in ionic strength at the same pH leads to lower values. According to film theory, δ is inversely related with k and the proportionality between them is given by the Fickian diffusivity ($\delta = D/k$). However, since D contains all the non-idealities of the system, it also changes with pH and I . Therefore, as we determined δ using experimental flux data, the effects of the non-idealities show up in the value of δ .

$J_{v\ lim}$ shows a relation with Z_{BSA} in Table 5-3. As Z_{BSA} increases due to a pH change, the repulsion between molecules increases as well, reducing the thickness and the density of the gel layer, and, as consequence, determining a higher limiting flux [32]. Ion strength plays also an important role in this matter, since the increase of ions in the system from 0.03 M to 0.15 M screened the electrostatic interactions between BSA molecules, reducing the repulsion.

Although only one value for δ was fitted ($\delta_{(z=L)}$), the calculation of local critical fluxes along the entire membrane was necessary, the obtained results for the different physicochemical conditions are plotted in Figure 5-5.

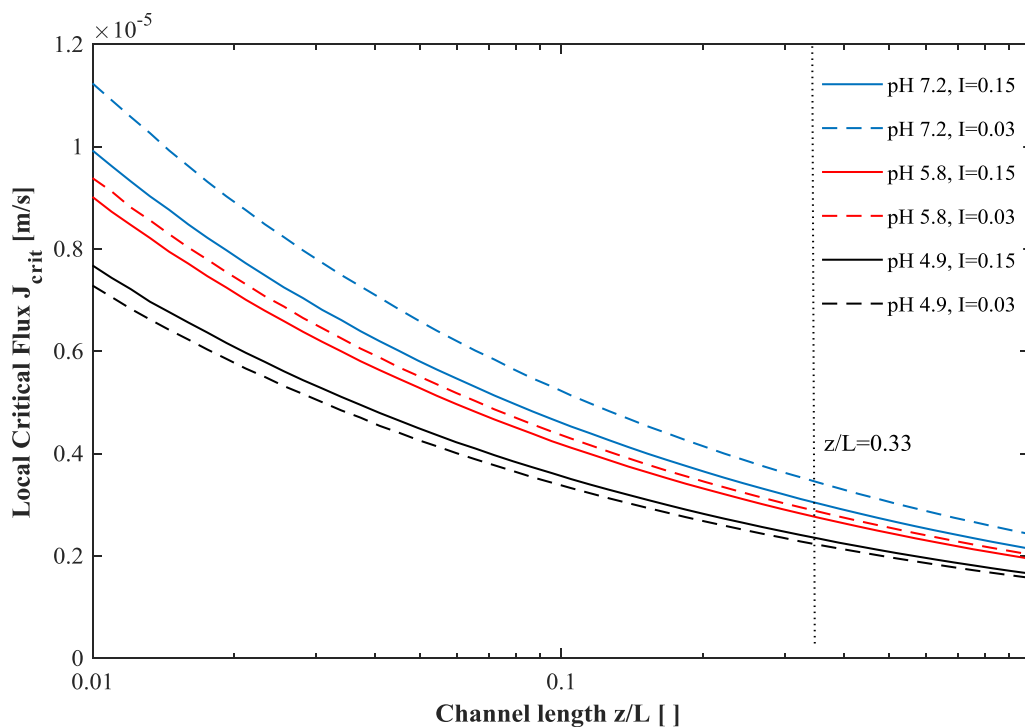


Figure 5-5. Local Critical fluxes along the channel length for different pH and ion strength values. In all the cases the feed was composed by BSA (0.5g/L), NaCl and water.

The local critical fluxes varied strongly along the membrane regardless the feed used in the experiment. This was due to the expression used to represent the thickening of the boundary layer along the membrane (Eq.5.1). As consequence, the limiting permeate flux at the entrance was 3-4 times higher than that at the outlet, and the local critical flux at $\frac{z}{L} = 0.33$ was similar to the overall flux value obtained with Eq. 5.2.

As expected, higher local critical fluxes were obtained at higher pH values (higher negative charge for Z_{BSA}). At pH 5.75 and 7.25, increasing ion strength leads to lower fluxes due to the screening of the electrical repulsion between BSA molecules, usually represented as thinner electrical double layers around the charged macromolecules. At the isoelectric point (pH4.9), the opposite behaviour was observed: The local fluxes were slightly higher at higher ion strength. At this pH, the number of positive and negative charges at the surface of BSA are the same, and their spatial distribution over the protein surface leads to intermolecular attraction and a compact gel. The increment of ions in the solution screened this attraction, leading to a higher permeate flux [31].

The way how BSA and ions influence each other can be seen in Figure 5-6, in which the concentration profiles of the solutes are shown for a specific position in the filtration channel ($z/L=0.33$). The BSA concentration grows exponentially in the concentration polarization layer towards the membrane surface, until it reaches its maximum at $\delta=113\mu\text{m}$, and form a gel. The steep increase of BSA influences the local concentration of the other ions, since electroneutrality must be maintained along the whole system. As a result, the concentration of the counterion Na^+ increases to compensate the negative charged BSA, while the concentration of the co-ion Cl^- decreases. Given that the BSA concentration is assumed constant in the gel layer, the concentration of ions was also assumed constant over the gel layer thickness. Additionally, local thermodynamic equilibrium was assumed at the membrane surface (Eqs. 5.28 to 5.30) to calculate the ions concentration just inside the membrane. These concentrations are similar to the concentrations in the permeate stream since the membrane pores were considerably bigger than the ions, so the friction of the transient ions with the membrane walls was considered negligible.

To enable the solution of the M-S equations, free passage of the ions through the membrane ($R_{\text{NaCl}}=0$) and total BSA rejection was assumed ($R_{\text{BSA}}=1$) for the calculations of the solute fluxes (Eq.5.10). These assumptions were experimentally checked at all feed conditions used in this study. Indeed, experimental R_{NaCl} fluctuated between 0.05 and -0.05, while R_{BSA} was never lower than 0.99. As shown in Figure 5-6, the calculated NaCl rejection coincides with our initial assumption.

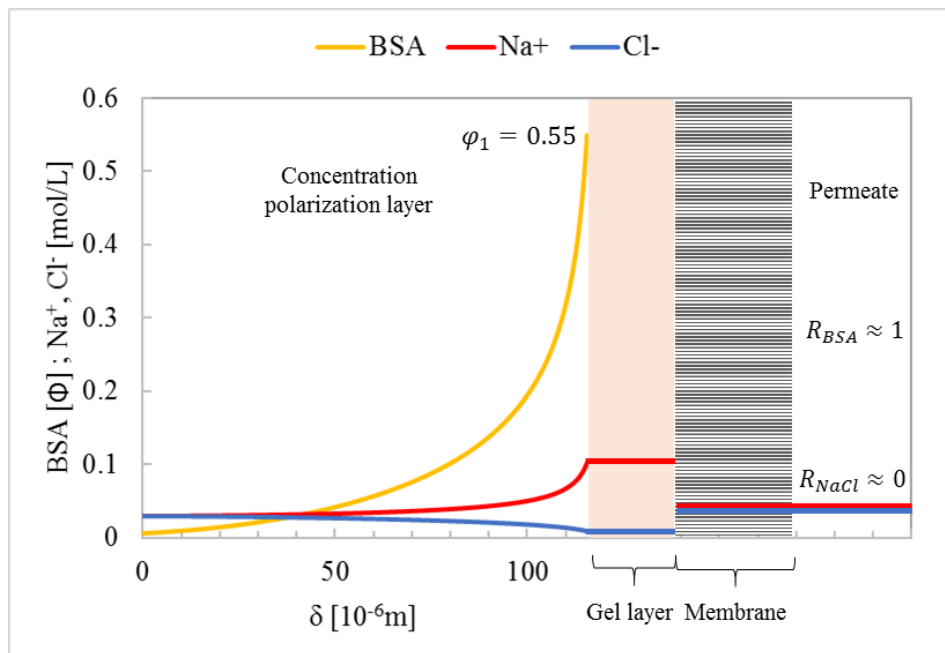


Figure 5-6. Solutes' concentration profiles corresponding to the position $z/L=0.33$ in an ultrafiltration channel at limiting conditions. The feed solution was at pH 7.2m and $I=0.03$ M (NaCl). The thickness of the gel layer and the membrane are not plotted to scale with respect to the thickness of concentration polarization layer.

The gel layer constitutes an extra resistance for the flow of liquid through the membrane. This is, however, not relevant for our model, since the local critical fluxes are determined by the force equilibrium in the concentration polarization layer.

5.4.2 Filtration in the Transition region

When part of the membrane is not covered by the gel layer, or when the entire membrane is not covered at all, the permeate flux is also influenced by the osmotic pressure of the system. Since the solutes concentrations at the surface of the 'uncovered section' of the membrane are different depending on the position along the membrane, the osmotic pressure is expected also to vary along the membrane length. For this reason, the M-S Equations had to be solved at every position z , considering $\delta_{(z)}$ to be the same as the values determined under limiting conditions. Figure 5-7 shows the predicted local fluxes obtained when a membrane was partially fouled. As consequence, two mechanisms (osmotic pressure and gel layer) coexisted within a filtration channel. The critical distance (z_{crit}), at which fouling starts at the membrane, separates both mechanisms, and was different depending on TMP.

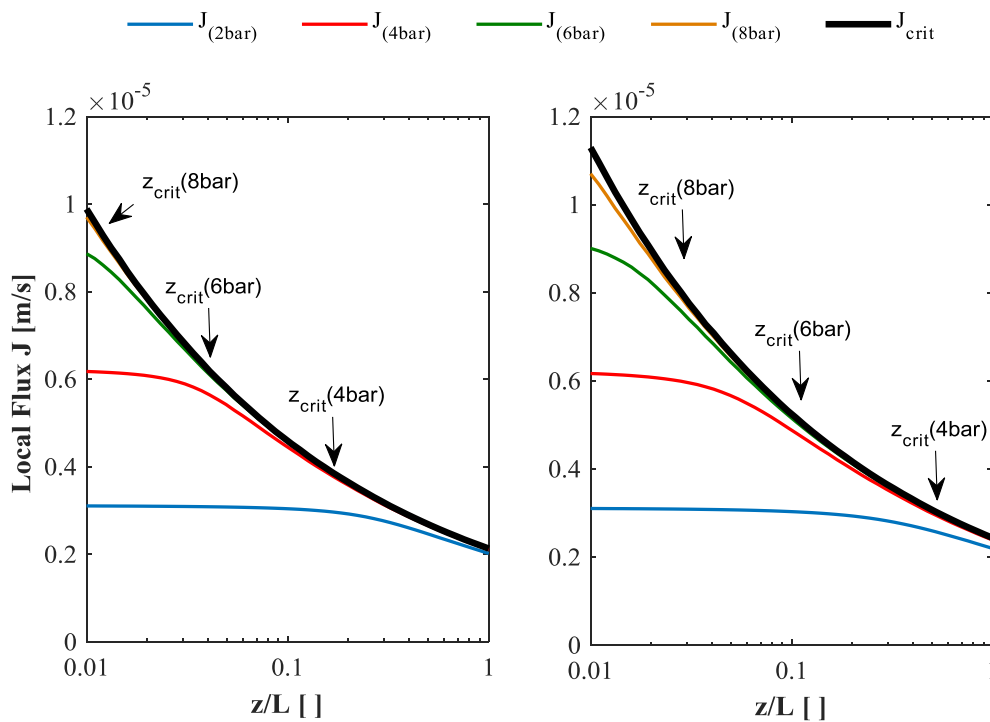


Figure 5-7. Local permeate fluxes due to two mechanisms (osmotic pressure and gel layer) during the desalination of BSA using a GH membrane at pH 7.2 and ion strength of $I=0.15$ M (left) and $I=0.03$ M (right). Fluxes from $z=0$ to z_{crit} are calculated considering the local osmotic pressures of the system (Eq.5.33). Fluxes from z_{crit} to $z=L$ are similar to J_{crit} , as obtained in section 5.4.1. X axis was plotted in logarithmic scale to show the transition between mechanisms in a clearer way.

As the pressure increases, the resulting local fluxes increase especially at the entrance of the channel, where the maximum local flux (the critical flux) is higher. In the predictions for an ionic strength of 0.15 M (Figure 5-7 - left), at a pressure of 2 bar, gel formation is just about to occur at the outlet of the membrane. At a pressure of 8 bar, the membrane is almost completely fouled and the limiting flux is nearly reached. Therefore, pressures higher than 8 bar would not alter the steady state permeate flux of the system. At lower ionic strength (Figure 5-7 - right), higher values for the critical fluxes and, consequently, for z_{crit} were obtained. Gel formation appears at a higher pressure than with the higher ionic strength of $I=0.15$ M, and the limiting flux is not yet achieved at a pressure of 8 bar. These results agree with the DLVO theory with respect to the screening effect of ions, and go in line with what has been observed experimentally by many authors for decades [4, 32].

It has been measured by other authors that for a given BSA concentration, the osmotic pressure gets lower as the ionic strength increases [33]. This would produce higher fluxes at higher I . Interestingly, this effect was not visible in the ‘uncovered’ membrane sections shown in Figure 5-7, in which $J_{osmo}(z)$ was always lower for $I=0.15$ M than for $I=0.03$ M. The reason is that both figures (Figure 5-7 left and right) are in fact not comparable. BSA concentrations at the membrane in the uncovered regions are much lower for $I=0.03$ M. The reason is that, at low ionic strength, the electrical potential gradient is greater (see Figure 5-8). This promotes the back diffusion towards the bulk of the retentate, lowering the increase of the BSA concentration.

Some UF models assume that when working in the transition region (see Figure 5-2), the permeate flux is entirely governed by the osmotic pressure. Under these assumption, there is not a consistent transition, but a contradiction between the flux defined by the osmotic pressure and the critical flux defined by the presence of the gel layer. Using uniquely the osmotic pressure approach, in the limit when BSA is becoming a gel, the flux for $I=0.03$ would be smaller than for $I=0.15$, when the opposite has been experimentally observed. Thus we feel that this interpretation does not hold in view of the experimental evidence.

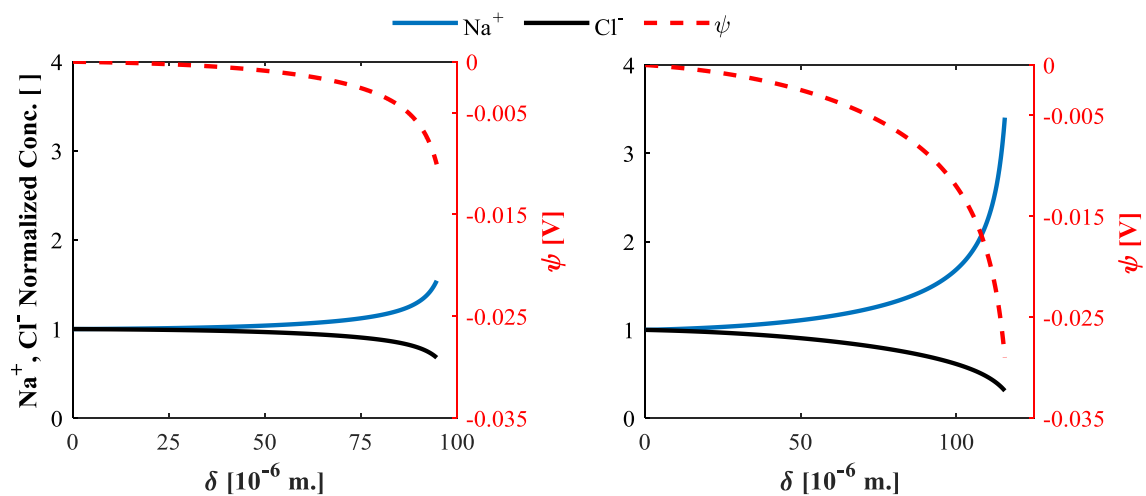


Figure 5-8. Normalized concentration profiles for Na^+ and Cl^- along the concentration polarization layer for the UF of BSA. The pH of the solutions was pH 7.2 and two ion strengths: $I=0.15$ (left) and $I=0.03$ (right) were studied at z_{crit} ($\varphi_1^W=0.55$). The resulting electrical potential is represented with dashed lines.

Figure 5-8 shows a comparison in the behaviour of the accompanying ions at two different ionic strengths. As the concentration of BSA increases along the concentration polarization layer, the concentration of Na^+ increases and that of Cl^- decreases. This change in concentrations is much

stronger at low ionic strengths. Therefore, this excess of Na^+ ions explains why higher osmotic pressures are observed under these conditions, compared to those at high ionic strengths. Another consequence of this asymmetric distribution of ions is that the electrical potential is much more negative at low ionic strengths, determining, as explained in Figure 5-6, an enhanced back diffusion of BSA towards the retentate bulk. Consequently, considering the electroneutrality condition (Eq. 5.12) during the resolution of the M-S Equations, and imposing a Donnan partitioning across the membrane (Eq. 5.30), we can accurately calculate the osmotic pressure in any position along the system for any pH and I . The resulting quantification of the electrical potential is an advantage of using the M-S Equations over other models where the electrical interactions between components are represented as an additional factor.

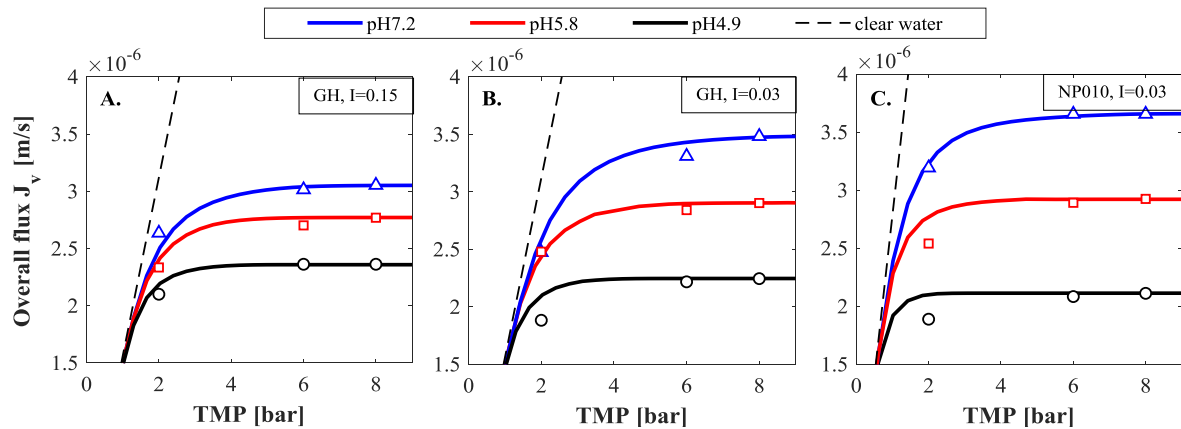


Figure 5-9. Overall permeate flux at different pH and I for two different membranes (GH and NP010). Continuous lines represented the model predictions and markers are the experimental measurements at steady state. Dashed lines are the fluxes using clear water.

The model was experimentally verified with measurements of the overall permeate flux under different physicochemical conditions (Figure 5-9). In general, a good accuracy was obtained for all the experiments. As expected, higher fluxes were obtained at lower ionic strengths, with the exception of the measurements at the isoelectric point, where an excess of ions screens the attraction between BSA molecules.

When comparing the effect of different membranes (Figure 5-9 B and C), somewhat similar limiting fluxes were obtained, regardless of the large difference in water permeability between the GH and the NP010 membranes. This similarity was expected as the local critical fluxes are determined by the equilibrium of forces in the concentration polarization layer, and not by the membrane. The same type of experimental observations have been reported by other authors [4, 34]. When working with fluxes lower than the limiting flux (Transition region), some parts of

the membrane remain uncovered and, consequently, some differences appeared in the flux due to the different permeability between both membranes. The GH membrane required a higher pressure to reach the limiting flux, especially at pH 4.9 and 5.8.

5.4.3 Experiments at constant flux

In industry, membrane filtration is mostly done at constant flux. Experiments under these conditions were performed to evaluate the applicability of our model. Figure 5-10 shows experimental measurements of TMP as function of time for different feed conditions. The left hand graph shows the difference in the pressure behaviour over time when the permeate flux was set higher and lower than the limiting flux. In the former case, no steady state was achieved and the pressure kept growing strongly, while in the latter case the pressure increased gently until it reached a plateau after some time. This plateau represents the steady state pressure, which is the equilibrium point where the drag due to convection is equal to the back diffusion effects due to the chemical and electrical potentials in the concentration polarization layer.

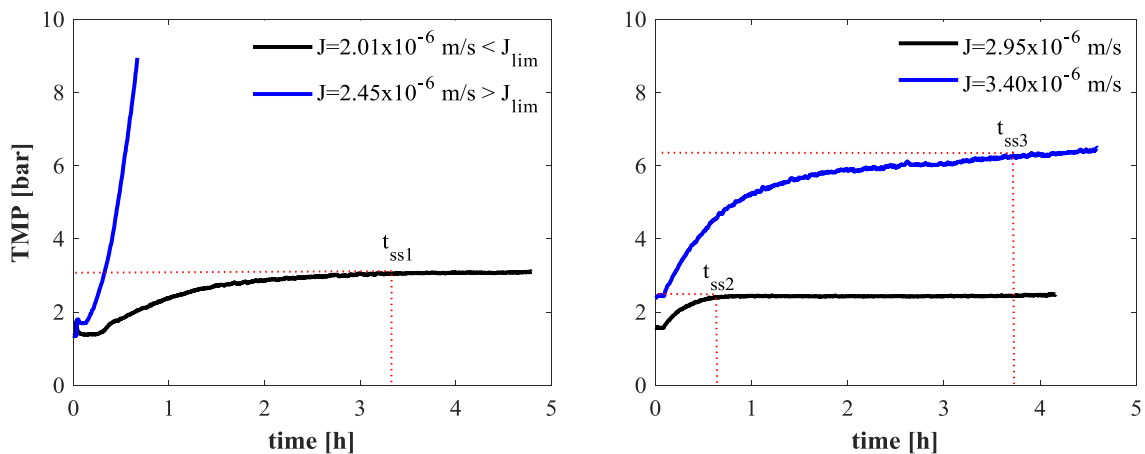


Figure 5-10. TMP as function of time for experiments at constant flux using GH membrane. The physicochemical conditions of the BSA solution were pH at 4.9, $I=0.03$ (left), and pH=7.2, $I=0.03$ (right).

In the right-hand graph of Figure 5-10, the comparison of the TMP evolution over time for two different permeate flows is shown for a larger pH. At a low permeate flow of $2.95 \times 10^{-6} \text{ m/s}$ (15% lower than J_{lim}), steady state was achieved in less than one hour, while at a higher flux (3% lower than J_{lim}), it took almost 4 hours to reach steady state. This clearly depicts the growth of the gel layer along the filtration channel over time. We conclude that at low fluxes, fouling only occurs in the outlet of the channel, while at higher fluxes, this fouling grows inwards towards

the channel inlet. Additionally, the fact that the increase of TMP over time becomes smaller shows that the system was stable and eventually will reach a steady state.

With the experimental measurements presented in Figure 5-10 is evident that below the limiting flux, in the transition region, fouling is already taking place over the membrane, as properly represented in our model. Consequently, it is incorrect to simplify the description of UF to a system that can go from ‘completely clean’ to ‘completely fouled’ in one instant. The transition region is quite important, and very relevant for practical UF operation.

At steady state, the combination of permeate flux and TMP are the same whether we operate the system at constant pressure or constant flux. Therefore, our model can be easily adapted to predict the steady state TMP, using as input the required value for the permeate flux. Figure 5-11 shows the accuracy of these predictions.

It is important to mention, however, that when the permeate flux was set close to J_{lim} , it was somewhat difficult to experimentally identify a steady state value for the TMP. The gel layer kept growing slowly and sometimes irregularly, implying that the duration of one experimental run might not capture the complete process of gel layer growth. Therefore, the next step would be to investigate the kinetics of the formation and growth of the gel layer. This will then enable the reliable prediction of the system performance over very long production runs.

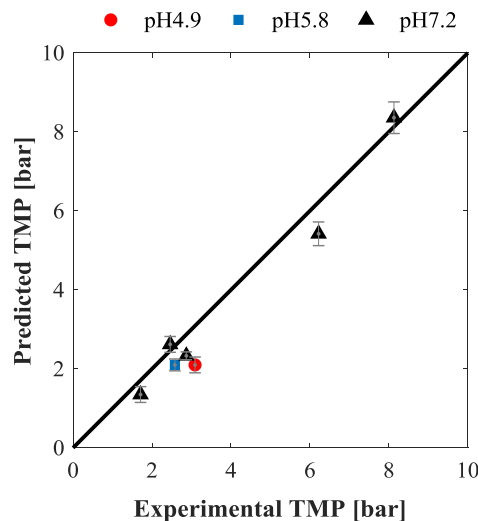


Figure 5-11. Comparison between model predictions of TMP and TMP measurements for experiments performed at constant flux and $I=0.03M$.

In this study we considered the ‘uncovered section’ of the membrane to be completely clean; hence, its original permeability was used in the calculations. This is obviously an oversimplification. Over time BSA will adsorb to the membranes due to the intermolecular interactions with the membrane surface, reducing slightly the local permeability. Since our model could well predict the experimental results, this effect was negligible under the conditions that were chosen and our assumption was justified; however this may be different with other conditions or during longer filtration runs.

5.5 CONCLUSIONS

A model to estimate the permeate flux at steady state of a UF system was developed taking into account not only the concentration profiles of the protein (BSA) but also the concentrations of the accompanying ions. The model was developed using modified Maxwell Stefan Equations expressed as function of the components’ volume fraction, which allowed the easier inclusion consideration of the non-idealities of the system (hydration, adsorption, electrical interactions and volume exclusion).

It was found that more than one mechanism can influence the permeate flux in a filtration system. For partially fouled membranes, two sections of the membrane can be distinguished, in which two different mechanisms determine the resulting local permeate fluxes. The uncovered section is mostly influenced by the osmotic pressure of the system, while in the section covered with gel, local critical fluxes, defined by the gel layer mechanism, are attained.

The model gave very good prediction of experimental results at different pH and ionic strengths, and could well describe the TMP during controlled-flux experiments, and the flux during controlled-TMP experiments. In fact, the steady state values for TMP and permeate flux were found to be the same whether the system was operated at constant pressure or constant flux.

The Maxwell-Stefan approach has thus proved effective in calculating the concentration profiles of the charged solutes along the concentration polarization layer. At the membrane, the Donnan equilibrium relation is the simplest way to calculate the concentration of the ions in the permeate and give accurate estimations of the osmotic pressure of the system. This methodology is in line with DLVO theory and allow us to quantify the contribution of the electrical interaction in the resulting permeate flux.

ACKNOWLEDGEMENTS

This work was carried out as part of a project of the Institute for Sustainable Process Technology (ISPT), The Netherlands: project number CM-20-05. We thank Bobby Oka Mahendra and Desiree Nieuwenhuijse for their contribution in the experimental part of this study within their Master thesis project at the Food Process Engineering group (Wageningen University).

NOMENCLATURE

a	Chemical activity []
C_g	Gel concentration [mol/m ³]
C_m	Concentration at the membrane [mol/m ³]
C_T	Total molar concentration [mol/m ³]
D	Fick Diffusion coefficient [m ² /s]
F	Faraday constant [Coulomb/mol]
I	Ion strength in Eq. 5.32[]
J	Volumetric Flux [m/s]
J_{crit}	Local critical flux [m/s]
J_{osmo}	Local flux determined only by the osmotic pressure [m/s]
J_v	Overall permeate flux [m/s]
k	Mass transfer coefficient [m/s]
L	Total length of the filtration channel [m]
L_p	Membrane permeability [m]
n	number of moles [mol]
m	Total number of components in mixture (including water as component m) []
P	Pressure [bar]
p	Permeate
R	Gas constant [J/(K mol)]
r	radius [m]
S	Entropy [J/K]

T	Temperature [K]
TMP	Transmembrane Pressure [Pa]
u	Linear velocities [m/s]
V	Volume [m ³]
\bar{V}	Molar volume (hydrated) [m ³ /mol]
x	Molar fraction []
w	Membrane surface
Z	Charge []
z	Position along the length of the filtration channel [m]
z_{crit}	Critical distance []

Greek letters

γ	Activity coefficient []
Π	Osmotic Pressure [Pa]
Π_{RS}	Osmotic Pressure due to excluded volume (Rigid Sphere)[Pa]
δ	Concentration polarization layer thickness [m]
\mathfrak{D}	Maxwell-Stefan diffusion coefficient [m ² /s]
\mathfrak{D}^V	Modified Maxwell-Stefan diffusion coefficient [m ² /s]
Γ	Thermodynamic factor []
μ	Chemical Potential [J/mol]
$\tilde{\mu}$	Electrochemical Potential [J/mol]
φ	Volume fraction []
ψ	Electrical potential [V]

APPENDICES

A1. Calculation of the modified M-S diffusion coefficient \mathfrak{D}_{14}^V

The M-S diffusion coefficient of BSA(\mathfrak{D}) is related to the Fick diffusion (D) coefficient in the following way:

$$D_{ij} = \mathfrak{D}_{ij} \Gamma_i \quad (5.A1)$$

In which Γ is the thermodynamic factor that corrects for the non-idealities of the system. In the case of BSA, Γ can be expressed as follows to account for volume exclusion:

$$\Gamma_{11} = x_1 \frac{d \ln a_1}{dx_1} \frac{d \varphi_1}{d \varphi_1} = x_1 \frac{d \ln a_1}{d \varphi_1} \frac{d \varphi_1}{dx_1} \quad (5.A2)$$

Considering the following approximations:

$$C_T \approx \frac{\varphi_4}{\bar{V}_4} \quad (5.A3)$$

$$\varphi_4 \approx (1 - \varphi_1) \quad (5.A4)$$

A new expression for x_i can be obtained:

$$x_i = \frac{\varphi_i}{\bar{V}_i C_T} \approx \frac{\varphi_i \bar{V}_4}{\bar{V}_1 (1 - \varphi_1)} \quad (5.A5)$$

Eq. 5.A5 for the case of BSA can be differentiated with respect to φ_1 using the quotient and chain rules:

$$\frac{dx_1}{d\varphi_1} = \frac{\bar{V}_4}{\bar{V}_1} \frac{1}{(1 - \varphi_1)^2} \quad (5.A6)$$

Combining Eq. 5.A2 5.A5 and 5.A6:

$$\begin{aligned} \Gamma_{11} &= \frac{\varphi_i \bar{V}_4}{\bar{V}_1 (1 - \varphi_1)} \frac{d \ln a_1}{d \varphi_1} \frac{\bar{V}_1 (1 - \varphi_1)^2}{\bar{V}_4} \\ &= (1 - \varphi_1) \varphi_1 \frac{d \ln a_1}{d \varphi_1} \end{aligned} \quad (5.A7)$$

Plugging Eq. 5.A7 into Eq. 5.A1:

$$\mathfrak{D}_{14} = \frac{D_{14}}{(1 - \varphi_1) \varphi_1 \frac{d \ln a_1}{d \varphi_1}} \quad (5.A8)$$

Considering Eq. 5.8, 5.A3 and 5.A4, the expression for the modified M-S diffusivity \mathfrak{D}_{14}^V can be obtained, as shown in Eq. 5.A9.

$$\mathfrak{D}_{14}^V = \mathfrak{D}_{14}(1 - \varphi_1) = \frac{D_{14}}{\varphi_1 \frac{d \ln a_1}{d \varphi_1}} \quad (5.A9)$$

The change of the Fick diffusivity D_{14} as function of concentration is shown in Eq. 5.A10. This empirical equation was obtained from data on the diffusivity of BSA at isoelectric conditions (pH 4.9) from the work of Fair et al. and Gaigalas et al. [35, 36]. By combining this equation with Eq. 5.A9 and Eq.5.23, the final expression for \mathfrak{D}_{14}^V as function of φ_1 can be obtained (Eq. 5.A11). This expression is useful at any pH and ion strength because the M-S coefficients represent only the friction between components and do not contain non-idealities due to electrical interactions.

$$D_{14} = 0.21 + 0.79 \exp(-4.1\varphi_1) \quad (5.A10)$$

$$\mathfrak{D}_{14}^V = D_{14}^\infty \frac{0.21 + 0.79 \exp(-4.1\varphi_1)}{\frac{1 + 4\varphi_1 + 4\varphi_1^2 - 4\varphi_1^3 + \varphi_1^4}{(1 - \varphi_1)^3}} \quad (5.A11)$$

A2. Calculation of the osmotic pressure.

Based on the work of Noordman et al., the osmotic pressure can be calculated by simply considering the concentration of the components of the mixture according to the Donnan distribution [26]. From Eq. 5.17 we can obtain the relation between osmotic pressure and water activity.

$$\ln x_4 + \ln \gamma_4 = -\frac{\bar{V}_4}{RT} \Pi$$

Since x_4 is a number that is very close to 1, then:

$$\ln x_4 \approx x_4 - 1.$$

$$\ln \gamma_4 = -\frac{\bar{V}_4}{RT} \Pi - (x_4 - 1)$$

$$\ln \gamma_4 = -\frac{\bar{V}_4}{RT} \Pi + x_1 + x_2 + x_3$$

$$\Pi = -\frac{RT}{\bar{V}_4} (\ln \gamma_4 - x_1 - x_2 - x_3) \quad (5.A12)$$

Even under concentrated conditions, the total number of moles in the system will be defined mostly by the amount of water in the system, thus $C_T \approx \frac{\varphi_4}{\bar{V}_4}$. Considering this relation and Eq. 5.A12 we can obtain the following relation for the osmotic pressure.

$$\begin{aligned}\Pi &= -\frac{RT}{\bar{V}_4} \left(\ln \gamma_4 - \frac{\varphi_1 \bar{V}_4}{\bar{V}_1 \varphi_4} - \frac{\varphi_2 \bar{V}_4}{\bar{V}_2 \varphi_4} - \frac{\varphi_3 \bar{V}_4}{\bar{V}_3 \varphi_4} \right) \\ \Pi &= -\frac{RT}{\varphi_4} \left(\frac{\ln \gamma_4 \varphi_4}{\bar{V}_4} - \frac{\varphi_1}{\bar{V}_1} - \frac{\varphi_2}{\bar{V}_2} - \frac{\varphi_3}{\bar{V}_3} \right)\end{aligned}\quad (5.A13)$$

The non-ideality produced by the excluded volume are due to BSA. Therefore, from our ‘imaginary’ binary system (Eq. 5.18), an expression for $\ln \gamma_4$ (Eq. 5.A14) can be derived in the following way:

$$\begin{aligned}\ln a_4 &= -\frac{\bar{V}_4}{\bar{V}_1} \left(\frac{\varphi_1 + \varphi_1^2 + \varphi_1^3 - \varphi_1^4}{(1 - \varphi_1)^3} \right) \\ \ln x_4 + \ln \gamma_4 &= -\frac{\bar{V}_4}{\bar{V}_1} \left(\frac{\varphi_1 + \varphi_1^2 + \varphi_1^3 - \varphi_1^4}{(1 - \varphi_1)^3} \right)\end{aligned}$$

In our system $x_4 \approx 1$, thus $\ln x_4 \approx x_4 - 1$, thus $\ln x_4 \approx -x_1$. Considering Eq. 5.A5 we obtain:

$$\frac{\varphi_1 \bar{V}_4}{\bar{V}_1 (1 - \varphi_1)} + \ln \gamma_4 = -\frac{\bar{V}_4}{\bar{V}_1} \left(\frac{\varphi_1 + \varphi_1^2 + \varphi_1^3 - \varphi_1^4}{(1 - \varphi_1)^3} \right),$$

which results in a simpler expression:

$$\ln \gamma_4 = \frac{\bar{V}_4}{\bar{V}_1} \frac{\varphi_1^4 - 3\varphi_1^2}{(1 - \varphi_1)^3}\quad (5.A14)$$

In the case of the permeate, where no BSA is expected, the system is considered ideal so $\ln \gamma_4 \approx 0$, and $\varphi_4 \approx 1$. Consequently Eq. 5.A13 reduces to Van’t Hoff equation:

$$\Pi = -RT(-2C_{2,3})\quad (5.A15)$$

Where C stands for the concentration of the ions in mol/m³. The factor 2 originates from the fact that the concentration of both ions is the same in the permeate, this value is commonly known as Van’t Hoff index.

REFERENCES

- [1] R. Baker, Membrane Technology and Applications 2nd ed., Wiley, California, USA, 2004.
- [2] G. Belfort, R.H. Davis, A.L. Zydney, The behavior of suspensions and macromolecular solutions in crossflow microfiltration, *J. Membr. Sci.*, 96 (1994) 1-58.
- [3] W.R. Bowen, J.I. Calvo, A. Hernández, Steps of membrane blocking in flux decline during protein microfiltration, *J. Membr. Sci.*, 101 (1995) 153-165.
- [4] S.P. Palecek, A.L. Zydney, Intermolecular electrostatic interactions and their effect on flux and protein deposition during protein filtration, *Biotechnol. Progr.*, 10 (1994) 207-213.
- [5] J.G. Wijmans, S. Nakao, C.A. Smolders, Flux limitation in ultrafiltration: Osmotic pressure model and gel layer model, *J. Membr. Sci.*, 20 (1984) 115-124.
- [6] M.C. Porter, Concentration polarization with membrane ultrafiltration, *Ind. Eng. Chem. Prod. Res. Develop.*, 11 (1972) 234-248.
- [7] R.D. Cohen, R.F. Probstein, Colloidal fouling of reverse osmosis membranes, *J. Colloid Interface Sci.*, 114 (1986) 194-207.
- [8] V.L. Vilker, C.K. Colton, K.A. Smith, The osmotic pressure of concentrated protein solutions: Effect of concentration and pH in saline solutions of bovine serum albumin, *J. Colloid Interface Sci.*, 79 (1981) 548-566.
- [9] R.H. Davis, J.D. Sherwood, A similarity solution for steady-state crossflow microfiltration, *Chem. Eng. Sci.*, 45 (1990) 3203-3209.
- [10] F.W. Altena, G. Belfort, Lateral migration of spherical particles in porous flow channels: application to membrane filtration, *Chem. Eng. Sci.*, 39 (1984) 343-355.
- [11] W.R. Bowen, P.M. Williams, The Osmotic Pressure of Electrostatically Stabilized Colloidal Dispersions, *J. Colloid Interface Sci.*, 184 (1996) 241-250.
- [12] W.R. Bowen, F. Jenner, Dynamic ultrafiltration model for charged colloidal dispersions: A Wigner-Seitz cell approach, *Chem. Eng. Sci.*, 50 (1995) 1707-1736.
- [13] P. Bacchin, P. Aimar, R.W. Field, Critical and sustainable fluxes: Theory, experiments and applications, *J. Membr. Sci.*, 281 (2006) 42-69.
- [14] P. Bacchin, P. Aimar, V. Sanchez, Model for colloidal fouling of membranes, *AIChE J.*, 41 (1995) 368-376.
- [15] A.L. Zydney, Stagnant film model for concentration polarization in membrane systems, *J. Membr. Sci.*, 130 (1997) 275-281.
- [16] R. Taylor, R. Krishna, Multicomponent Mass Transfer, John Wiley & Sons, Inc, New York, 1993.

- [17] J.A. Wesselingh, R. Krishna, Mass Transfer in Multicomponent Mixtures, VSSD, Delft, 2000.
- [18] R. Krishna, Describing mixture permeation across polymeric membranes by a combination of Maxwell-Stefan and Flory-Huggins models, *Polymer*, 103 (2016) 124-131.
- [19] C.P. Ribeiro, B.D. Freeman, D.R. Paul, Modeling of multicomponent mass transfer across polymer films using a thermodynamically consistent formulation of the Maxwell–Stefan equations in terms of volume fractions, *Polymer*, 52 (2011) 3970-3983.
- [20] N. El Kadi, N. Taulier, J.Y. Le Huérou, M. Gindre, W. Urbach, I. Nwigwe, P.C. Kahn, M. Waks, Unfolding and Refolding of Bovine Serum Albumin at Acid pH: Ultrasound and Structural Studies, *Biophys. J.*, 91 (2006) 3397-3404.
- [21] B. Halle, Protein hydration dynamics in solution: a critical survey, *Philosophical Transactions of the Royal Society of London. Series B: Biological Sciences*, 359 (2004) 1207-1224.
- [22] Prasad S. Sarangapani, Steven D. Hudson, Kalman B. Migler, Jai A. Pathak, The Limitations of an Exclusively Colloidal View of Protein Solution Hydrodynamics and Rheology, *Biophys. J.*, 105 (2013) 2418-2426.
- [23] G. Scatchard, I.H. Scheinberg, S.H. Armstrong, Physical Chemistry of Protein Solutions. IV. The Combination of Human Serum Albumin with Chloride Ion¹, *J. Am. Chem. Soc.*, 72 (1950) 535-540.
- [24] C. Tanford, S.A. Swanson, W.S. Shore, Hydrogen Ion Equilibria of Bovine Serum Albumin¹, *J. Am. Chem. Soc.*, 77 (1955) 6414-6421.
- [25] N.F. Carnahan, K.E. Starling, Equation of State for Nonattracting Rigid Spheres, *The Journal of Chemical Physics*, 51 (1969) 635-636.
- [26] T.R. Noordman, T.H. Ketelaar, F. Donkers, J.A. Wesselingh, Concentration and desalination of protein solutions by ultrafiltration, *Chem. Eng. Sci.*, 57 (2002) 693-703.
- [27] D.G. Leaist, The role of supporting electrolytes in protein diffusion, *The Journal of Physical Chemistry*, 93 (1989) 474-479.
- [28] O. Annunziata, D. Buzatu, J.G. Albright, Protein Diffusiophoresis and Salt Osmotic Diffusion in Aqueous Solutions, *The Journal of Physical Chemistry B*, 116 (2012) 12694-12705.
- [29] M.D. Reboiras, H. Pfister, H. Pauly, Activity coefficients of salts in highly concentrated protein solutions: I. Alkali chlorides in isoionic bovine serum albumin solutions, *Biophys. Chem.*, 9 (1978) 37-46.
- [30] J.A. Wesselingh, P. Vonk, Ultrafiltration of a large polyelectrolyte, *J. Membr. Sci.*, 99 (1995) 21-27.

- [31] P. Walstra, *Physical Chemistry of Foods*, Marcel Dekker Inc., New York, 2003.
- [32] R.S. Faibish, M. Elimelech, Y. Cohen, Effect of Interparticle Electrostatic Double Layer Interactions on Permeate Flux Decline in Crossflow Membrane Filtration of Colloidal Suspensions: An Experimental Investigation, *J. Colloid Interface Sci.*, 204 (1998) 77-86.
- [33] C. Ersch, L.L.C. Meijvogel, E. van der Linden, A. Martin, P. Venema, Interactions in protein mixtures. Part I: Second virial coefficients from osmometry, *Food Hydrocolloids*, 52 (2016) 982-990.
- [34] S.P. Palecek, S. Mochizuki, A.L. Zydney, Effect of ionic environment on BSA filtration and the properties of BSA deposits, *Desalination*, 90 (1993) 147-159.
- [35] B.D. Fair, D.Y. Chao, A.M. Jamieson, Mutual translational diffusion coefficients in bovine serum albumen solutions measured by quasielastic laser light scattering, *J. Colloid Interface Sci.*, 66 (1978) 323-330.
- [36] A.K. Gaigalas, V. Reipa, J.B. Hubbard, J. Edwards, J. Douglas, A non-perturbative relation between the mutual diffusion coefficient, suspension viscosity, and osmotic compressibility: Application to concentrated protein solutions, *Chem. Eng. Sci.*, 50 (1995) 1107-1114.

Chapter 6

General Discussion

6.1 MAIN FINDINGS AND CONCLUSIONS

This study was aimed at understanding membrane separation by ultrafiltration and nanofiltration, and capture this understanding in an integrated model. Emphasis was put on multicomponent, concentrated feed mixtures, since these are the type of mixtures typically used in the food and biotechnology industry. Membrane processes involving porous synthetic membranes were investigated theoretically and experimentally. The following is a small summary and discussion on our main findings and their applications.

The study intended to analyse membrane processes as close as possible to ‘real conditions’. This implies using feed solutions that truly resemble the type of feed mixture used in industry. We even went further and used a pilot scale set up that resembled the type of staged processes used at industrial level. In **Chapter 2**, we performed the study of a 3-stage nanofiltration cascade system for the purification of oligosaccharides. We found that the overall separation efficiency depended not only on the process conditions but also on the feed composition. Additionally, under some specific conditions, the trade-off between purity and yield was overcome by using a cascaded process. A model based on mass balances was developed to calculate the concentration of every component of the mixture in every stream of the system as a function of time. Although very accurate results were obtained with the dynamic model, it was necessary to perform single stage experiments to gather experimental data on the membrane rejection at specific concentrations. Therefore, it was clear that at least at the pilot scale level, the challenge was not really to represent the cascade system, but to model the membrane rejection itself at different conditions (concentration and composition).

To reduce the number of experiments, the next step was thus to model membrane rejection. In **Chapter 3**, the first step was to understand the effect of the solute molecular shape on membrane rejection. Since the molecular shape influences the probability of a molecule to enter a cylindrical pore, we considered different ways to represent the shape of elongated molecules such as oligosaccharides. Based on modelling and experimental measurements, we showed that representing these elongated solute molecules as capsules was much more accurate than considering them to be spherical. Additionally, the importance of using the entire pore size distribution during the calculations was demonstrated.

The next step was to assess the effect of the concentration on membrane rejection. As reported by many authors, in concentrated multicomponent systems, solutes influence each other’s rejections [1, 2]. It has been observed that the addition of an ‘extra’ component to single solute

systems lowers the rejection of the initial solute, even resulting in negative rejections in some cases. In **Chapter 4**, we could understand this by using Maxwell-Stefan equations to represent the cross-effects between components. We explained the observations using three mechanisms: thermodynamic non-idealities (hydration) in the concentration polarization layer, osmotic pressure effects in membrane pores, and the effect of the pressure gradient in the diffusion of the solutes through the membrane pores. Interestingly, the outcome of these interactions did not necessarily decrease the process efficiency, and an optimum feed concentration was determined at around 20% w/w for the purification of an oligosaccharide mixture.

Additional to the non-idealities described in the previous chapter, it is known that electrical interactions between charged components (sometimes also with the membrane), can take place in the filtration system, influencing the process performance. Therefore, in **Chapter 5**, a model system composed of BSA, Na⁺, Cl⁻ and H₂O was used to study these interactions and their effect on the permeate flux. The presence of protein in the system implies that fouling may occur, caused by the formation of a gel layer on the membrane surface. Again, the Maxwell-Stefan equations were used to account for the cross effects and the non-idealities of the system (hydration, Cl⁻ absorption, electrical interactions and volume exclusion). Local fluxes were calculated by considering the increase in the thickness of the boundary layer along the membrane length. When the system was completely covered by the gel layer, the local fluxes were at their maximum value (local critical fluxes). On the other hand, when the system was only partially covered, the local fluxes of the 'clean' section were determined by the local osmotic pressure difference, and the fluxes of the covered section were the local critical fluxes. The magnitude of these local fluxes were strongly influenced by the physico-chemical conditions of the feed (pH and ionic strength). These conditions determined the osmotic pressure in the system and the presence of fouling.

This study therefore contributes with new insights on membrane filtration by extending the previously available theory with the quantitative representation of more complex systems (food streams). Apart from their predictive role, the developed models allow us to understand and elucidate the mechanisms taking place during the separation process, giving insight for the development of new strategies. The qualitative and quantitative accuracy of the integrated model that was developed, has as an additional practical implication that less experiments will be needed to design and implement industrially relevant processes in the food and biotechnology industry.

6.2 SIMILAR OBSERVATIONS IN OTHER SYSTEMS

In this section we discuss some additional findings that complement those that were reported within the context of the previous chapters.

The observed decrease in the rejection of the solutes with increasing feed concentration was studied in **Chapter 4**; to verify if the same phenomenon occurs in different systems, additional experiments were performed. We used a system that resembles the composition of the permeate stream of whey UF. The feed was prepared by mixing lactose, KCl and CaCl₂. Using a NF membrane, the rejection of lactose was investigated at different concentrations, first as a single solute and then after adding KCl and CaCl₂ to the feed mixture (Figure 6-1).

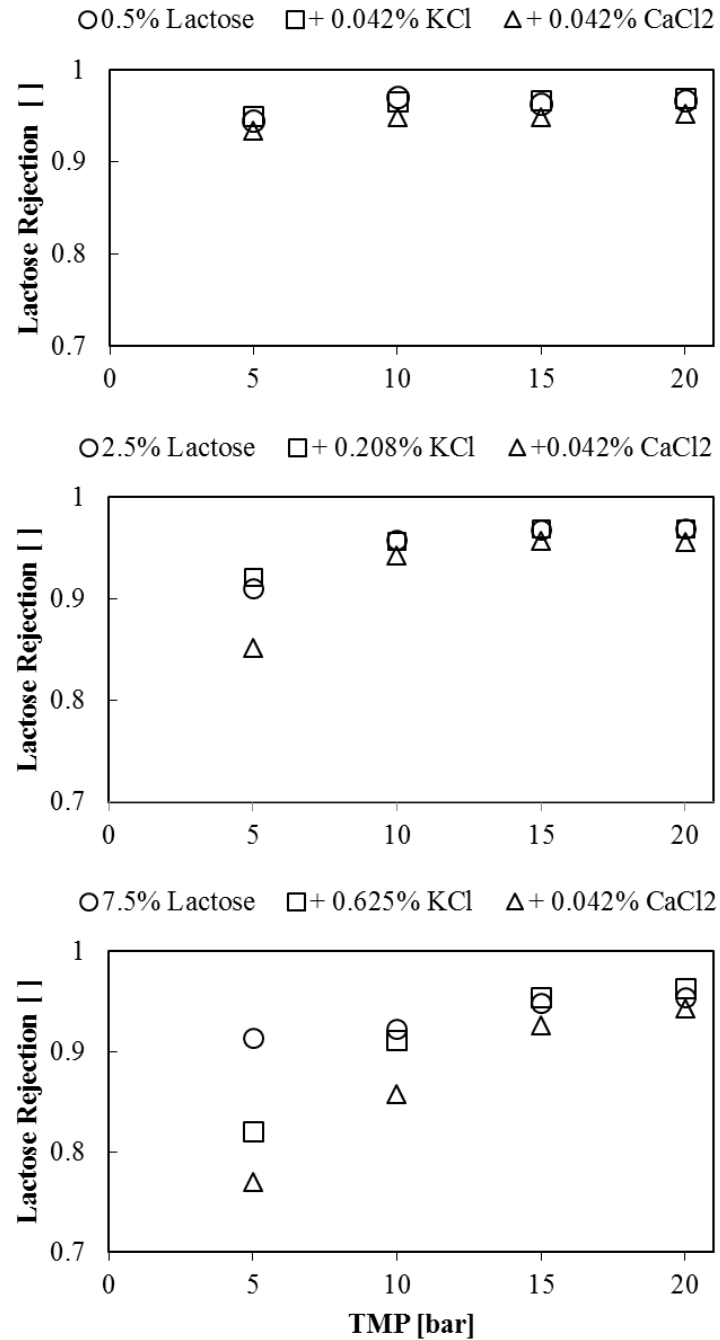


Figure 6-1. Effects of adding salts (KCl and CaCl₂) in the rejection of lactose at different concentrations. A cellulose acetate membrane GE-CK (MWCO ≈ 300Da) was used for these experiments in a spiral wound module. ○ = only lactose, □ = lactose + KCl, △ = lactose + KCl + CaCl₂.

One can see that the lactose rejection decreases as the salts are added to the feed. At low concentrations, the effect of adding KCl is negligible but it becomes important at higher concentrations (Figure 6-1C). The presence of CaCl₂ affects the rejection of lactose somewhat more strongly than KCl. Again, as the system becomes more concentrated, the effect of CaCl₂ is stronger.

Since the effects are almost negligible at high transmembrane pressures, it may be that the decrease in the rejection of lactose can be explained by the reduction in convection due to an increase in the osmotic pressure difference over the system. The rejection of KCl and CaCl₂ salts was around 0.4 and 0.6 respectively (results not shown), thus a polarization effect and a consequent contribution in the osmotic pressure difference was expected. To quantitatively support this the concentration profiles of all the components should be solved and the osmotic pressure over the system should be calculated. This is, however, a complicated task considering that the ions in the solution interact with the membrane material, and this interaction influences their transport in the system. Additionally, the high concentration of lactose in the concentration polarization layer is expected to influence the activity of the transient ions due to a hydration effect, similarly as what happened among sugars in **Chapter 4**.

The system in Figure 6-1 differs from the oligosaccharide system analysed in **Chapter 4** in that the added solute here (the salts) can actually enter the NF pores. As consequence, the resulting cross-effects should be considered also inside the membrane pores, including the membrane polymer as a component of the system. This requires knowledge on the interactions of the transient solutes (especially the charged ones) with the membrane polymer(s) at the process conditions. Unfortunately, these interactions are not well understood yet, and despite some studies using molecular dynamics, few work has been done on the subject.

These results confirmed the high impact of concentration in the rejection of solutes in multicomponent systems. It also demonstrates the importance of modelling to understand and predict the behaviour of a system that can be designed and optimized in function of these strong interactions. It is evident that membrane and feed should not be regarded separately but assessed together as a one only system. Further discussion on this aspect is presented in the coming sections.

6.3 REDUCING THE GAP BETWEEN THEORY AND REALITY BY MAKING MORE REALISTIC MODELS.

To represent the filtration of complex, practically relevant feed mixtures, the description of many phenomena should be integrated in a model. This goes beyond the consideration of the thermodynamic non-idealities of the mixtures. Other physical aspects of the process must be also included, such as the molecular shape (**Chapter 3**), the pore size distribution (**Chapter 3, 4**) and the influence of the module length (**Chapter 5**), etc. All this together represents a complicated set of equations, which are not only complex by itself to set but also difficult to numerically solve, and requires the prior knowledge of the values of many parameters. Therefore it is important to take into account only those phenomena that are most relevant. This is not just important for practical application but just as much for distinguishing those phenomena that determine the system's behaviour and those that are not relevant for the system within its targeted context.

6.3.1 Interactions between components

With the exception of the electrical interactions (electroneutrality), all the other interactions (hydration, excluded volume) can be safely neglected at diluted conditions. Even in concentrated systems, friction between neutral solutes is not relevant due to the low solute molar fraction (**Chapter 4**). In the case of ions, friction becomes slightly more important, and the cross M-S diffusivities (\mathfrak{D}_{ij}) have to be calculated, but high accuracy is not needed [3]. Our general conclusion is therefore that the observed interaction in concentrated systems is predominantly of a thermodynamic nature.

6.3.2 Molecular shape

For elongated molecules, considering them as capsules instead of as spheres is definitely necessary for the calculation of membrane rejection, especially for nanofiltration (**Chapter 3**). In the case of sugars with a degree of polymerization of 2 (sucrose, lactose, maltose, trehalose), the assumption of sphericity still yields acceptable results. For longer sugars, however, assuming sphericity leads to an estimation of the rejection that significantly lower than the real value, which in industrial applications might lead to wrong design and to a distorted estimation of processing costs.

Solute shape considerations are only relevant when the size of the solute molecule is smaller but not much smaller than that of the pore. For solutes that are bigger than the pores ($r_s > r_p$),

total rejection ($R=1$) can be safely assumed, as it normally happens with proteins in UF processes (**Chapter 5**). When the solute is much smaller than the pore ($r_s \ll r_p$), its shape is also irrelevant since the rejection is low. This is normally the case of small ions or some small neutral molecules (urea, boron, glucose) during UF or MF processes. Therefore, shape should be considered when separating components that are very similar in size, thus using a membrane that has intermediate rejection for these components.

6.3.3 Pore size distribution

Considering the pore size distribution of a membrane in the estimation of the rejection greatly increases the computational requirements. However, incorporation of the pore size distribution is generally necessary in most of the NF separations for multicomponent mixtures (**Chapter 3 and Chapter 4**). In the case of UF, this incorporation is less crucial as long as total rejection can be assumed for the retained molecules and as long as the permeating molecules are considerably smaller than the pores. In that case the rejection of these small solutes can be calculated using just the average pore size.

6.3.4 Membrane length

The inclusion of the effect of the membrane channel/module length requires the consideration of an additional dimension and significantly increases the complexity of the model. It implies the calculation of local variables (e.g. local fluxes, local pressure, local concentration, etc.) and subsequent integration over the channel length. If the system contains macromolecules that can induce membrane fouling, and the membrane module is long (as it normally is at industrial scale), and is operated not too far from the limiting flux (as is usual for practical purposes), the resolution into local fluxes will indeed be required for correct estimation of the overall permeate flux (**Chapter 5**). When operating below the overall critical flux, or when fouling can be ruled out from the nature of the feed constituents, an average distance for the boundary layer thickness can be estimated, and from it an average permeate flow can be calculated without having to resolve the local variables. Likewise, if the membrane module is short in length, local variables may not change too much along the membrane, and average values may be safely used.

6.4 APPLICABILITY OF THE FINDINGS

This work has shown, that the development of membrane and process should become more integrated. We showed that the accumulation of rejected components, such as higher-DP, on the membrane, may positively influence the transmission of the smaller components; thus enhancing the resolution of the separation (**Chapter 4**). In effect, the concentration polarization layer acts as an additional active layer on top of the membrane. One result was that separations at around 20 weight% solids were found to be more efficient than separations at lower concentrations. Thus, we would like to argue that the traditional separation in tasks between membrane developers, aiming at better permeance, system designers, aiming at limiting concentration polarization, and system users, aiming at fast and reliable separations, should be taken down. By integrating the understanding of the interaction between components, significant improvements in the overall performance of systems may be obtained, without requiring radically new membranes or module designs, and at the same time reducing the overall use of water for dilution, and consequently also reducing the energy requirements per kg of solute separated.

Some generalizations can be made with the knowledge acquired along this thesis. We target them to two important players in membrane development: membrane and module manufacturers and membrane system users.

6.4.1 Membrane and module manufacturers

Awareness and understanding of the underlying phenomena occurring during membrane separation gives insight in the characteristics that a membrane should have to be more efficient. The way to go for membrane manufacturers might not be too evident considering the complexity of the systems in many industrial applications. Based on observations in our lab and on literature data, we believe that selectivity and pressure resistance are aspects that can still be improved in the membrane manufacturing. Our reasoning for this is explained in the following sections.

6.4.1.1 Improve permeability or selectivity?

All synthetic membranes have a trade-off between selectivity and permeability, regardless the type of material that they are made out of, and regardless whether they are dense or porous [4]. The membrane permeability L_p is defined as follows:

$$L_p = J \frac{\Delta z}{\Delta P},$$

in which J is the permeate flux, ΔP is the pressure gradient and Δz is the thickness of the membrane selective layer, which most of the times is included in the L_p term, yielding the permeance: $L_p/\Delta z$. It is thus logical to believe that the permeance of a membrane can be improved by reducing Δz . Therefore, manufacturers indeed have created very thin selective layers. Values of $\Delta z \approx 100$ nm have already been reached with industrial membranes in the case of thin-film composite membranes (TFC). Nevertheless, the effect of the porous support of the membrane, which is commonly considered to have a negligible resistance for mass transfer, does become relevant with such thin selective layers [4]. Therefore, reducing the thickness of the selective layer further does not guarantee an equivalent increase in the membrane permeance.

The second parameter in the permeance is the permeability. Improving membrane permeability indeed could reduce the processing costs for dilute feed streams, but this is not the case for concentrated systems, as many food streams are (**Chapter 4** and **Chapter 5**). A higher permeate flux implies stronger concentration polarization, and stronger dominance of the phenomena related to this. Operating at larger fluxes will lead to a higher solutes concentrations at the membrane surface, and, as consequence, a larger difference in the osmotic pressure over the selective membrane layer. This has already been observed in RO seawater desalination, in which an increase of a factor of 5 in the membrane permeability only decreases the overall energy consumption by 3.7% [5].

Selectivity, on the other hand, is linked with the membrane pore size distribution. As assessed in **Chapter 3**, narrowing the pore size distribution will evidently improve the membrane selectivity. To achieve this, many strategies have been tested at lab scale. One of the most promising techniques is to use block copolymers that innately self-assemble into well-defined structures with regular periodicity. Isoporous membranes with 15 nm. pores have been obtained in this way with excellent results in the removal of viruses, maintaining high permeate flux [6]. Efforts now are focused on reducing the size of the pore to the NF spectrum.

A membrane with a narrower pore size distribution (higher selectivity) could lead to higher efficiency at high concentrations. We found in **Chapter 4** that the transport through the larger pores becomes more important at high concentrations, reducing the rejection of all the solutes in the system. With a uniform pore size, this effect does not occur and only the transport of the

solutes that are smaller than the pore ($r_s > r_p$) gets enhanced by the thermodynamic effects at high concentrations. As consequence, permeate solutions with high purity and high concentration (due to low or even negative rejections) could be obtained. Therefore, in the permeability – selectivity trade-off, an increase in membrane selectivity seems to be much more promising for the improvement of overall process performance in concentrated systems.

6.4.1.2 Should we build more pressure resistant NF membranes?

In the final part of **Chapter 4**, the effect of pressure on the transport of solutes across a porous membrane was discussed. We found that in concentrated NF systems the pressure gradient becomes a very important mechanism for the transport of solutes, due to a severe limitation in convection. As consequence, the pressure tolerance of NF membranes / membrane modules may become limiting, since the concentration polarization will induce high osmotic pressure differences over the membrane. Further improvement of the selectivity of the membrane – for example by narrowing the pore size distribution – will only exacerbate this effect, requiring larger pressure differences.

The objective of operating the system at higher pressures is not augmenting the permeate flux but enhancing the flux of the small solutes towards the permeate. It was already mentioned in the previous section that increasing permeance is not really a fruitful strategy for concentrated systems. It is better to focus on maximizing the transport of the molecules that have to be removed from the feed. A good strategy seems to be making use of the pressure gradient, which is a driving force that has been overlooked over the years due to its insignificance at diluted conditions (**Chapter 4**).

Consequently, more robust NF membranes are definitely needed. Osmotic pressure differences in concentrated NF systems can reach values close to 20 bar. Therefore, the manufacturing of novel NF membranes and membrane modules that would allow (resist) the processing of concentrated solutions at high pressures (30-40 bar) would indeed enhance the possibilities of nanofiltration in the food industry.

6.4.2 Membrane system users

The understanding of the filtration process, captured in its mathematical representation, is a powerful tool for membrane users for the improvement of the separation process. We believe that feed and membrane must be seen as one integrated system and the design and optimization of the process must consider the complexity of the resulting interactions and benefit from it.

The usefulness of our findings and models for membrane users is further discussed in the next sections.

6.4.2.1 Using a model or keep doing experiments?

In general, modelling is less expensive than carrying out an experimental programme. It is a task that involves not too many persons and that pursues not only predictive purposes, but more importantly, the understanding of the process. This understanding will guide the process designer to find new opportunities for improvement. The total parametric space is so large that it is impossible to investigate all possibilities purely experimentally; thus one needs a guide through this parametric space, which quantitative understanding can offer. In addition, mechanistic understanding will enable the designer to extend beyond the conventional boundaries, and find possibilities that would be difficult to find with a purely experimental programme.

Indeed, in chapter 2, it was demonstrated that, for a known design, measurements in the correct domain result in right predictions. However, in real large systems, the combinations of pressures, concentrations and crossflow velocities becomes too large to be approached with an empirical methodology. Therefore, a mechanistic insight, operationalised by modelling to predict the membrane rejection at different conditions facilitates the optimization and control of such processes. Nevertheless, experiments should never be completely eliminated since verification and validation of the model results always remain necessary.

6.4.2.2 What to maximize? Overall productivity or purity?

During the separation of two solutes by membrane filtration, we almost always have a trade-off between product purity and productivity or yield. This is an inherent characteristic of membrane separations (selectivity-permeability trade-off). Nevertheless, during this research, we identified ways to overcome this trade-off.

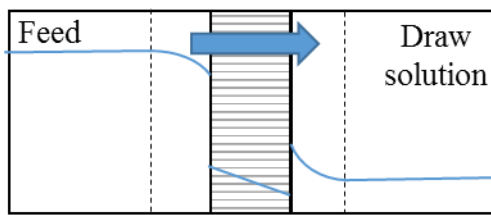
The first way is the efficient use of cascades, as shown in **Chapter 2**. Under specific conditions, purity and yield can be increased simultaneously. Likewise, in **Chapter 4**, it was demonstrated that at high concentrations the transport of small molecules was promoted through the membrane, increasing the yield of the process, its productivity (lower dilution) and purity. Evidently, we can make use of this phenomenon to benefit the overall performance of the separation.

The relative importance between productivity and purity depends on the specific application. If the value of a feed mixture increases strongly after an increase in purity, it is obvious that we should prioritize purity, like in high-value, low-volume separations (mostly for biomedical applications). The opposite happens in the case of lower-value products, for which it is better to keep the productivity high.

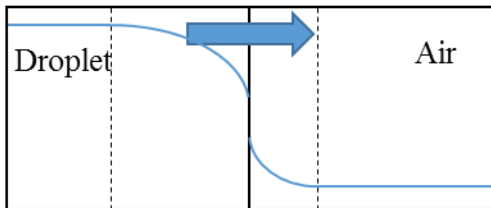
6.4.2.3 Applications in other processes

Although only systems with porous membranes have been covered in this thesis, the approach can be extended to other type of filtration processes. For example, forward osmosis and reverse osmosis, which are processes that are used for concentration purposes, can be modelled using a similar approach as done in this thesis, especially for the representation of the concentration polarization layer. Similarly, some concepts and strategies can be used for other type of processes taking place at high concentrations such as: evaporation, drying, condensation, crystallization. In all these processes the proper representation of mass transport is critical. As in filtration, concentration gradients originate near the interface and non-idealities play an important role in the final results (See Figure 6-2). We expect that the same conclusions will result, with respect of the types of non-idealities that are important in the systems.

A.) FORWARD OSMOSIS



B.) SPRAY DRYING



C.) CRYSTALLIZATION

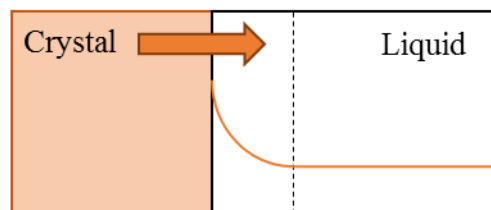


Figure 6-2. Schematic representation of other processes in which the concepts presented in this thesis can be applied. Blue and brown lines represent the concentration profiles of water and solute respectively. A.) Forward Osmosis: Water diffuses down its concentration gradient to a phase with high concentration of solutes (draw solution). B.) Spray drying: Water moves towards the air, producing gradients in concentration inside the droplet and in a film layer in the gas phase. C.) Crystal gets dissolved in an unsaturated liquid, producing the solute to migrate towards the liquid phase.

6.5 CONCLUDING REMARKS.

While membrane separations such as UF and NF have been investigated thoroughly, in almost all cases this has been done for dilute streams. This simplifies the descriptions, and avoids the necessity to understand the complexity of concentrated, multicomponent feed systems.

This thesis shows that, by not taking this approach but by deliberately seeking this complexity, new opportunities can be found. The non-idealities, or specific interactions that emerge in these concentrated systems can be detrimental, but can also enhance the separation. This can be only

found and embraced by a quantitative understanding of these properties, preferably operationalised in a model based on mechanistic insight.

It is remarkable that after so many years of research in membrane processes, we are only now starting to learn the possibilities that are created by this emergence. Potentially, this could lead to more concentrated process streams, smaller factories, lower energy use (since less dehydration is necessary when streams remain more concentrated).

To model these emergent system properties, one needs to consider all length scales. Starting from the atomic/molecular level, all the way up until the scaling up at the industrial level. In the case of membrane separations, the complete understanding of the interactions at a molecular level is not yet attained. In this thesis we have mostly discussed on the interaction between the components of the mixture. Nevertheless, the interaction of these components, especially the charged ones, with the membrane is also important and, unfortunately, its understanding is still in its infancy.

Insights in the emergent properties resulting from interactions between solutes and membrane polymer(s) may allow us to create not just better membranes, but to create much better integrated systems of membranes, process systems and feed streams. Only a small number of polymers are currently used for this purpose, and in many cases, their applicability in membranes was discovered by serendipity [4]. The insight in the complexity of the feed and the membrane materials together, will bring us to a next step in separation processes based on membranes.

REFERENCES

- [1] G. Bargeman, J.M. Vollenbroek, J. Straatsma, C.G.P.H. Schroën, R.M. Boom, Nanofiltration of multi-component feeds. Interactions between neutral and charged components and their effect on retention, *J. Membr. Sci.*, 247 (2005) 11-20.
- [2] C.W. van Oers, M.A.G. Vorstman, R.v.d. Hout, P.J.A.M. Kerkhof, The influence of thermodynamic activity on the solute rejection in multicomponent systems, *J. Membr. Sci.*, 136 (1997) 71-87.
- [3] J.A. Wesselingh, R. Krishna, *Mass Transfer in Multicomponent Mixtures*, VSSD, Delft, 2000.
- [4] H.B. Park, J. Kamcev, L.M. Robeson, M. Elimelech, B.D. Freeman, Maximizing the right stuff: The trade-off between membrane permeability and selectivity, *Science*, 356 (2017).
- [5] J.R. Werber, A. Deshmukh, M. Elimelech, The Critical Need for Increased Selectivity, Not Increased Water Permeability, for Desalination Membranes, *Environmental Science & Technology Letters*, 3 (2016) 112-120.
- [6] S.Y. Yang, I. Ryu, H.Y. Kim, J.K. Kim, S.K. Jang, T.P. Russell, Nanoporous Membranes with Ultrahigh Selectivity and Flux for the Filtration of Viruses, *Adv. Mater.*, 18 (2006) 709-712.

Summary

SUMMARY

The mechanisms behind membrane processes such as ultrafiltration and nanofiltration are not yet completely understood when multicomponent, concentrated solutions are used as feed, as is usually the case in the food and biotechnology industry. Under concentrated conditions, the interactions between the mixture components become important and the prediction of permeate flux and rejection is not possible using currently available models. This PhD thesis reduces the gap in the understanding of these complex systems, enabling a better process design and optimization. Thus, the aim was to improve the accuracy of the predictions of pressure driven filtration by implementing new concepts and descriptions that result from considering the fundamental underlying phenomena acting under realistic concentrated conditions.

In Chapter 1, a general introduction is presented, in which the relevance, motivation and scope of this thesis are outlined. The importance of key aspects in modelling the filtration of complex mixtures (solutes' shape, pore size distribution, molecular interactions, molecular friction, viscosity and osmotic pressure) is also explained. Finally, the Maxwell-Stefan approach and its advantages are briefly introduced.

The overall behaviour of a staged nanofiltration system is described in **Chapter 2**. A three-stage cascade system for the purification of oligosaccharides is modelled. An optimal combination of process parameters dependent on the feed mixture composition was determined, and under some conditions, the typical trade-off between purity and yield could be overcome. Nevertheless, single stage experiments were still essential to obtain information on the membrane rejection under specific conditions.

To avoid the need of these experiments, the transport of solutes through membrane pores was studied in **Chapter 3**. Here, we revisited the effects of the molecular shape of solutes on membrane rejection for nanofiltration systems. For the estimation of the rejections, elongated solutes could best be described as capsule-shaped. This description yielded a more accurate approach than regarding them as perfect spheres. Additionally, the consideration of a pore size distribution instead of a uniform pore size was included in the analysis. This pore size distribution was used as a 'given input' in the model built for concentrated conditions presented in the next chapter. These two new elements gave rise to better description compared to previous approaches.

In Chapter 4, the effect of high concentrations was assessed using as a model system the nanofiltration of a multicomponent mixture of oligosaccharides. The Maxwell-Stefan equations were used, to capture the interactions between the components in the system. The thermodynamic effects due to hydration were found to be very important specially at the membrane interface, in which a local equilibrium between a concentrated (retentate) and a diluted phase (membrane pores) is present. Additionally, effects emerging from the pore size distribution and high osmotic pressure were found and represented into an integrated model. Finally, we found that the importance of the different transport mechanisms (convection and diffusion due to concentration and pressure gradients) differs greatly between concentrated and diluted conditions, leading to not just quantitatively but also qualitatively different rejections in concentrated systems. The developed model could explain all observations including the negative rejections obtained for smaller sugars at concentrated conditions. In literature, negative rejections are only explained for systems with charged molecules, which is precisely the type of system studied in the next chapter.

In Chapter 5, the ultrafiltration of a system composed of BSA, NaCl and H₂O was assessed. To do so, non-idealities due to hydration, Cl-adsorption to BSA, electrical interactions and excluded volume were taken into account. Once again a model based on the Maxwell-Stefan Equations was developed and validated with experimental data. The influence of the pH and the ionic strength on the performance of the system was explained and quantitatively predicted considering the electrical potential as an additional driving force in the system. This representation of the system allowed us to accurately estimate the degree of fouling of the membrane (length of the membrane covered by gel) and the permeate flux under many different process conditions. Thus more than one mechanism can influence the permeate flux when working under the limiting flux, and this needs to be taken into account for obtaining accurate predictions.

In Chapter 6, the findings and conclusions of this thesis are discussed. Opportunities for improvement for membrane manufacturers and membrane users are analysed within the scope of the application of membrane technology in food processes. Remaining challenges about scientific aspects that could not be covered in this thesis are also presented.

Acknowledgements

I would like to thank to all the FPE group for the support during these 4 years. Thank you Remko for the interesting and challenging discussions during our meetings, figuring things out became a really pleasant activity during my time in the group. Thank you Anja and Albert for your supervision and for letting me ‘see the forest through the trees’.

Thanks to all the rest of the staff and to my fellow PhD colleagues for these 4 years. Special thanks to Lu and Anton for being my paranymphs. Thanks to Juliana and Andrea for all the Mexican food and drinks that I got without the necessity of washing dishes. Thank you Jaap for the trips to the European capital of culture, and for being a fan of Dexter Holland. Thank you Pina and Birgit for the multiple invitations to dinners and events at your house. Thank you Ali and Jun for being good and quiet officemates. Thank you Martin for the Canadian F1 grand prix, I waited 15 years to finally make it.

I also want to thank Ana María for all her love and support since we started our masters in The Netherlands. It has been a long road, but all the effort will eventually pay off. Thanks to my parents and sisters for their occasional visits and for their continuous support. Thank you to all my high school friends in Ecuador who were permanently (almost daily!) in contact with me. Special thanks to Frank López for the amazing cover design.

Finally, I would like to give my heartfelt thanks to my students (Zulhaj, Koen, Patrick, Maria, Daniel, Desiree, Jaap, Esther and Bobby), who worked very hard alongside me. This thesis belongs also to them.

About the author

Curriculum vitae



Photo: Maxim van Asseldonk

Víctor Hugo Aguirre Montesdeoca was born on April 13, 1985 in Quito – Ecuador. He studied Food Engineering from 2003 to 2008 at Universidad San Francisco de Quito, from where he graduated (*summa cum Laude*). During this time he spent 1 year in a study abroad program at Michigan State University. After working in the food industry for 4 years, he decided to continue with his studies and pursued a Master degree in Food Technology at Wageningen University. He finished his master with distinction (*cum Laude*) in 2014, and his MSc thesis ‘Optimization of oligosaccharide purification in nanofiltration cascades’ led to his PhD project within Food Process Engineering group on the Membrane Filtration of Food Streams.

Besides science, he has a big interest in tennis and music.

List of publications

This thesis

Victor Aguirre, A. Van der Padt, R.M. Boom, Anja E.M. Janssen. Modelling of membrane cascades for the purification of oligosaccharides. *J Memb Sci*, Volume 520, 2016.

Victor Aguirre, Jaap Bakker, R.M. Boom, Anja E.M. Janssen, A. Van der Padt. Ultrafiltration of elongated molecules. (*accepted in J Memb Sci*)

Victor Aguirre, Anja E.M. Janssen, R.M. Boom, A. Van der Padt. Nanofiltration of concentrated oligosaccharide solutions – hydration and pore size distribution effects (*submitted for publication*)

Victor Aguirre, Anja E. M. Janssen, A. Van der Padt, R. M. Boom. Modelling UF performance by integrating local (critical) fluxes along the membrane length. (*submitted for publication*)

Others

Nirmal V Patil, Thom Schotel, Carol Rodríguez, **Victor Aguirre**, Jos Sewalt, Anja EM Janssen and Remko Boom. Continuous purification of galacto-oligosaccharide mixtures by using cascaded membrane filtration. *J Chem Technol Biot*, Volume 91, 2015.

Overview of completed training activities

Discipline specific activities

Courses

- Numerical methods for chemical engineers (OSPT, Eindhoven - Netherlands, 2015)
- Advanced thermodynamics (OSPT, Delft - Netherlands, 2016)
- Process intensification (OSPT, Delft - Netherlands, 2016)
- International School of modelling (VirProFood, Anacapri - Italy, 2016)
- Statistical uncertainty analysis of dynamic models (PE&RC, Wageningen - Netherlands, 2017)
- Physical Chemistry Winter School (WUR/TU Delft, Han-Sur-Lesse - Belgium, 2018)

Conferences and meetings - Oral Presentations

- 11th International Congress on Membranes and Membrane processes ICOM 2017 (NAMS, San Francisco - USA, 2017)
- Symposium ISPT day (ISPT, Amersfoort - Netherlands, 2017)
- Symposium Thermodynamics and Phase Transitions in Food Processing (WUR, Wageningen - Netherlands, 2018)
- Netherlands Process Technology Symposium 2018 (ISPT, Twente - Netherlands, 2018)

Conferences - Poster Presentations

- Conference Euromembrane 2018 (EMS, Valencia - Spain, 2018)

General courses

- VLAG PhD week (VLAG, Baarlo - Netherlands, 2015)
- Data Management Planning (VLAG, Wageningen - Netherlands, 2016)
- Techniques for writing and presenting a scientific paper. (WGS, Wageningen – Netherlands, 2016)
- Writing Grant Proposals (Wageningen into languages, Wageningen – Netherlands, 2017)
- Introduction to R (VLAG, Wageningen – Netherlands, 2017)
- Chemometrics (VLAG, Wageningen – Netherlands, 2017)
- Career Assessment (WGS, Wageningen – Netherlands, 2017)
- Bayesian Statistics (PE&RC, Wageningen – Netherlands, 2017)

Optional activities

- Preparation of research proposal (Wageningen – Netherlands, 2014)

- PhD study tour (Germany and Switzerland, 2016)
- PhD study tour (Canada, 2018)
- Weekly group meetings
- Teaching: Transfer Processes (2014, 2015, 2016), Thesis rings (2016, 2017)

The research described in this thesis was carried out in the framework of the Institute of Sustainable Process Technology (ISPT) under the project 'CM-20-05'.

Cover design by Frank Lopez || Novotrendmedia

Printed by Digiforce || ProefschriftMaken

Propositions

1. The efficiency of filtration processes can be improved by operating at more concentrated conditions.

(this thesis)
2. Membrane retentions are determined by chemical activities and not by concentrations.

(this thesis)
3. Trial and error approach should only be a last resource for scientists.
4. Modelling is understanding.
5. Self-learning is the future of education at every level.
6. The smarter your phone, the dumber you get.

Propositions belonging to the thesis, entitled
'Membrane filtration of food streams: Mechanisms and modelling'.

Victor Aguirre

Wageningen, 12th November 2018